A NOVEL COMPOUND TARGETING MICROGLIAL ACTIVATION

INAUGURAL-DISSERTATION

TO OBTAIN THE ACADEMIC DEGREE

DOCTOR RERUM NATURALIUM (DR. RER. NAT.)

SUBMITTED TO THE DEPARTMENT OF BIOLOGY, CHEMISTRY AND PHARMACY

OF FREIE UNIVERSITÄT BERLIN

BY

PHILIPP JORDAN

aus

Beckum, Deutschland

2018

This work was carried out at the Max-Delbrück-Centrum für Molekulare Medizin in the Helmholtz Association from November 2013 to September 2017 under the supervision of Prof. Dr. Helmut Kettenmann and Dr. Susanne Wolf.

1st Reviewer: Prof. Dr. Udo Heinemann
Max-Delbrück-Centrum für Molekulare Medizin
Macromolecular Structure and Interaction
Robert Rössle Str. 10
13125 Berlin

2nd Reviewer: Prof. Dr. Helmut Kettenmann
Max-Delbrück-Centrum für Molekulare Medizin
Cellular Neurosciences
Robert Rössle Str. 10
13125 Berlin

Date of defense: 20.03.2019

ACKNOWLEDGEMENTS

I thank Prof. Dr. Helmut Kettenmann for the opportunity to work on this fantastic project, for the supervision and funding, and to work in such a wonderful lab. Thanks to Prof. Dr. Udo Heinemann for being my university supervisor. I am very grateful for invaluable support and supervision from Dr. Susanne Wolf for the excellent supervision, many discussions and ideas and a lot of support through the development of this project, as well as for critical comments on this thesis. Furthermore, I would like to the thank the FMP screening unit of Jens Peter von Kries for the help in realisation the high throughput screen, the "Medicinal Chemistry" of Marc Nazaré for the help in chemical questions, in particular Edgar Specker, who was of great help identifying the chemical structures of compound C1.0 and the setting up the SAR for compound C4.0. Thanks to Matthias Endres and Golo Kronenberg for providing the stroke mouse model and Amanda Costa, who did the behavioural experiments.

Special thanks to the wonderful technicians, Regina Piske and Maren Wendt for the help throughout the years with all experiments, Irene Haupt for the preparation of a tremendous amount of microglia for the high throughput screen, and all other technicians and Azubis who help to make the life of an PhD student easier. Special thanks to Birgit Jarchow for her support and invaluable help in all organisational matters and bureaucratic challenges.

I would also particularly like to thank all my fellow PhD students, without whom the last years would have not been the same. It has been an amazing time, with help and support both intellectually and socially. Thanks especially to Petya Georgieva, Maria Pannell, Daniele Mattei, Felipe Sassi, Nadine Richter, Dong Le, Feng Hu, and Masataka Ifuku, as well as Alice Buonfiglioli, Amanda Costa, Dilansu Güneykaya, Verena Haage, Francesca Logiacco, Meron Maricos, Niklas Meyer, Stefan Wendt, and Olga Bakina (and everyone else who I forgot to mention here!). It was a wonderful time with you all.

This thesis is dedicated to my whole family: Ingrid und Claus, Carsten, Catharina, and Victoria. You have been there for me whenever and wherever needed with support and understanding. Without you I wouldn't be there where I am right now.

TABLE OF CONTENTS

Acknowledgements ii

List of abbreviations viii

List of figures x

List of tables xiii

1 Introduction 1

1.1 A small history of microglia 1

1.1.1 Origin 1

1.1.2 Capabilities 2

1.1.3 Physiology 2

1.1.4 Pathophysiology 3

1.2 Nitric Oxide 3

1.2.1 The history as a biologically active molecule 3

1.2.2 The unique properties as a biological messenger 4

1.2.3 Nitric oxide synthesis: Isoforms and mode of action 5

1.2.4 The biological function of nitric oxide 6

1.2.5 Regulation of iNOS 7

1.3 Nitric Oxide in Stroke 9

1.3.1 Stroke – an overview 9

1.3.2 The double role of nitric oxide in stroke 9

1.3.3 Treatment of Stroke 11

1.4 Aim of this thesis 11

2 Material and Methods 13

2.1 Material 13

2.1.1 Chemicals and reagents 13

2.1.2 Buffers 14

2.1.3 Commercial kits 15

2.1.4 Primer 15
2.1.5 Tools and plasticware 15
2.1.6 Devices 16
2.1.7 Software 17
2.2 Methods 17
2.2.1 Mice 17
2.2.2 Primary cultured cells 18
2.2.3 Immortalised cell lines 20
2.2.4 Nitric Oxide quantification 21
2.2.5 AlamarBlue assay 21
2.2.6 Enzyme-linked Immunosorbent Assay 22
2.2.7 Microchemotaxis assay 23
2.2.8 Propidium iodide based proliferation and cell death assay 24
2.2.9 Flow cytometry 25
2.2.10 Quantitative PCR 26
2.2.11 High throughput screening (HTS) 27
2.2.12 Enzymatic activity assay 29
2.2.13 Intravenous Pharmacokinetic Study in Mice 30
2.2.14 Middle cerebral artery occlusion 30
3 Results 33
3.1 Screening for compounds inhibiting nitric oxide release in microglia 33
3.2 Four compounds decrease the LPS induced NO release. 43
3.3 The NO release is regulated independently from the pro-inflammatory stimulus. 48
3.3.1 IFNγ induced NO release is regulated in a dose dependent manner in primary microglia 48
3.3.2 PolyIC induced NO release is regulated in a dose dependent manner in primary microglia. 50
3.4 Selective regulation of LPS induced, IL1β, IL6, and TNFα release in primary microglia. 52

3.4.1 Selective inhibition of LPS induced release of IL1ß in primary microglia. 53

3.4.2 Selective inhibition of LPS induce release of IL6 in primary microglia 54

3.4.3 Selective inhibition of LPS induce release of TNFα in primary microglia 55

3.5 The compounds show an analogous effect on primary macrophages as they show on microglia. 57

3.5.1 LPS induced NO release is reduced by compound C1.0 and C4.0 in a dose depended manner. 58

3.5.2 C1.0 and C4.0 do not interfere with metabolic activity in LPS stimulated macrophages. 59

3.5.3 IFNγ induced NO release in primary macrophages is regulated in a dose dependent manner..... 60

3.5.4 PolyIC induced NO release in primary macrophages is regulated in a dose dependent manner..... 62

3.6 The different regulation of LPS induced pro-inflammatory cytokines release in primary macrophages. 63

3.7 Compound C1.0 and C4.0 do influence the AlamarBlue, PI and NO readout in high concentrations. 67

3.7.1 High doses of C1.0, C4.0, and DMSO increase the measured values of nitric oxide. 67

3.7.2 The AlamarBlue readout is affected by C1.0, C4.0, and DMSO. 68

3.7.3 The readout of PI is shifted by high concentrations of C1.0, C4.0, and DMSO. 71

3.7.4 Compound C1.0 and C4.0 are soluble in the used concentration range but precipitate in high concentrations..... 72

3.7.5 C1.0 and C4.0 do not act as a NO-Scavenger. 74

3.8 The compounds effect on microglial phagocytosis and migration. 76

3.8.1 Neither compound C1.0 nor C4.0 shows an effect on the basal and stimulated microglial phagocytosis. 76

3.8.2 C1.0 and C4.0 show a diverse effect on the microglial migration. 78

3.9 The compounds interference with the metabolism, cell death, and cell number of cells of the healthy brain. 82

3.9.1 The positive effect of the compounds on microglial metabolic activity. 83
3.9.2 The compounds positive effect on the cell number of astrocytes and microglia 84
3.9.3 Compound C1.0 and C4.0 show no effect on the cell death. 86
3.10 Structure action relationship analysis (SAR) of compound C4.0 reveal an inconsistent mode of action 87
3.11 C1.0 is able to reduce the NO release of previously activated microglia 91
3.12 Compound C1.0 includes two distinct two diastereomers. 92
3.12.1 S-S is the active conformation of compound C1.0 96
3.12.2 The IC50 value of the active *S-S* conformation C1.0a is 104 nM. 98
3.13 Treatment with C1.0, C1.0a, or C1.0b does not modify the iNOS's mRNA regulation. 102
3.14 C1.0a does not directly regulate the NO-Synthesis iNOS, eNOS, or nNOS 104
3.15 The pharmacokinetics and ADME of C1.0 in healthy adult mice 106
3.15.1 Mice survive C1.0 for at least 24 hours. 106
3.15.2 C1.0 passes the blood brain barrier in healthy adult mice. 107
3.16 Compound 1.0 ameliorates neuronal deficits in a rodent model of mild cerebral arterial occlusion (MCAO) 109
3.16.1 C1.0 treatment has no significant impact on the stroke lesion volume ... 111
3.16.2 C1.0 improves the laterality in mice. 112
3.16.3 The forced movement on the rotarod is not improved by C1.0. 113
3.16.4 C1.0 treatment enhances the mice capability in the pole test. 114
4 Discussion 116
4.1 The distinct functions of Nitric Oxide 116
4.2 The HTS yield two compounds of different structure and capabilities. 117
4.3 Compound C4.0 misses a structure action relationship. 119
4.4 The selective NO inhibition by C1.0. 121
4.5 C1.0 passes the blood brain barrier in *in-vivo* 127

4.6 A proof of concept study: C1.0 improves extrapyramidal motor skills and laterality in an *in-vivo* model of ischemic injury 128

4.7 C1.0a is a novel compound targeting NO release in microglia and macrophages – an outlook 130

5 Summary 132

6 Zusammenfassung 133

Eidesstattliche Erklärung 134

LIST OF ABBREVIATIONS

ADP	Adenosine-5'-Diphosphate
ATP	Adenosine-5'-Triphosphate
BCA	Bicinchoninic Acid
BSA	Bovine Serum Albumine
cDNA	Complementary Deoxyribonucleic Acid
CNS	Central nervous system
DMEM	Dulbecco's Modied Eagle Medium
DMSO	Dimethyl Sulfoxide
DNA	Deoxyribonucleic Acid
EDTA	Ethylenediaminetetraacetic acid
eNOS	endothelial nitric oxide synthase
FCS	Fetal calf serum
GABA	γ-aminobutyric acid
HBSS	Hank's balanced salt solution
HTS	High Throughput Screen
IC50 value	half maximal inhibitory concentration
IFNγ	Interferon γ
IL1β	Interleukin 1 ß
IL10	Interleukin 10
IL13	Interleukin 13
IL4	Interleukin 4
IL6	Interleukin 6
iNOS	inducible nitric oxide synthase
IP3	Inositol triphosphate
LPS	Lipopolysaccharide
MCAO	middle cerebral artery occlusion
M-CSF	Macrophage colony stimulating factor
MRI	magnetic resonance imaging
nNOS	neuronal nitric oxide synthase
NO	Nitric oxide
PBS	Phosphate Buffered Saline
PCR	Polymerase Chain reaction

PolyIC	Polyinosinic-polycytidylic acid
qPCR	Quantitative Polymerase Chain Reaction
RNA	Ribonucleic Acid
ROI	Region Of Interest
RT	Room temperature
SAR	Structure Action Relationship
SD	Standard deviation
SDS	Sodium Dodecyl Sulfate
SE	standard error
SEM	Standard error of the mean
TLR	Toll-Like Receptor
TNFα	Tumor necrosis factor α

LIST OF FIGURES

Figure 3.1: Illustration of the HTS setup using the microglial cell line BV2. 34
Figure 3.2: Illustration of the reduction in compounds during the screening process. 35
Figure 3.3: Illustration of the plating scheme of the compound validation with primary cultured neonatal microglia. 36
Figure 3.4: LPS induced nitric oxide release and metabolic activity in primary cultured neonatal microglia in the presence compounds. 38
Figure 3.5: Illustration of an ideal IC_{50} curve 39
Figure 3.6: The dose dependent reduction of LPS induced NO in microglia 40
Figure 3.7: Illustration of the assignment of the compound concentrations. 44
Figure 3.8: Validation of the dose dependent reduction of LPS induced microglial NO release scaled to a 96 well plate. 45
Figure 3.9: Validation of the dose dependent influence on LPS elevated microglial metabolic activity scaled to a 96 well plate. 47
Figure 3.10: IFNγ induced NO release in microglia and the reduction by the compounds. 50
Figure 3.11: The reduction of polyIC induced NO release in microglia by the 4 compounds. 52
Figure 3.12: Dose dependent influence on LPS induced IL1ß release in microglia. 54
Figure 3.13: Dose dependent influence on LPS induced IL6 release in microglia. 55
Figure 3.14: Dose dependent influence on LPS induced TNFα release in microglia. 56
Figure 3.15: Dose dependent reduction of LPS induced NO release in macrophages. .. 59
Figure 3.16: Dose dependent influence on LPS elevated macrophages metabolic activity. 60
Figure 3.17: Dose dependent reduction of IFNγ induced NO release in macrophages.. 62
Figure 3.18: Dose dependent reduction of polyIC induced NO release in macrophages. 63
Figure 3.19: Dose dependent influence on LPS induced IL1ß release in macrophages. 64
Figure 3.20: Dose dependent influence on LPS induced IL6 release in macrophages... 65
Figure 3.21: Dose dependent influence on LPS induced TNFα release in macrophages. 66
Figure 3.22: Direct dose dependent influence on the read out of the Griess assay..... 68

Figure 3.23: Direct dose dependent influence on the readout of the AlamarBlue assay. 71
Figure 3.24: Direct dose dependent influence on the read out of the PI-based proliferation and cell death assay. 72
Figure 3.25: Solubility the compounds in PBS. 74
Figure 3.26: Compounds dose dependent NO savaging ability. 75
Figure 3.27: Modulation of the basal and LPS stimulated phagocytosis in microglia... 77
Figure 3.28: Modulation of microglial chemotaxis by compound C1.0 and C4.0..... 79
Figure 3.29: Modulation of microglial motility by compound C1.0 and C4.0. 81
Figure 3.30: Compounds influence on the metabolic activity of non-stimulated neurons, astrocytes, microglia, and oligodendrocytes. 83
Figure 3.31: Compounds influence on the proliferation of non-stimulated neurons, astrocytes, microglia, and oligodendrocytes. 85
Figure 3.32: Compounds influence on the cell death of non-stimulated neurons, astrocytes, microglia, and oligodendrocytes. 86
Figure 3.33: Structure action relationship analysis of compound C4.0. 90
Figure 3.34: Impact of compound C1.0 on the NO release of pre-stimulated microglia. 92
Figure 3.35: Possible chiral structure of compound C1.0. 94
Figure 3.36: HPLC chiral separation of C1.0. 95
Figure 3.37: Dose dependent influence of the two separated fractions on the LPS induced NO release in microglia. 96
Figure 3.38: Identification of the chiral structure of compound C1.0 97
Figure 3.39: Dose dependent reduction of LPS induced NO release in microglia of compound C1.0, C1.0a, and C1.0b. 99
Figure 3.40: Dose dependent scavenging effect on NO by compound C1.0, C1.0a, and C1.0b 100
Figure 3.41: Dose dependent scavenging influence of the NO concentration of NO enriched medium of compound C1.0, C1.0a, and C1.0b..... 101
Figure 3.42: Compounds influence on the LPS stimulated and non-stimulated iNOS mRNA transcription in microglia. 103
Figure 3.43: Modulation of the eNOS enzyme activity by compound C1.0a..... 105
Figure 3.44: Modulation the iNOS enzyme activity by compound C1.0a 105
Figure 3.45: Modulation of the nNOS enzyme activity by compound C1.0a 106
Figure 3.46: C1.0a's blood plasma concentration over a time period of 24 hours after a single shot intravenous injection. 107
Figure 3.47: Tissue specific concentration of C1.0a over time period of 4 hours. 108

Figure 3.48: Tissue specific concentration of C1.0a in relation to the blood plasma concentration. 109
Figure 3.49: Illustration of the time line of the stroke application and the behaviour test. 111
Figure 3.50: Volume of the stroke lesion 7 days after stroke. 112
Figure 3.51: Head turning preference before and after stroke with and without compound treatment. 113
Figure 3.52: Time spend on the rotarod before and after stroke with and without compound treatment. 114
Figure 3.53: Time needed to turn and to descend in the pole test before and after stroke with and without compound treatment. 115

LIST OF TABLES

Table 1.1:	List of Nitric Oxide Synthase isoforms	6
Table 3.1:	Parameters and their significance of the calculated IC_{50} curve.	42
Table 3.2:	Compound name translation.	43
Table 3.3:	Compound concentrations.	44
Table 3.4:	Description of the linear regression curves of the compounds influence the Griess assay.	68
Table 3.5:	Description of the linear regression curves of the compounds influence the AlamarBlue assay.	71
Table 3.6:	Description of the linear regression curves of the compounds influence on the PI-based proliferation and cell death assay.	72
Table 3.7:	Description of the linear regression curve of the compounds NO scavenging ability.	76
Table 3.8:	Statistical comparison of the basal phagocytosis.	78
Table 3.9:	Statistical comparison of the LPS induced phagocytosis.	78
Table 3.10:	Statistical comparison of the compound induced chemotaxis.	79
Table 3.11:	Statistical comparison of ATP induced chemotaxis in the presents of the compound.	80
Table 3.12:	Statistical comparison of the compound modified motility.	81
Table 3.13:	Statistical comparison of the ATP induced motility in the presents of the compound.	82
Table 3.14:	Statistical analysis of the compounds influence on the metabolic activity of non-stimulated neurons, astrocytes, microglia, and oligodendrocytes.	84
Table 3.15:	Statistical analysis of the compounds influence on the proliferation of non-stimulated neurons, astrocytes, microglia, and oligodendrocytes.	86
Table 3.16:	Statistical analysis of the compounds influence on the cell death of non-stimulated neurons, astrocytes, microglia, and oligodendrocytes.	87
Table 3.17:	Statistical analysis of the compound's impact on the NO release of pre-stimulated microglia.	92
Table 3.18:	Statistical analysis of the NO dose response curve using a 2-way ANOVA	100
Table 3.19:	Statistical analysis of the metabolic activity dose response curve using a 2-way ANOVA	101

Table 3.20: Statistical analysis of the scavenger dose response curve using a 2-way ANOVA 102
Table 3.21: Statistical analysis of the compounds influence on the non-stimulated iNOS mRNA transcription in microglia. 103
Table 3.22: Statistical analysis of the compounds influence on the LPS stimulated iNOS mRNA transcription in microglia. 104

1 INTRODUCTION

1.1 A small history of microglia

In 1919, almost a hundred years ago, the Spanish neuroscientist Pio del Rio Hortega described microglia for the first time [1–5]. He used the term "microglia" to define a subpopulation of cells within the "third element" of brain cells, which was defined by Ramón y Cajal a few years earlier [5,6]. In a series of followed publications [7–9], Pio del Rio Hortega characterised the physiology and pathophysiology of microglia. Most of his observations and assumptions made back then still hold true today. He postulated that microglia adopt different morphologies depending on their vicinity and activation[1]. Only recently the microglial heterogeneity was addressed again [10]. Microglia originate from the mesoderm [3,11] and populate the brain during early development, which was shown by Ginhoux and colleagues in 2010 [12]. They perform diverse functional tasks, such as migration and phagocytosis [4], which is until today considered as a hallmark of microglia. Following del Rio Hortegas fundamental research on microglia made in the 1920s, the field did not advance for decades, and the existence of microglia was even denied by some neuroscientists. The interest in microglia came back in the 1960s with studies on the injured facial nerve by the group of Georg Kreutzberg [13]. This interest accelerated sustainably. Today, microglial research focuses on many aspects of the brain, ranging from brain development [14–16], synaptic plasticity [17,18], and sex differences [19,20], and in different types of disease such as stroke [21–23], cancer [24], multiples sclerosis [25–27], and psychiatric diseases such as schizophrenia [28,29] and autism, to age related diseases such as dementia [14] and Alzheimer's disease [30–33].

1.1.1 Origin

In today's publications, microglia are often introduced as "the resident macrophages of the brain", pointing out one of their most studied feature: their contribution to the innate and adaptive immunity. Although microglia and monocyte-derived macrophages share the same functions and expression of markers, they derived from a different origin [3,11,12]. In mice, microglia

arise from myeloid progenitor cells and migrate from the yolk sac into the central nervous system (CNS) between embryonic day 8.5 and 9.5 [12]. Around 5 days later at E15, the formation of the blood brain barrier (BBB) begins and shields the microenvironment of the CNS against the rest of the body. This consecutive timeline distinguishes microglia from other tissue specific macrophages, such as Langerhans cells [34], Kupffer cells [35], and Alveolar macrophages [36–38]. While those are replaced by bone marrow derived macrophages (BMDM) over a lifespan, the BBB protects microglia. Microglia age concurrent with the brain. Yet, they can be replaced to some extend by microglia precursors [14].

1.1.2 Capabilities

Microglia and macrophages do inherit the same functions, pathways and activation pattern, yet differ in their morphology and tissue specific tasks [39–42]. In the healthy mature CNS, microglia have a ramified morphology, characterised by a small soma and long thin cellular processes. This phenotype was previously considered to be a "resting" state. However, this view came to an end, as Nimmerjahn showed that in physiology microglia processes are highly dynamic while their cell body remains immobile [43]. Microglia monitor the brain homeostasis [44]. An alteration in the homeostasis, be it induced by infection, trauma, ischemia, neurodegenerative diseases, or altered neuronal activity, leads to microglial activation [41]. To detect signals from the micro-environment, microglia express different receptors, like Toll-like receptors (TLR), purinergic receptors, neurotransmitter receptors, receptors for neurohormones as well as for cytokines and chemokines [40,41]. TLRs recognise structurally conserved molecules of different pathogens such as viruses, bacteria, parasites, and fungi [45]. Purinergic receptors are involved in paracrine and autocrine signalling [41]. An increase in extracellular ATP is associated with cell death and serves as a danger signal in the inflammatory process [46]. Neurotransmitter receptors, like glutamate and gamma-aminobutyric acid (GABA) receptors, sense alterations in the neuronal activity, a sign of neuronal malfunction or lesions [47]. In addition, microglia also express receptors for neurohormones and -modulators, such as opioid and histamine receptors, to detect changes in the brain homeostasis. A variety of cytokine and chemokine receptors enable cell-cell communication [40] and the modulation of the immune response.

1.1.3 Physiology

Even though microglia are characterised as immune cells, they are of great importance in the developing and mature brain [14,48]. During the development of the brain, microglia proliferate

and accumulate in areas presenting high densities of apoptotic neurons to facilitate neuronal turnover during developmental cell death. Apart from clearance of dead cells, microglial phagocytosis controls the number of neural precursors in proliferative regions of the developing brain [15,18]. This regulation of neurogenesis continues throughout adulthood in well-defined areas in which the existence of neuronal stem cells persists. In addition to their impact on the number of neurons, microglia are also involved in the neuronal wiring. Microglia play a role in the axonal outgrowth and positioning. They engulf dendritic spines and are required for synaptic pruning. As recent studies have shown, does microglial modulation and regulation of neuronal activity and synaptic plasticity continue in the mature CNS [17,41,49,50].

1.1.4 Pathophysiology

Upon activation, microglia change their morphology, gene expression, and functional behaviour, resembling activated BMDMs. Microglia retract their thin processes and acquire an amoeboid morphology [40]. They become motile and start migrating towards the epicentre of a danger signal. This transformation is initiated by a change in the composition of cell surface proteins for cell-cell and cell-matrix interaction, as well as the secretion of proteins and enzymes to rearrange and disintegrate the extracellular matrix (ECM) [51]. In areas of pathological events, induced microglial proliferation can increase the density locally [41,52]. Activated microglia change their repertoire of released cytokines and chemokines, in order to trigger and regulate an immune response and attract other immune cells, like BMDMs, neutrophils, T-cells, or natural killer cells (NK-cells). Microglia enhance their basal phagocytosis to fight pathogens as well as to clear cell debris left behind. As a first line defence mechanism against pathogens, microglia release nitric oxide (NO) and activate the complement system [53–55].

1.2 Nitric Oxide

1.2.1 The history as a biologically active molecule.

Nitric oxide is a colourless free radical gas under standard conditions with the chemical formula of NO[56]. The action of nitric oxide in the body is of a paradoxical nature. It is both, a regulatory molecule and an agent which is cytotoxic, mutagenic, and probably carcinogenic [57–60]. It was long

believed that its biosynthesis was exclusive to microorganisms. This was disproven in 1987 by Hibbs et al., showing that nitric oxide can be produced by macrophages upon LPS stimulation and that it is playing an important role in the innate immune system [61]. In the same year, Ignarro et al. could show that nitric oxide is the primary endogenous vasodilator regulating the cardio vascular system [62]. As a consequence of its importance for the human body, the leading scientific journal Science proclaimed nitric oxide as the "Molecule of the Year" in 1992 [63]. Only 6 years later, in 1998, the Nobel Prize in Physiology or Medicine was awarded jointly to Robert F. Furchgott, Louis J. Ignarro and Ferid Murad "for their discoveries concerning nitric oxide as a signalling molecule in the cardiovascular system" [64].

1.2.2 The unique properties as a biological messenger

The unique physical and chemical properties of nitric oxide distinguish it from other biological messenger molecules. It is one of the smallest signalling molecules in the human body and a free radical. Both properties are responsible for its distinct behaviour.

In the human body, the gaseous nitric oxide is solved in the cytosol and extracellular liquids. Its relatively small size allows it to diffuse freely across biological barriers, as the cell membrane and bacteria wall. Therefore, nitric oxide can neither be stored nor actively transported. However, there are some evidence that the cell is able to direct the diffusion using connexins or relocate the place of synthesis. The diffusion coefficient of nitric oxide in water (2.60×10^{-5} cm²/s) is higher than those of oxygen (2.10×10^{-5} cm²/s) and carbon dioxide (1.92×10^{-5} cm²/s), which leads to locally and temporally restricted gradients of sufficient nitric oxide concentrations [65–67]. The lack of storage and the rapid and free diffusion results in a short range undirected signalling.

Nitric oxide belongs to the group of reactive oxygen species (ROS) and is a free radical [68]. Free radicals are atoms, molecules or ions that have an unpaired electron. This unpaired electron is highly reactive towards other molecules. In contact with other molecules, nitric oxide will react spontaneously and undirected [69]. These rapid undirected reactions lead to the very short lifespan of nitric oxide. Prominent reactions of nitric are with oxygen (O2) and water (H2O), forming other highly reactive oxygen species, like peroxynitrite (ONOO-) or hydrogen peroxide (HOOH) [70]. Important biological reactions are with nucleic acids (DNA and RNA) causing mutations, with lipids causing peroxidation and leading to a membrane break-down, with proteins causing loss of function and leading to early degradation, and with biological molecules blocking them permanently [71]. The reaction with proteins and biological molecules do not always cause a loss of

function but are also used for regulation and storage [72–74]. Proteins can be regulated and post-transcriptional modified by nitrosylation of their sulfhydryl groups [75]. It was postulated that nitric oxide reacts reversible with heme B. However, its function is not fully understood [76].

Taken the physical and chemical properties together, nitric oxide reacts undirected ubiquitously but locally and temporally restricted.

1.2.3 Nitric oxide synthesis: Isoforms and mode of action

In mammalians, nitric oxide is produced by nitric oxide synthases (NOS). In human as well as in mice three major isoforms of NOS are known: eNOS, nNOS, and iNOS [59,60,77]. eNOS and nNOS are constitutively expressed. Their activation status is regulated via the cytosolic calcium concentration (Ca^{2+}) [78]. iNOS is calcium independent, it is regulated on a transcriptional level [58]. The nomenclature of eNOS and nNOS derives from its predominant location within the human body: eNOS is most frequently expressed in endothelial cells (endothelial NOS) and nNOS is most frequently found in neurons (neuronal NOS). The nomenclature of iNOS nomenclature derives from its inducible expression (inducible NOS). Another used nomenclature lists the NOS chronologically by their first successful cloning. nNOS was the first isoform to be purified and cloned, in 1990 and 1991 respectively. Later on, it was given the name NOS1. The second one on the list was iNOS, thus named NOS2, purified and cloned in 1991. The purification and cloning of eNOS followed one year later in 1992, respectively named NOS3. In this thesis, I will stick to the nNOS, eNOS, and iNOS nomenclature emphasising the different expression of iNOS compared to nNOS and eNOS.

The cloning of NOS cDNAs from human, rodent and other species has revealed that NOS isoforms comprise a family of structurally related enzymes. Amino acid sequence identity between isoforms is high (50% - 60%) and for each isoform conservation between mammalian species is even higher (85% for iNOS and 95% for nNOS and eNOS) [54,59]. The intron-exon structure of the NOS genes is conserved suggesting: that the NOS gene family evolved by gene duplication and evolutionary pressure for the preservation of structure and function [79].

Name	Abbrevi-ation	Alternative name	Location	Regula-tion
Inducible Nitric Oxide Synthase	iNOS	NOS2	immune system cardiovascular system	translation
Endothelial Nitric Oxide Synthase	eNOS	NOS3	endothelium	Ca^{2+} sensitive
Neuronal Nitric Oxide Synthase	nNOS	NOS1	Nervous system Skeletal muscle	Ca^{2+} sensitive

Table 1.1: List of Nitric Oxide Synthase isoforms

Though the three isoforms differ in their expression, they all share the same catalytic synthesis of nitric oxide from L-arginine [59,60,72,80]. The protein contains two separate catalytic domains, a reductase domain, and an oxygenase domain. Both domains are linked by a calmodulin binding domain. In order to form an active catalytic complex, the synthase forms a homodimer in which the reductase domain of one protein aligns with the oxygenase domain of the second protein. The binding of calcium to calmodulin changes the arrangement of both catalytic domains and activates the enzyme. eNOS and nNOS require a high amount of calcium to trigger this conformational change. iNOS, even though it is considered calcium independent, requires trace levels to function. Calcium levels found in the cytosol of resting cells are sufficient. [81]. The main substrates of the nitric oxide formulation are the proteinogenic amino acid L-arginine, providing the nitrogen, and dioxygen, providing the oxygen. The amine group of L-arginine is oxidised to citrulline via a two-step monooxygenation reaction. In addition, this reaction consumes 2 mol of O2 and 1 ½ mol of NADPH per mole of NO formed [82–84]. This reaction requires relative tightly bound cofactors: Tetrahydrobiopterin (BH4), flavin adenine dinucleotide (FAD), Flavin mononucleotide (FMN), and Heme-B [81,85,86].

1.2.4 The biological function of nitric oxide

In mammals nitric oxide is involved in three major processes: It is ubiquitously short range messenger in the cardiovascular system [87–89], it is a specific neuronal transmitter in the CNS [73,90–94], and it is an undirected weapon used by the immune system [41,95,96]. Those three processes are mainly regulated by the three isoforms eNOS, nNOS, and iNOS respectively.

Nitric oxide is of critical importance as a mediator of vasodilation in the cardiovascular system. The pulsatile stretch of endothelial cells induces calcium influx into the cytoplasm causing an

increase in cytoplasmic calcium concentration. The elevated calcium concentration actives the endothelial expressed eNOS. The synthesised nitric oxide diffuses into the surround smooth muscles cells and activates the guanylate cyclase, which induces relaxation by inhibition of calcium influx via increased intracellular cGMP concentration, the activation of K+ channels, which leads to hyperpolarization and relaxation, and the stimulation of cGMP-dependent protein kinase that activates myosin light chain phosphatase causing the dephosphorylating of the myosin light chains and muscle relaxation [97,98].

In the CNS, nitric oxide severs as a neurotransmitter between nerve cells. It functions as a retrograde neurotransmitter important for long term potentiation and therefore has an impact on learning and memory. Stimulation of the NMDA receptor activates the neuronal NOS, nNOS, via an elevation of cytoplasmic calcium concentration. Due to its physical and chemical properties, described above, nitric oxide does act non-specifically on all neurons within its range. It diffuses into the presynaptic neuron, as well as those neurons that are not directly connected by synapses. The short half-life of nitric oxide restricts its action temporal and its fast degradation do not require any additional cellular reuptake or enzymatic breakdown [99,100].

The immune system takes advantage of the radical nature of nitric oxide. In the first line of defence, macrophages and microglia produce excessive amounts of nitric oxide to target parasites, bacteria, and viruses. Pathogen stimulation, such as bacterial LPS, or paracrine cytokines, like interferon-γ, induces iNOS protein synthesis. As noted above, iNOS is independent of the cellular calcium concentration, once synthesised it produces nitric oxide constantly until the protein is degraded, leading to cytotoxic concentrations. Those high concentrations of nitric oxide react unspecific with nucleic acids (DNA and RNA), lipids, and proteins (see above). This reaction affects the host and invader to the same extant. The damage to other host cells evokes yet another immune reactions, potentiating the inflammation [59,95,96].

1.2.5 Regulation of iNOS

While the regulation of the constitutively expressed eNOS and nNOS is directly linked to the regulation of the Ca^{2+} level in the cell, the regulation of iNOS takes place on a transcriptional level and is calcium independent. Under physiological conditions, evidence for baseline iNOS expression has been elusive, yet under pathological conditions, the iNOS expression is upregulated tremendously in cells of the monocyte lineage.

Microglia and macrophages express iNOS in response to an external pathogen stimulus, like lipopolysaccharide (LPS), and paracrine cytokines, like interferon-γ (IFNγ), interleukin-1ß

(IL1ß), interleukin-6 (IL6), tumour necrosis factor-α (TNFα), and hypoxia. Those stimuli act more or less directly on the transcription of iNOS. Like the protein sequence, the promotor region of iNOS shares a high degree of homology with other species. It is packed with numerous binding sites for transcription factors such as AP-1, ARE, C/EBP, c-ETS-1, CREB, GATA, HIF, HSF, IRF-1, NF-1, NFAT, NF-κB, NF-IL6, Oct-1, PEA3, p53, Sp1, SRF and STAT-1α [58,101–111]. Here, I will shortly outline the function of NF-κB, STAT-1α, and HIF. NF-κB is one of the most prominent transcription factors in this list. It is a key regulator of the immune system and responses to cell stress, cytokines, free radicals as nitric oxide itself, and bacterial and viral antigens [106,112,113]. NF-κB is present in the cytoplasm in an inactive state. Upon activation, it translocates to the nucleus, binds to its binding site and induces the transcription of iNOS. Stimulation with polyinosinic:polycytidylic acid (polyIC) activates NF-κB via the TRIF pathway [114,115]. Stimulation of the Toll-like receptor 4 (TLR4) with LPS activates NF-κB via the MyD88 pathway [115]. In addition, this pathway triggers the activation of the transcription factors CREB and AP-1. Cytokines, like IFNγ, are using the transcription factor STAT-1α to induce iNOS transcription [116,117]. Upon stimulation with IFNγ JAK is activated, which phosphorylates STAT-1α. Phosphorylates STAT-1α relocates into the nucleus and induces transcription of iNOS. HIF is a major regulator of oxygen homeostasis within cells. Unlike the transcription factors described above, HIF is a sensor and regulator in once [118,119]. Upon low oxygen concentration HIF changes its conformation, becomes activated and induces iNOS transcription. Nitric oxide itself can regulate induction of iNOS. In microglial and macrophages NO causes an upregulation of the cellular cGMP concentration, the enhancement of transcription factor p53 activity, which inhibits the iNOS promoter, reduction of the HIF-1 activity, inhibition of cytokine induced NF-κB activity [120,121], and tyrosine nitration of STAT-1α [122]. This negative feedback regulation is tissue dependent and might even be reversed for some tissues [123]. Posttranscriptional and posttranslational modifications of iNOS play a minor role in the regulation of iNOS. Several factors are known to destabilise iNOS mRNA or iNOS protein [54]. Most of those factors have a general effect on mRNA and protein stability, lacking iNOS specificity.

1.3 Nitric Oxide in Stroke

1.3.1 Stroke – an overview

Nitric oxide plays an eminent role in Stroke. It has a positive as well as a negative effect on the outcome of stroke, depending on the concentration, the location and the time point of synthesis.

A stroke is defined as the sudden death of brain cells in a localised area due to lack of oxygen and energy supply [124]. It is caused by insufficient blood flow, as a result of a clogged blood vessel (ischemic stroke), or bleeding (haemorrhagic stroke) [125]. Within minutes after oxygen deprivation neurons start dying in the stroke core area which induces an inflammation. Even a temporary interruption of the blood flow can cause a chronic loss of brain function. Areas hit by a stroke, suffer a great deal of damage and do barely recover, leaving the patient behind with severe cognitive disabilities. These disabilities are directly linked to the loss of neurons within the focal area of the stroke, meaning a loss in the ability to speech occurs when the corresponding area is hit. Major signs of stroke are a loss of motor functions (side specific face dropping, arm or leg weakness), and coordinative functions, speech difficulty, impaired vision, sudden dizziness, and severe headaches [126,127].

For the last 15 years, stroke was the second most frequent cause of death worldwide outrun by ischaemic heart disease, another ischaemic triggered disease [128]. In 2015 stroke was accounting for more than 6.2 million deaths worldwide, about 6 % of all causes of death and about 0.1 % of the world population [129]. In Germany, approximately 196 000 people, 2.4 % of the German population, per year are affected by first-ever stroke events. With about 63.000 deaths yearly, stroke is the third most frequent cause of death in Germany. Compared with the global statistics, the stroke death rate did decrease by 40 % between the year 1998 and 2008. This reduction is largely due to the widespread establishment of stroke units all over Germany [130,131].

1.3.2 The double role of nitric oxide in stroke

NO plays a two-sided role in stroke. It is neuroprotective and neurotoxic at the same time [57,70,92,132–136]. Studies have shown an enhancement and exacerbation in the outcome of stroke for both, an elevated and a reduced NO concentration. The complex consequences of NO are driven by the various sources, the concentrations, the location, and the time point of synthesis within the stroke. During a stroke, NO is produced by all three NOS isoforms eNOS, nNOS, and iNOS.

eNOS and nNOS are consecutively expressed in the brain, while iNOS is only induced in inflammatory processes. eNOS is predominantly expressed in the vascular endothelial cells and choroid [137,138]. Although it generates NO only in a small amount, it plays a crucial role in the regulation of cerebral blood flow, the protection of the blood brain barrier, and the reduction of oxidative stress. Here, NO acts as a scavenger for oxygen free radicals, an inhibitor for expression of adhesion molecules, and a promotor of platelet aggregation and lymphocytes adhesion [89]. An elevation in eNOS driven NO dilates the blood vessels locally, reducing the blood pressure and increasing the blood flow within that region. Both effects reduce the infarct size significantly and are related to an improved outcome in stroke [139]. Whereas, the inhibition of eNOS - achieved by utilising a knockout-mouse or eNOS-specific inhibitors - leads to significantly reduced cerebral blood flow, and thus subsequently results in a greater infarct size [140–142]. NO generated by nNOS, which is expressed in a small subset of neurons, has opposing effects on the health of the neurons, depending on the produced NO concentration. In low concentrations, NO is used for retrograde signalling. At these low concentrations, NO has a neuroprotective function, stabilising the synapses and therefor the neurons. It scavenges oxygen free radicals and interacts with the vasodilating pathway in endothelial cells resulting in an increased blood perfusion [143,144]. However, a misguided regulation of nNOS leading to an elevation of the NO concentration reveals its neurotoxic properties. Upon an inflammation, the Ca^{2+} levels rise inter- and intracellular, due to dying cells in the proximate range. This elevation in Ca^{2+} ions causes a direct activation of nNOS leading to an increase in NO concentration. Unlike eNOS and nNOS, iNOS is regulated on the transcriptional level. In the brain, iNOS is predominantly produced by microglia and in the case of a stroke by infiltrating macrophages. It is also reported, that astrocytes and endothelial cells can express iNOS [145,146]. As described above, is the iNOS protein not detectable under physiological conditions. Upon a proinflammatory stimulus, the iNOS protein synthesis is upregulated and iNOS starts producing NO in high concentrations. This regulation leads to a delay of iNOS driven NO. In an ischemic stroke, iNOS is produced from 6 up to 12 hours after the incident but can last for more than a week [147]. Microglia and Macrophages use NO as a first response mechanism to fight infiltrating pathogens, like fungi, bacteria, and other parasites. To do so, it uses high concentrations of NO which reacts unspecific with pathogens and more specific with other immune cells to trigger an amplified response. In a stroke, these elevated NO concentrations react with all cells in range leading to an universal cell death, especially of sensitive neurons. The amplification in the immune response does increase the area of inflammation leading to an enlarged stroke area and exacerbated the outcome.

1.3.3 Treatment of Stroke

State of the art treatment of stroke is the restoration of blood flow to the area of critical energy supply in a minimal amount of time. Time is the most crucial factor in stroke treatment. The outcome of stroke is directly correlated with the duration of critical energy supply in the affected brain region. In Europe the period from the onset of stroke to the first treatment could be decreased tremendously in the last decades, archived by educating the people for early sings of stroke, a fast infrastructure, and the creation of stroke core units [130,131]. Depending on the type of stroke these treatments can be completely different and opposing. In case of an ischemic stroke, the reperfusion is accomplished by a chemical and surgical disruption of the underlying thrombus, the dilution of the blood and an increase in blood pressure. In the case of a haemorrhagic stroke, the first steps taken are the decrease in blood pressure to reduce the bleeding into the brain tissue and closing the disrupted blood vessel. Both treatments diverge entirely, hence the type of stroke has to be assessed prior to treatment.

The main goal of both approaches is the restoration of the blood flow, but both are missing out the peculiarities of the cells of the brain, the neurones, astrocytes, oligodendrocytes, and the immune system, including the brain own microglia and the infiltrating immune cells. Over the last decades, numerous studies tried to improve the effect on those cells by target the excitotoxicity (rapid release and inhibited reuptake of the excitatory glutamate as a result of energy failure) [148,149], the oxidative and nitrosative stress (increased level of NO and oxygen free radicals) [53,149–154], and inflammation (infiltrating macrophages and neutrophils) [155–157]. So far none of these studies led to drugs approved or ischemic and haemorrhagic stroke [126,131,158].

1.4 Aim of this thesis

Recent studies shown, that microglia activation play an important role in the development, progression and outcome of in different types of disease such as stroke [21–23], cancer [24], multiples sclerosis [25–27], and psychiatric diseases such as schizophrenia [28,29] and autism, as well as dementia [14] and Alzheimer's disease [30–33]. Yet, a drug targeting specifically microglial activation is still missing. This thesis is an attempt to identify and characterise a novel compound targeting mi-

croglia activation. The main aim is to discover a compound able to modulate the proinflammatory activation of microglia in broad but defined range with a focus on the regulation of induced NO release.

2 MATERIAL AND METHODS

2.1 Material

2.1.1 Chemicals and reagents

Chemical	Company
Adenosine-5'-Triphosphate (ATP)	Sigma Aldrich, St. Louis, USA
ß-mercaptoethanol	Sigma Aldrich, St. Louis, USA
Bovine serum albumine (BSA)	Carl Roth, Karlsruhe, Germany
Dnase	Life Technologies GmbH, Darmstadt, Germany
dNTPs	Life Technologies GmbH, Darmstadt, Germany
Dimethyl Sulfoxide (DMSO)	Sigma Aldrich, St. Louis, USA
DTT	Life Technologies GmbH, Darmstadt, Germany
Dulbeccos Modified Eagles Medium	Life Technologies GmbH, Darmstadt, Germany
Fetal calf serum (FCS)	Life Technologies GmbH,
Fluorescent latex beads	Darmstadt, Germany
Hank's balanced salt solution (HBSS)	Life Technologies GmbH, Darmstadt, Germany
HEPES	Carl Roth, Karlsruhe, Germany
IFNγ, recombinant murine	Peprotech, Rocky hill, USA
Lipopolysaccharide (LPS) from E.coli	Enzo Life sciences, Farmingdale, USA
Oligo DT	Life Technologies GmbH, Darmstadt, Germany
Penicillin/Streptomycin	Life Technologies GmbH, Darmstadt, Germany
Phosphate-buffered saline (PBS)	Life Technologies GmbH, Darmstadt, Germany
Poly I:C	Invivogen, San Diego, USA
Poly-L-lysine	Sigma Aldrich, St. Louis, USA
RNase Out	Life Technologies GmbH, Darmstadt, Germany
Sodium chloride (NaCl)	Carl Roth, Karlsruhe, Germany
Sodium Dodecyl Sulfate (SDS)	Sigma Aldrich, St. Louis, Germany

Chemical	Company
Superscript II Reverse Transcriptase	Life Technologies GmbH, Darmstadt, Germany
SYBR green Select Mastermix	Life Technologies GmbH, Darmstadt, Germany
EDTA/Trypsin	Biochrom, Berlin, Germany
Clodronate Disodium Salt	Merck KGaA, Darmstadt, Germany.
DMEM/F-12, GlutaMAX™ supplement	Life Technologies GmbH, Darmstadt, Germany
L-Glutamine	Life Technologies GmbH, Darmstadt, Germany
AlamarBlue	Invitrogen, Darmstadt, Germany
RPMI 1640	Life Technologies GmbH, Darmstadt, Germany
Protease inhibitor cocktail	Roche, Berlin, Germany
RIPA buffer	Sigma-Aldrich, Munich, Germany
Tissue Tek Compound (OCT)	Weckert Labortechnik, Kitzingen, Germany
Tris-base	Carl Roth GmbH, Karlsruhe, Germany
Tris-HCl	Carl Roth GmbH, Karlsruhe, Germany
Triton X-100	Carl Roth GmbH, Karlsruhe, Germany
Trypan blue	Sigma-Aldrich, Munich, Germany
Tween 20	Merck, Hohenbrunn, Germany
M-CSF, murine	Invitrogen, Darmstadt, Germany
Sulfanilamide	Sigma-Aldrich, Munich, Germany
H3PO4 (85 %)	Sigma-Aldrich, Munich, Germany
Naphthylethylene	Sigma-Aldrich, Munich, Germany
Sodium nitrite	Sigma-Aldrich, Munich, Germany
Propidium Iodide	Invitrogen, Darmstadt, Germany
Isoflurane	Forene, Abbot, Wiesbaden, Germany

2.1.2 Buffers

Buffer	Ingredients
DMEM complete	DMEM
	10 % FCS
	2 mM L-glutamine
	100 U/ml penicillin
	100 µg/ml streptomycin
HEPES buffer	Aqua dest. sterile filtered
	0.9% NaCl

Buffer	Ingredients
L929 fibroblast cond. Medium	1/3 DMEM from confluent L929 fibroblast grown for 2 days mixed with 2/3 DMEM
FACS buffer	PBS + 2% v/v FCS

2.1.3 Commercial kits

Kit	Company
ELISA Mouse IL-1β/IL-1F2 Duo Set	Bio-Techne GmbH Wiesbaden-Nordenstadt Germany
ELISA Mouse IL-6	Bio-Techne GmbH Wiesbaden-Nordenstadt Germany
ELISA Mouse TNF-α	Bio-Techne GmbH Wiesbaden-Nordenstadt Germany
Diff-Quik stain	Medion Grifols Diagnostics AG, Düdingen, Switzerland

2.1.4 Primer

Primer name	Sequence
iNOS forward	TCACGCTTGGGTCTTGTTCA
iNOS reverse	TGAAGAGAAACTTCCAGGGGC
βActin forward	CGTGGGCCGCCCTAGGCACCA
βActin reverse	CTTAGGGTTCAGGGGGGC

2.1.5 Tools and plasticware

Plastic ware	Company
4-well plate	Thermo scientific, Rockford, USA
6-well plate	BD Biosciences, Heidelberg, Germany
12-well plate	BD Biosciences, Heidelberg, Germany
24-well plate	BD Biosciences, Heidelberg, Germany
96-well plate (transparent)	BD Biosciences, Heidelberg, Germany
Cell strainer, 70 µM	NeoLab, Heidelberg, Germany

Plastic ware	Company
Glass coverslip	Thermo Fischer Scientific, Walldorf, Germany
Pasteur pipette	Carl Roth, Karlsruhe, Germany
T75 cell culture flask	Greiner Bio-one, Frickenhausen, Germany
384-well plate	Corning, New York, USA
Polycarbonate filter	Thermo-Scientific, Rockford, USA

2.1.6 Devices

Devices	Company
Centrifuges 5417R and 5810R	Eppendorf, Hamburg, Germany
Incubator Steri-Cult Forma	Thermo-Scientific, Rockford, USA
Microplate reader Infinite M200	Tecan, Männedorf, Switzerland
Monochromator Polychrome II	Till photonics, Gräfelfing, Germany
qPCR machine7500 Fast Real Time PCR System	AB Applied Biosciences, Foster City, USA
Shaking platform SSM4	Stuart scientific, Stone, United Kingdom
Spectrophotometer Nanodrop 1000	PeqLab Biotechnologie, Erlangen, Germany
Thermocycler T3000	Biometra, Göttingen, Germany
Thermomixer	Compact Eppendorf, Hamburg, Germany
Boyden chamber	Neuroprobe, Bethesda, MD, USA
Flow Cytometry Systems	Becton Dickinson GmbH, Heidelberg, Germany
EL406	Biotek, Winooski, USA
Freedom Evo	Tecan, Maennedorf, Switzerland
Safire2	Tecan, Maennedorf, Switzerland
Pharmascan 70/16	Bruker BioSpin, Bruker, Billerica, USA
Small Animal Monitoring & Gating System	SA Instruments, New York, USA
Rotarod	TSE Systems, Chesterfield, USA

2.1.7 Software

Software	Company
Adobe Design Standard CS6	Adobe Inc, San Jose, USA
GraphPad Prism	GraphPad Software Inc., La Jolla, USA
ImageJ	National Institute of Health, USA
Microsoft Office	Microsoft, Redmond, USA
R statistics package	R Foundation for Statistical Computing, Austria.
FACSDiva	Becton Dickinson GmbH, Heidelberg, Germany
FlowJo	FlowJo LLC, Ashland, USA
Pipeline Pilot	Biovia, San Diego, USA
Paravision 5.1	Bruker BioSpin, Bruker, Billerica, USA
Analyze 10.0	AnalyzeDirect, Inc., Overland Park, USA

2.2 Methods

2.2.1 Mice

All *in-vitro* experiments were carried out using C57BL/6N mice originating from Charles River Laboratories in Sulzfeld, Germany. The animals were bred in the animal facilities of the Max-Delbrück-Centrum für Molekulare Medizin in Berlin-Buch according to the LaGeSo (Landesamt für Gesundheit und Soziales) regulations (TVV: X9023/12). All animal experiments preformed in the laboratories of the Max-Delbrück-Centrum für Molekulare Medizin and the Charité were conducted according to the German guidelines for animal care and were approved in advance by the LaGeSo.

In-vivo pharmacokinetic and ADME (absorption, distribution, metabolism, and excretion) studies in mice were performed by the external company Touchstone Biosciences (Plymouth Meeting, USA). The company states that all experiments were performed according to the guidelines of the United States Food and Drug Administration (FDA) and the European Medicines Agency (EMA).

2.2.2 Primary cultured cells

2.2.2.1 Primary cultured neonatal microglia

Primary cultured neonatal microglia were prepared from the cerebral cortex and midbrain of new-born C57BL/6N mice (postnatal day 0 – 3) as described previously [159]. The mice were sacrificed by cervical dislocation using a scissor, the brain was extracted, and the meninges and cerebellum were removed and transferred into ice cold HBSS. The dissected brains were washed 3 times and resuspended in 400 µL trypsin (0.1 mg/mL) and DNase (5 µg/mL) in PBS for not longer than 2 minutes. The reaction was blocked by adding 5 mL DMEM complete. The supernatant was discarded, and 1 mg DNase was added, followed by a mechanical dissociation using first a Pasteur pipette and secondly a glass pipette. The cells were centrifuged for 10 min at 130g at 4°C and the supernatant was discarded. The pellet was resuspended in DMEM complete and plated (2.5 brains/flask) in Poly-L-Lysine coated T75-flasks. The cells were washed after 2 days with PBS 4 times and incubated for another 7 days in DMEM complete to gain a confluent cell level. Afterwards, the medium was replaced with DMEM complete containing 33% L929 conditioned medium inducing microglia proliferation and maturation. The cells were harvested 2 days later by shaking the flask slowly for 30 min at 150 rpm at 37 °C. Microglia transits into the medium while the astrocytes remain attached to the flask. The supernatant was transferred into a falcon tube and centrifuged for 10 min at 130 g at 4 °C, washed once with DMEM complete and plated according to the experimental setup. The remaining flasks were refilled with 15 mL DMEM complete containing 33% L929 to induce microglia proliferation and maturation again. This process can be performed 3 times in total.

2.2.2.2 Primary cultured neonatal astrocytes

The preparation of primary cultured neonatal astrocytes followed the preparation of primary cultured neonatal microglia preparation, as it is explained above in Primary cultured neonatal microglia. After the third shake-off of microglia, the remaining astrocytes were washed harshly with DMEM complete and then trypsinated. The reaction was blocked with DMEM complete. The cells were transferred into a falcon tube, washed with PBS twice and seeded into T25 flasks. The astrocyte culture was expanded incubating them with DMEM complete under cell culture conditions (37 °C, 5% CO2, and 95% humidity) for several days. Afterwards, the astrocytes were trypsinated, washed with DMEM complete and PBS and plated according to the experimental setup.

2.2.2.3 Primary cultured bone marrow derived macrophages

Primary cultured bone marrow derived macrophages were isolated from the tibia and femur of adult (P49-56) C57BL/6N Bone mice as previously described (Marim et al., 2010). In summary, mice were killed by cervical dislocation. The skin of the mice legs was removed, and the hip joint was excavated from the surrounding muscles. The leg was separated from the body by dislocation, washed shortly with ice cold 70% ethanol in double-distilled water followed by ice-cold PBS, and immediately transferred into fresh ice-cold PBS for storage. Afterwards, all muscles were removed carefully, the feet were removed by dislocation, and the tibia and femur were separated. All following steps were carried out under the cell culture hood. The bones were cut open and flushed with up to 20 mL of ice-cold PBS. The flow through was collected in a petri dish on ice. It was used for up to 4 bones. The flow through was transferred into a falcon tube and centrifuged for 10 min at 500 g at 4 °C. The supernatant was removed, and the pellet was resuspended in 5 mL ammonium chloride solution for 3 – 5 minutes to lyse the erythrocytes. The cells were washed 2 times with PBS at room temperature (for 10 min at 200 g at 4 °C). The pellet was resuspended in DMEM complete containing 10 ng/mL M-CSF and an additional 100 units/ml penicillin and 100 µg/ml streptomycin. 16 bones were plated into one 10 mL petri dish for one day. The cells were washed with PBS, resuspended in DMEM complete containing 10 ng/mL M-CSF and additional 100 units/ml penicillin and 100 µg/ml streptomycin again, and plated into 10 mL petri dish (4 bones / petri dish). The cells were cultured for 6 additional days to allow differentiation. The medium was changed if needed. Afterwards, the cells were trypsinated, washed with PBS and plated according to the experimental setup

2.2.2.4 Primary cultured neurons

Primary cultured neurons were kindly provided by Florian Hetsch from the laboratory of Prof. Dr. Rathjen. The primary neurons were obtained as descripted in his thesis: “Induction of Synapses by Agrin in Cultured Cortical Neurons”. This culture is a mixed cell culture in favour of neurons.

Neurons were grained from pregnant mice at day 15 of gestation. The brains were extracted from the embryos, the olfactory bulbs and meninges were discarded as well as the mid- and hindbrain. The brains were transferred into a falcon tube and incubated in S1 solution for 15 min at 37°C in a water bath. The brain was trypsinated, washed with NB complete and a single cell suspension was created by mechanical dissociation using a glass pipette. The cells were washed once again with NB complete, counted, and seeded at a density of 2.65×10^5 cells/cm² on a petri dish. The cells were incubated for 5 up to 15 days.

2.2.3 Immortalised cell lines

All immortalized cell lines used were taken from the stock of our laboratory, including those for the high throughput screen. They were freshly thawed, cultivated with DMEM complete in a T75 flask, and split according to the cell line. Therefore, the cell culture flask was slightly shaken by hand to detach all loose cells and the old medium, including loose cells, was removed thoroughly. The flask was washed twice with warm (37 °C) PBS. 4 mL of an EDTA/Trypsin solution was added, and the flask was incubated for 3-5 min under cell culture conditions. Afterwards, the flask was shaken roughly by knocking it against a hard surface to bring all cells into solution. Detachment and health of the cells were examined under the microscope. If needed, the incubation with the EDTA/Trypsin solution was extended. The reaction was blocked adding 10 mL of DMEM complete. The cell suspension was transferred into a flacon tube and washed once with PBS (centrifugation at 300 g for 10 min at 4 °C). The cells were resuspended in fresh warm (37 °C) DMEM complete and singularised by pipetting them vigorously with a 10 mL pipette. 1 mL of this cell suspension was mixed with 10 – 20 mL fresh preheated (37 °C) DMEM complete and transferred into a new T75 cell culture flask. The flask was incubated under cell culture conditions until the next splitting.

2.2.3.1 BV2 microglia cell lines

The immortalized murine microglia cell line BV2[160] is frequently used as a substitute for primary microglia cultures. The BV2 cell line was freshly thawed and used until the 15th splitting cycle. 1 mL of frozen cell suspension was placed directly into a 37 °C water bath until everything was liquefied. The cell suspension was then mixed with 10 mL preheated cell culture medium and transferred into a T75 cell culture flask. Once more, 10 mL cell culture medium was added and then incubated under cell culture condition for 2-3 days before first splitting. The cells were incubated under cell culture conditions up to a confluence of 80% which resulted in splitting every 2 to 3 days at a dilution of around 1:20 depending on the actual cell concentration.

2.2.3.2 OLN-93 oligodendrocyte cell lines

The immortalized murine oligodendroglia precursor cell line OLN-93 [161]were incubated up to a confluence of 60% which resulted in splitting every 3 to 4 days at a dilution of around 1:10 depending on the actual cell concentration.

2.2.4 Nitric Oxide quantification

The total concentration of nitric oxide (NO) in cell culture supernatant was determined using the Griess assay. The Griess assay measures the total amount of nitrite (NO_2^-), a breakdown product of NO, by the formation of a chromophore with a red pink colour.

Microglia, either BV2 cell line or primary cultured neonatal microglia, or primary cultured bone marrow derived macrophages were plated onto a 96 well plate, let adhere and stimulated for a defined time. Cell-number per well, incubation time and stimulation reagent are given separately for each experiment. 100 µL of cell culture supernatant was transferred into a new 96 well plate and 100 µL freshly mixed Griess reagent were added. Griess reagent was composed of reagent A (100 mg Naphthylethylenediamine in 50 mL aqua dest.) and reagent B (1 g Sulfanilamide, 6 ml H3PO4 (85 %) in 44 mL aqua dest.) mixed 1:1. The solution was slightly shaken, and the absorbance of the colorimetric reaction was determined in a microplate reader at a wavelength of 550 nm. In parallel, the defined amount of sodium nitrite dissolved in DMEM complete as a standard was measured.

The concentration of nitrite was calculated by a linear regression of the standard curve. For statistical analysis of different experiments, the ration of the experimental condition to its positive control was used, in the following named foldchange.

2.2.5 AlamarBlue assay

AlamarBlue is used as an oxidation-reduction indicator in cell viability assays for both aerobic and anaerobic respiration. It determines the reductive potential of the cytosol. The assay is based on the cell permeable dye resazurin. Resazurin is a non-toxic, cell permeable compound, blue in colour and nearly fluorescent. Upon entering a living cell, the acid cytoplasm reduces it irreversible to resorufin, a compound that is red in colour and highly fluorescent. This change in colour and fluorescence can be measured. The reduction of resazurin depends on the number of living cells and the reductive potential of those. Dead cells lose their reductive potential, activated cells increase their reductive potential, therefore AlamarBlue indicates cell proliferation, cell death, and the metabolic activity of cells.

Prior to this experiment, cells were seeded into a 96 well plate. The cells were let adhere under cell culture condition and incubated according to the experimental setup. Cell number per well,

the volume of cell culture medium per well, as well as time to let cells adhere, stimulating substance and incubation time under stimulating condition are given separately for each experiment.

The supernatant of the prior prepared 96 well plate was removed thoroughly and replaced with 100 µL of fresh warm (37 °C) AlamarBlue DMEM (1/10th volume) mixture. The plate was then incubated for around 3 h under cell culture conditions. The conversion of resazurin to resorufin was measured by absorbance (absorbance wavelength of 570 nm and a reference wavelength of 600 nm). A baseline of unspecific absorbance was measured in wells containing AlamarBlue DMEM mixture without cells and subtracted from all values. For statistical analysis of different experiments, the ration of the experimental condition to its positive control was used, in the following named foldchange.

2.2.6 Enzyme-linked Immunosorbent Assay

The release of the pro-inflammatory cytokines, TNFα, IL1ß, and IL6, were determined by Enzyme-linked Immunosorbent Assay (ELISA). A kit from R&D Systems was used and the assay was performed as written in the manufacturer's protocol.

In brief, a 96 well plate was coated with the capture antibody of the specific cytokines dissolved in 100 µL PBS per well. The concentrations of the specific antibodies are given by the manufacturer. The plate was incubated airtight over night at room temperature. The next day, the capture antibody solution was removed, and the plate was washed 4 times with 300 µL per well washing buffer (PBS + 0.05% Tween-20). Residual liquid was removed by tapping the 96 well plate upside down onto a tissue paper. To prevent unspecific binding the plate was incubated with 300 µL per well blocking buffer (PBS + 1% BSA) for 1 hour at room temperature and afterwards washed 4 times with 300 µL per well washing buffer, as done before. Afterwards, 100 µL per well of the cell culture supernatant was applied and incubated for 2 hours. If not otherwise stated all cell culture supernatant were diluted 1:10 in PBS. In parallel, this step was also applied for the standard. The cell culture supernatant was taken from cells, either BV2 cell line, primary cultured neonatal microglia, or primary cultured bone marrow derived macrophages, cultured according to the experimental setup. The plate was washed 4 times with 300 µL washing buffer, as mentioned before. 100 µL of detecting antibody dissolved in PBS + 1% BSA was added and incubated for 2 hours. The concentrations of the antibody are given by the manufacturer. The plate was washed 4 times with 300 µL washing buffer per well, as done before. 100

µL streptavidin coupled horseradish peroxidase (HRP) provided by the manufacturer, in a dilution of 1:200 in PBS + 1% BSA, was added per well and the plate was incubated for 30 min at room temperature. Afterwards, the plate was washed 4 times with 300 µL washing buffer per well. To start the HRP reaction, 100 µL of HRP substrate was added per well and incubated for 20 min at room temperature, protected from light continuously shaking. This reaction was stopped by applying 100 µL of 1 M H_2SO_4 to each well. The total amount of the designated cytokine was measured directly in a microplate reader at a wavelength of 455 nm and was normalised to a wavelength of 540 nm.

The exact concentration of the cytokine was calculated by interpolating the values to a linear regression based on the standard and dividing these calculated values with a deployed dilution of the cell culture supernatant. For statistical analysis of different experiments, the ration of the experimental condition to its positive control was used, in the following named fold change.

2.2.7 Microchemotaxis assay

Migration was assessed using a 48-well microchemotaxis Boyden chamber (Neuroprobe, Bethesda, MD, USA) in combination with a polycarbonate filter (8 µm pore size; Poretics). The Boyden chamber, originally introduced by Boyden for the analysis of leukocyte chemotaxis, is ideally suited for the quantitative analysis of different migratory responses of cells, including chemotaxis, haptotaxis, and chemokinesis. The assay was performed as described before by Masataka Ifuku. In brief, the lower and upper compartment of the Boyden chamber were separated by the polycarbonate filter. Prior to assembling, the lower compartments were filled with around 30 µL warm (37 °C) serum-free DMEM. The upper compartments were filled with fresh 5 x 10^4 microglial cells suspended in 50 µL serum-free DMEM per well. The cells were incubated for 6 hours under cell culture conditions. Afterwards, the Boyden chamber was disassembled, and the polycarbonate filter was fixed and stained using the Diff-Quik stain (Medion Grifols Diagnostics AG, Düdingen, Switzerland) as described in the protocol. The filter let dry over night and was fixed on a coverslip the next day. Remaining microglia on the upper side of the filter were removed suing a wet cotton swab.

The rate of microglial migration was calculated semi-automatic, described by the following steps. First, the area of each well was photographed using a 20 × bright-field objective. The total amount of the area covered by microglia was measured in pixels using a colour-based threshold in the image process software ImageJ (selecting colours in the hue range of 150 (upper)-240 (lower), which are specific for the migrated cells stained in red-violet). Exemplary, the total

amount of microglia was counted by hand in images with a low, medium, and high calculated area, to prove a linear regression. The number of migrated microglia were calculated by interpolating the values to the linear regression assessed before. For statistical analysis of different experiments, all data were normalised to ATP induced chemotaxis.

2.2.8 Propidium iodide based proliferation and cell death assay

The relative cell proliferation and cell death were measured using propidium iodide (PI). PI is a fluorescent dye that binds into the nucleotide pair of guanine and cytosine and can, therefore, intercalate into DNA and RNA. It is not able to pass the cell membrane of healthy living cells and therefore binds only the DNA/RNA of damaged and apoptotic cells. In an unbound state the absorptions maximum of PI is at 488 nm and the emissions maximum 590 nm, upon binding to DNA/RNA the spectrum shifts to longer wavelength, respectively 535 nm and 617 nm. The emission intensity of PI bound to DNA/RNA measured at 535 nm increases by 20 to 30 % compared to unbound PI. The physical characteristics are used to determine the relative number of dead cells in a cell culture setup. This assay can determine the relative proliferation compared to control conditions, but not the absolute number of new cells. Additionally, the assay can determine the cell death relative to the complete number of cells.

To determine the relative proliferation and cell death, the cells were seeded into a 95 well plate, let adhere for 24 hours and afterwards treated for an additional 48 hours. Cell number per well, the volume of cell culture medium per well, as well as time to let cells adhere, stimulating substance and incubation time under stimulating condition are given separately for each experiment. The supernatant was removed carefully, and the cells were washed once carefully with warm (37 °C) HBSS, to not lose any dead cells. 100 µL per well PI solution in HBSS (1/200) was added to the cells and incubated for 10 minutes to measure the emission intensity of dead cells. After gaining the dead cell signals, all cells were killed to determine the total amount of cells. To do so, 10 µL of DMSO was added to each well and incubated for 30 minutes under cell culture conditions. Afterwards, the emission intensity of all cells was measured.

All signals were corrected for the background noise, subtracting the blank signal. Cell proliferation was calculated relative to the control conditions, dividing the treatment condition by the control condition. Cell death was calculated relative to the total amount of cells, dividing the signal of dead cells by the signal of the total cells.

2.2.9 Flow cytometry

In flow cytometry, cells are stained with fluorophore-conjugated antibodies specific to certain cell types or cell properties. These antibodies can be directed against surface markers, such as the CD antigens, or against intracellular proteins, such as transcription factors. A suspension of stained cells is running through the flow cytometer in a way that allows the machine to illuminate every single cell with different lasers. The cytometer is equipped with a set of filters and detectors that measure the presence of bound fluorophore-conjugated antibodies and the light-scattering properties of each cell. The light-scattering properties of a cell are in the first instance its size, measured by the amount of light that is able to pass through the cell in a direct way (forward scatter or FSC) and its granularity, measured by the amount of light that is scattered perpendicular to the laser beam (side scatter or SSC).

Flow cytometry is sometimes generally referred to as fluorescence-activated cell sorting (FACS). More precisely, this refers to the flow cytometry systems by Becton Dickinson (BD), used here. In the following, the term fluorescence-activated cell sorting will be used when the technique was applied to actually sort cells for the use in further assays. Otherwise, the general term flow cytometry will be used.

2.2.9.1 Cell surface staining for flow cytometry

Suspensions of $5x10^5$ - $1x10^6$ cells were centrifuged and the supernatant was discarded. Cells were washed with 2 ml PBS and resuspended in 100 µl PBS. Fluorophore-conjugated antibodies were added at the appropriate amounts. After vortexing, cells were incubated with the antibodies for 15 min at 4 °C in the dark. 2 ml PBS was added, the cells were centrifuged, and the supernatant was discarded. For immediate analysis, cells were resuspended in 100 – 200 µl PBS.

2.2.9.2 Propidium iodide staining for flow cytometry

Propidium iodide (PI) staining was used to distinguish between dead and living cell by flow cytometry. PI staining was performed after the Phagocytosis-Assay for flow cytometry and/or cell surface staining for flow cytometry. The cell suspension was centrifuged at 300 rcf for 10 min at room temperature. The supernatant was discarded and resuspended in 250 µL PI dissolved in FACS buffer (PBS + 2% v/v FCS) with an end concentration of 50 µg/mL. The cell suspension was incubated for 5 – 10 min before measured by flow cytometry. PI negative cells were considered alive, while PI positive cells as dead.

2.2.9.3 Flow cytometry-based phagocytosis assay

The phagocytosis assay determines the general phagocytosis activity of cell lines or cultured cells by their uptake of fluorescent beads. This assay is based on the phagocytic uptake of fluorescent beads by cells. The number of incorporated beads will be measured by flow cytometry.

Prior to the experiment, cells were plated onto a Ø 3.5 cm petri dish, non-coated surface, and treated with stimulation reagents. Cell number, stimulating reagent and incubation time are given for each experiment separately.

30 µL of Fluoresbrite BB Carboxylate Microspheres 4.5 µm latex beads were incubated with 1 mL sterile filtered FCS for 30 min constantly shaking at 1000 rpm at room temperature. The beads were centrifuged for 2 min at 3000 g at room temperature. The supernatant was discarded, and the remaining pallet was resuspended in 3 mL HBSS. The prior prepared cell culture plates were washed carefully with ca. 3 mL of HBSS, the supernatant was removed, and the HBSS-bead solution was added. This was incubated for exact 30 min in an incubator at 37 °C under normal cell culture conditions. The supernatant was transferred into a flow cytometry tube and 2 mL of ice cold HBSS was added. The remaining cells were detached by scratching them vigorously and transferred into a separate flow cytometry tube. Both FACS-tubes were centrifuged immediately for 10 min at 300 g at 4 °C. The supernatant was discarded, and the cell pellet was resuspended in 250 µL FACS buffer. If required, the cell surface staining protocol and/or the propidium iodide staining protocol was applied afterwards. Otherwise, the cell suspension was measured directly by flow cytometry. Flow cytometric data were acquired with FACS-Diva. The median intensity of the bright blue beads was calculated using FlowJo version 7.6.5 or later. The data from each experiment were normalised to the unstimulated media control.

2.2.10 Quantitative PCR

The same stimulation protocol as for the Flow cytometry-based phagocytosis assay was applied. Cells were seeded overnight, treated with 2.5 µM C1.0 in DMSO, 125x10-5 v/v DMSO respectively, plain medium only for 1 hour, followed by an additional stimulation with 1 µg/mL LPS for 24 hours. Total RNA was isolated using the RNeasy Plus Mini Kit (Qiagen). On-column DNase 1 (Qiagen) digestion was performed and total RNA was eluted in RNase-free water. RNA yield was measured using a Nanodrop 1000 (Nanodrop) spectrophotometer and quality was assessed using an Agilent 2100 Bioanalyzer (Agilent). Samples were stored at -80°C until further

use. First-strand cDNA synthesis was done with the SuperScript II reverse transcriptase (Invitrogen) using oligo-dT primers12–18 (Invitrogen) according to the manufacturer's instructions. Quantitative real-time PCR (qRT PCR) reactions were performed in a 7500 Fast Real-Time thermocycler (Applied Biosystems) using the SYBR Select Master Mix (Applied Biosystems) according to the manufacturer's instructions. cDNA input ranged between 1 and 5 ng/µL of total RNA transcribed into cDNA. The expression results were normalized to the expression of ß-actin by the same cells. Primers used are the following: iNOS forward TCACGCTTGGGTCTTGTTCA, iNOS reverse TGAAGAGAAACTTCCAGGGGC, ßActin forward CGTGGGCCGCCCTAGGCACCA, and ßActin reverse CTTAGGGTTCAGGGGGGC.

2.2.11 High throughput screening (HTS)

The high throughput screening was established, tested, carried out, and analysed in the facilities of Leibniz-Forschungsinstitut für Molekulare Pharmakologie im Forschungsverbund Berlin e.V. (FMP) using a robotic setup. The HTS was performed in two separate rounds, first with the microglia cell line BV2 testing the compound library in a single shot approach and validation in concentration dependent approach and followed up by testing primary cultured neonatal microglia in a concentration dependent approach. Cytotoxicity and the effect of NO release were determined using the AlamarBlue assay and the Griess assay, respectively.

2.2.11.1 Compound Library

The library used in this screen was designed by the ChemBioNet, a cooperative of the FMP, the Max-Delbrück-Center for Molecular Medicine (MDC), the Helmholtz-Centre for Infection Research (HZI), and the University of Konstanz. It consists of 16544 compounds, selected to satisfy the basis of the maximum-common substructure principle. The compounds are arranged on 384-well microtiter plates, containing a 10 mM compound solution dissolved in 100 % DMSO placed in columns 1 to 22. DMSO is placed in column 23 and 24 as an internal control. Therefore, one place holds 352 compounds per plate and 32 controls.

2.2.11.2 HTS: a single shot approach

The first round of the screen was performed as following. BV2 cells were seeded into a 384-well assay plate (3683, Corning, New York, USA) at a concentration of 5000 cells per well and 40 µL DMEM per well using a dispenser (EL406, Biotek, Winooski, USA). The cells led to adhere to the plate for 24 hours at standard cell culture conditions (37 °C, 5% CO2, and 95% humidity).

The compounds of the ChemBioNet library were pre-diluted with DMEM to an end-concentration of 500 µM, using a robotic liquid handler (Freedom Evo, Tecan, Maennedorf, Switzerland). After 1 h pre-incubation with the compounds, the cells in column 1 to 23 were stimulated with 1 µg/mL LPS (10 µl of 5 µg/ml LPS solution), while column 24 was left unstimulated. This results in a final compound concentration of 5 µM compound, 0.05 % DMSO. The cells were incubated for 48 hours under standard cell culture conditions, followed by adding 25 µL of premixed 2-fold Griess reagent. The colorimetric change was measured using a plate reader (Safire2, Tecan, Maennedorf, Switzerland). Active compounds were identified by a decreased Z-scores of lower than -5, described below in "Experimental Design and Statistical Analysis for HTS" of the absorbance signal.

2.2.11.3 HTS: concentration dependent validation and cytotoxicity determination

Positive compounds were validated for their reduction in NO concentration and tested for cytotoxic potential in a concentration dependent manner. A dilution series of 10 sequential 2-fold dilutions were rearranged onto a new 384-well plate, ranging from 0.0195 µM up to 20 µM (0.0195, 0.0391, 0.0781, 0.1563, 0.3125, 0.6250, 1.25, 2.5, 5, 10, and 20 µM). The concentrations ranging up to 5 µM were obtained by diluting the previously described mother plate in DMSO, and the protocol was repeated exactly as for the preceding screen (BV2 cell concentration 5000 cells/well, primary microglia cell concentration: 50000 cells/well). 10 µM and 20 µM were acquired by transferring 1 µL and 2 µL from the 500 µM pre-dilution plate. Each concentration was measured in duplicates and normalised to the positive control. Values were plotted against the compound concentration to calculate the IC_{50} value. Compounds cytotoxicity was measured using the AlamarBlue assay (see page 21 AlamarBlue assay). In parallel, a second batch of plates was prepared as described above, but instead of the Griess reagent 5 µL of the AlamarBlue solution was added after 48 hours and measured after an additional incubation for 4 hours under cell culture conditions. Due to missing control samples for data normalisation, the absolute AlamarBlue values were plotted.

2.2.11.4 Experimental Design and Statistical Analysis for HTS

Data were pre-processed (initial graphical quality control and data normalization) by Martin Neuenschwander at the FMP using in-house software, and reports containing chemical structures where generated using Pipeline Pilot (Biovia).

Data were normalized for each plate by using statistically robust estimators as described in Brideau et al. [162].

The Z-score, also named standard score, specifies by which number of standard deviations a measured value is above or below the overall mean signal. Here, x_i is the measured signal of a single sample, Median is the median signal on a plate without the controls, and MAD is the median absolute deviation on a plate without the controls.

$$\boldsymbol{Z-score} = {\boldsymbol{x_i - Median}}/{\boldsymbol{MAD * 1.48258}}$$

The percentage of NO concentration was calculated relative to the unperturbed state. negControl is the median of the unstimulated cells (without LPS stimulation and treatment), posControl is median of untreated but stimulated cells (= 100% LPS-induced, non-treated) on a plate.

$$\boldsymbol{Percent\ Activity} = {\boldsymbol{x_i - negControl}}/{\boldsymbol{|posControl - negControl|}}$$

The Z'-factor is a statistical parameter to the quality of an assay itself, without the intervention of any test compounds. It is commonly used to measure the effective dynamic signal range of HTS assays and serves as a quality control. δ^p and δ^n are the standard deviations of the positive and negative controls respectively, and μ^p and μ^n are the mean values of the positive and negative controls of a plate.

$$\boldsymbol{Z'} = \mathbf{1} - {\mathbf{3} * (\boldsymbol{\delta^P + \sigma^N})}/{\boldsymbol{|\mu^P - \mu^N|}}$$

The IC_{50} value of the compounds was calculated with a four-parameter log-logistic function. The fitting of the curve was done with the Pipeline Pilot curve fit module for determining dose-response curves using ILRS algorithm. The IC_{50} value is represented as "a", the Hill-coefficient which determine the steepness of the IC_{50} curve at the inflection point is represented as "b", and the upper (left) and lower (right) plateau (activity asymptotes) are represented as "c" and "d".

$$\boldsymbol{f(x)} = {\mathbf{c} + (\mathbf{d} - \mathbf{c})}/{\mathbf{1} + \mathbf{e}^{(\boldsymbol{b}*(\boldsymbol{log}(\boldsymbol{x}) - \mathbf{log}(\boldsymbol{a}))}}$$

2.2.12 Enzymatic activity assay

The enzyme activity assay was conducted in the laboratories of Eurofins (Hamburg, Germany). In brief, the test compound, reference compound or water (control) are added to a buffer containing 44 mM Tris-HCl (pH 8.0), 0.5 mM NADPH, 4 µM FAD, 12 µM BH4, 3 mM DTT, 0.1875 µg/ml

calmodulin, 2 mM CaCl2 and 28 nM [3H]L-arginine and 50 nM arginine. Thereafter, the reaction is initiated by the addition of the enzyme (about 6 µg) and the mixture is incubated for 30 min at 37°C. Basal NO concentration was measured omitting the enzyme from the reaction mixture. Following incubation, the reaction is stopped by adding an ice-cold buffer containing 20 mM Tris-HCl (pH 5.0), 2 mM EDTA and 2 mM EGTA. NO was either measured directly using the Griess assay, or indirectly by measuring the citrulline concentration. The results are expressed as a percent inhibition of the control enzyme activity. iNOS was isolated from overexpressing E.coli, eNOS was isolated from Human Umbilical Vein Endothelial Cells (HUV-EC-C) cell line, and nNOS was isolated from wistar rat cerebellum.

2.2.13 Intravenous Pharmacokinetic Study in Mice

The intravenous pharmacokinetic study in mice was carried out by the company Touchstone Biosciences (Plymouth Meeting, USA) according to their standard procedures. In brief, 3 male adult mice of the CD-1 strain were fasted overnight. 5 mg/kg compound was given intravenously in one shot. After 5, 15, 30 min, and 1, 2, 4, 6, 8, and 24 hours blood samples were collected from the vein and analysed via Liquid chromatography-mass spectrometry. After 24 hours all mice were killed. The intravenous tissue distribution study in mice was carried out by the same company. In brief, 3 male adult mice of the strain CD-1 per time point (4 time points) where fasted overnight. 5 mg/kg compound was given intravenously. After 30 min, 1, 2, or 4 hours the blood, brain, heart, liver, and kidney were extracted and the level of compound concentration for each organ and the blood were calculated using Liquid chromatography-mass spectrometry.

2.2.14 Middle cerebral artery occlusion

As a model for stroke, the middle cerebral artery occlusion (MCAO) in mice was used. In total 24 adult male mice (13 weeks old, C57BL/6) were analysed after a 30 minutes left-sided MCAO. All mice were handled according to governmental (LaGeSo - G0249/15) and internal (MDC/Charité) rules and regulations, having free access to food and water over the whole experiment. Animals were randomly attributed to treatment paradigms, and experimenters were blinded at all stages of interventions. The mice were injected intraperitoneally (i.p.) every day for the 7 days, subsequently of the behavioural tests, with the compound (n=11) or with the vehicle (125×10^{-5} v/v DMSO, n=13).

2.2.14.1 Induction of cerebral ischemia

Mice were anesthetized for induction with 3 - 4% isoflurane and maintained in 1.5% isoflurane in 70% N_2O and 30% O_2 using a vaporizer. MCAO was essentially performed as described elsewhere (Endres et al.) [163]. In brief, brain ischemia was induced with a silicone rubber-coated monofilament 7-0, diameter 0.06 - 0.09 mm, length 20 mm; diameter with coating 0.19 ±0.01 mm; coating length 9-10 mm. The filament was introduced into the internal carotid artery up to the anterior cerebral artery. Thereby, the middle cerebral artery and anterior choroidal arteries were occluded. The filament was removed after 30 min to allow reperfusion.

2.2.14.2 Determination of infarct volume:

2.2.14.2.1 Magnetic Resonance Imaging

MRI was performed using a 7 Tesla rodent scanner (Pharmascan 70 / 16, Bruker BioSpin, Bruker, Billerica, USA) with a 16 cm horizontal bore magnet and a 9 cm (inner diameter) shielded gradient with an H-resonance-frequency of 300 MHz and a maximum gradient strength of 300 mT/m. For imaging a 20mm - 1H-RF quadrature-volume resonator with an inner diameter of 20 mm was used. Data acquisition and image processing were carried out with the Bruker software Paravision 5.1. During the examinations, mice were placed on a heated circulating water blanket to ensure a constant body temperature of 37 °C. Anaesthesia was induced with 2.5% and maintained with 2.0 – 1.5% isoflurane (Forene, Abbot, Wiesbaden, Germany) delivered in an O_2 / N_2 mixture (0.3 / 0.7 L/min) via a facemask under constant ventilation monitoring (Small Animal Monitoring & Gating System, SA Instruments, New York, USA). For imaging the mouse brain, a T2-weighted 2D turbo spin-echo sequence was used (imaging parameters TR / TE = 4200 / 36 ms, rare factor 8, 4 averages, 32 axial slices with a slice thickness of 0.5 mm, the field of view of 2.56 x 2.56 cm, matrix size 256 x 256).

2.2.14.2.2 Image Analysis

Calculation of lesion volume was carried out with the program Analyze 10.0 (AnalyzeDirect, Inc., Overland Park, USA). The hyperintense ischemic areas in axial T2-weighted images were assigned with a region of interest tool. This enables threshold-based segmentation by connecting all pixels within a specified threshold range about the selected seed pixel and results in 3D object map of the whole stroke region. Further, the total volume of the whole object map was automatically calculated.

2.2.14.3 Motor deficits assessment:

2.2.14.3.1 Accelerated Rotarod Test

The Rotarod test was performed to access motor coordination using a treadmill with a diameter of 3 cm (TSE Systems, Chesterfield, USA). This test was performed with accelerating velocity (4 – 40 rpm) and maximal velocity was achieved after 300 s. The time until the animals dropped was measured. Animals were trained on day 2 and 3 before MCAO, and the baseline was taken on the day before MCAO. Tests were always performed four times and means were used for statistical analysis.

2.2.14.3.2 Pole Test

A vertical pole (80 cm high with a rough surface) was used for this test, to analyse extrapyramidal motor locomotion. Mice were placed head upward on the top of the pole. The time taken to orientate the body completely downwards, making a 180° turn (t turn), and to reach the floor with all four paws (t down) were recorded. If the animal was unsuccessful at either task, it was scored the maximum time that any other animal from the same experimental group took to perform the task. Animals were trained on day 2 and 3 before MCAO, and the baseline was taken on the day before MCAO. Tests were always performed after the accelerated Rotarod test and repeated four times and means were used for statistical analysis.

2.2.14.3.3 Corner Test

Each mouse was placed on a cage containing two vertical boards attached to each other forming an angle of 30° in 2 of the corners. The side chosen to leave the corner once it made contact to the boards with its whiskers was observed within 10 trials per day. Whereas healthy animals leave the corner without side preference, mice after stroke preferentially leave the corner towards the non-impaired (i.e., left) body side (Zhang et al.) [164]. Baseline side preference was accessed on day 5 before MCAO and the mice were tested again on day 6 after MCAO.

3 RESULTS

3.1 Screening for compounds inhibiting nitric oxide release in microglia

Elevated NO concentration in the CNS is a mayor risk factor for neuronal cell death. The main source of NO in the CNS are proinflammatory activated microglia. In order to identify novel compound targeting the proinflammatory induced release of NO in microglia, we performed a high throughput screen with the ChemBioNet [165,166] library containing 16544 small molecules. The ChemBioNet library was designed to exhibit a high degree of chemical diversity and to be enriched with putative bioactive compounds. The library was corrected for biological instable molecules and molecules that overshoot the "Lipinski rule of five"[167–169] to ensure general bio availability. The screen was executed in two steps: first, the library was tested on the microglial cell line BV-2, which allowed an HTS approach[170], followed by a validation of the positive results using primary cultured neonatal microglia. The cells were stimulated with 1 µg/mL LPS to induce a proinflammatory response and trigger the production and release of NO. Figure 3.1 illustrates the overall experimental strategy of the HTS.

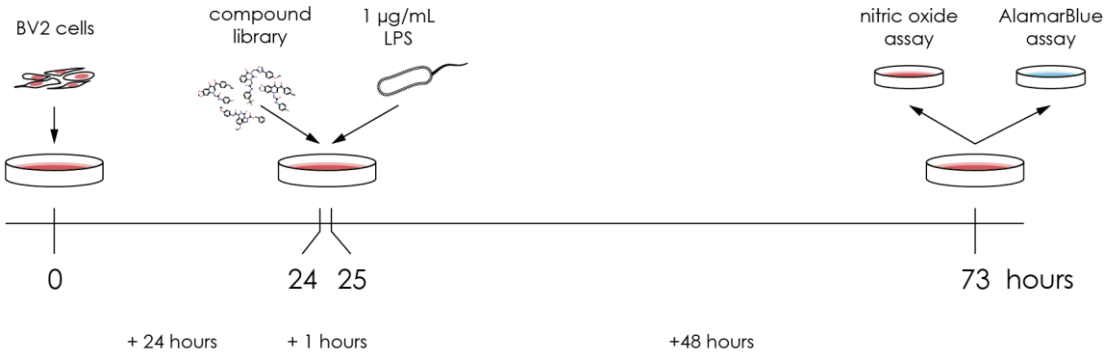

Figure 3.1: Illustration of the HTS setup using the microglial cell line BV2.
BV2 cells were seeded 24 hours prior to the treatment with the FMP compound library. 1 hour after treatment 1 µg/mL LPS were added and the cells were incubated for additional 48 hours. NO concentration was assessed using the Griess assay, the metabolic activity was measured using AlamarBlue.

The first run of the HTS was conducted with the complete library of 16544 compounds on the BV-2 cell line. BV-2 cells can be easily cultured and expanded to fulfil the high demand of cells in this HTS; over 90 million cells were needed for the initial run. BV-2 cells show a similar activation pattern as primary microglia[160,171] but do vary in the magnitude of their response[170]. Therefore, BV-2 cells are a good compromise for the requirement of a high cell number and the resembling of microglia function and regulation. 24 hours prior to the begin of the HTS 5000 BV-2 cells per well were seeded into a 384-well plate. The cells were pre-treated with 5 µM compound for 1 hour, followed by an additional stimulation with 1 µg/mL LPS for another 48 hours. The NO concentration in the supernatant was measured using a modified Griess assay. Each plate of the screen contained 352 different compounds, 16 times the positive control of untreated LPS stimulated cells, and 16 times the negative control of untreated unstimulated cells (see Figure 3.3). The difference in the signal between the positive and the negative control showed a mean Z'-factor of 0.75. Compounds with a Z-score of below -5 were considered as active compounds. 503 of the 16544 tested compounds (3 %) reached this goal. Out of those 503 positive compounds,

we picket the 352 most active ones for further concentration-dependent validation in reducing the NO release and to assess their cytotoxic.

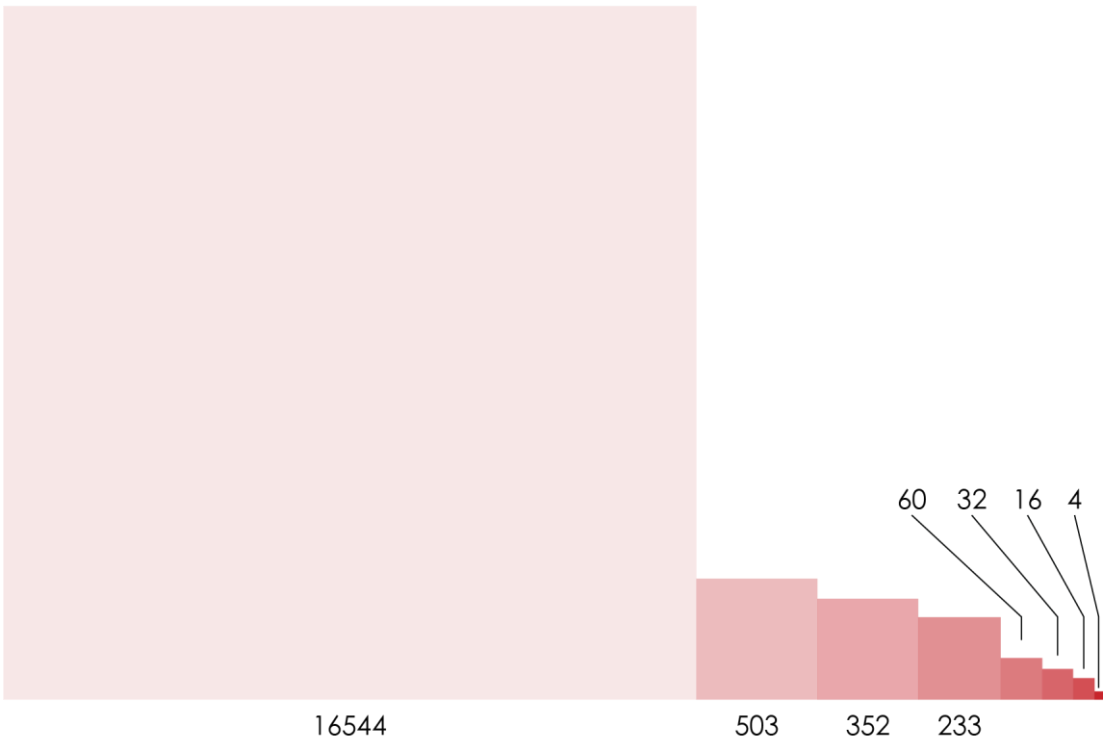

Figure 3.2: Illustration of the reduction in compounds during the screening process
In a step by step the library of 16544 compounds were narrowed down to 4 hit compounds. After the initial NO screen in BV2 cells 503 positive compounds remained. 352 compounds were further analysed, 233 of them showed a dose dependent reduction, and 60 of those were not cytotoxic. 32 compounds were validated in primary microglia. 16 showed a satisfactory reduction in NO and 4 of them a superior reduction in NO.

The concentration-dependent validation was carried out similar to the above described initial one-shot run. We applied the compounds in a concentration range starting from 20 µM down to 0.0195 µM in 2-fold dilution sequence (20, 10, 5, 2.5, 1.25, 0.6250, 0.3125, 0.1563, 0.0781, 0.0391, and 0.0195 µM). The impact on the NO release and the effect on the BV-2 cell viability was tested in parallel, using a modified Griess and AlamarBlue assay. 233 of the tested 352 compounds showed a dose dependent decrease of NO concentration. However, in only 60 cases this reduction in NO was independent of the BV-2 cell viability, as those compounds showed no effect in the AlamarBlue.

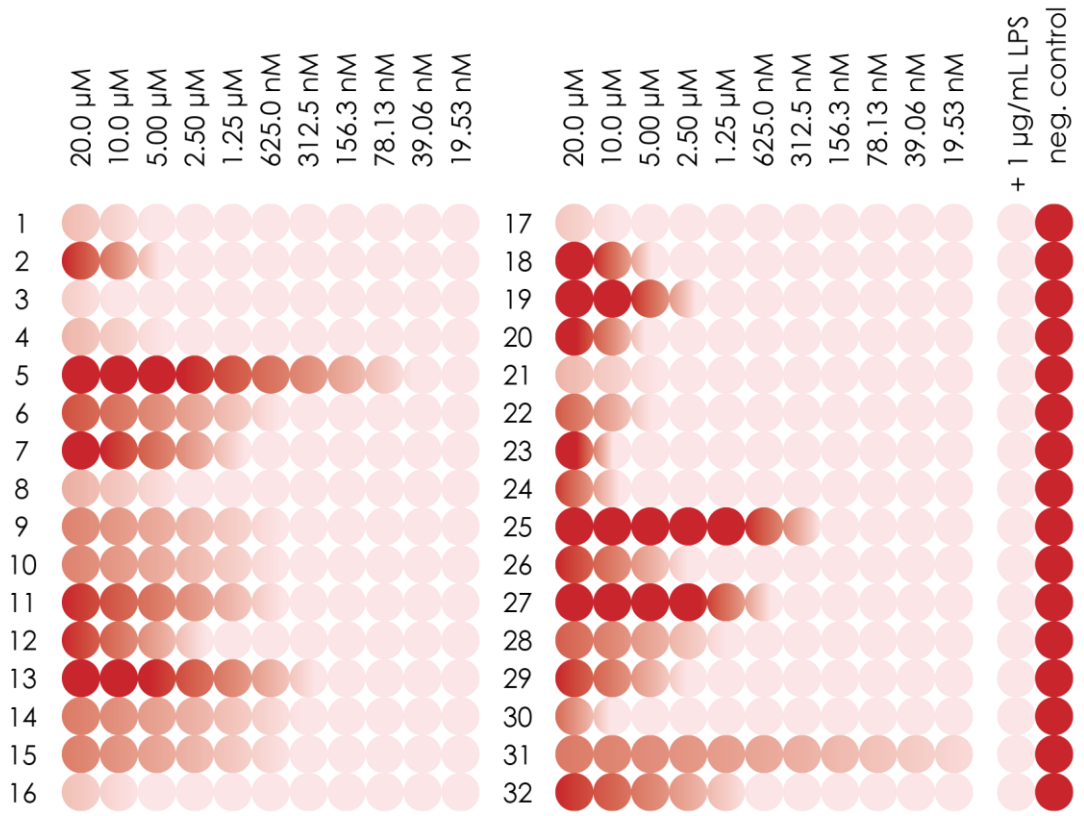

Figure 3.3: Illustration of the plating scheme of the compound validation with primary cultured neonatal microglia.
Primary cultured neonatal microglia were seeded 1 day before compound treatment into a 384 well plate. The 32 compounds were added in the concentrations 20, 10, 5, 2.5, 1.25, 0.6250, 0.3125, 0.1563, 0.0781, 0.0391, and 0.0195 µM (left to right). One hour later 1 µg/mL LPS was added. After 48 hours the NO concentration was measured (high NO concentration = dark red, low NO concentration = light red). Untreated wells severed as negative control (neg. control, most far right) and with 1 µg/mL LPS as positive control (+ 1µg/mL LPS, left to the negative control.)

To overcome the disadvantages of the BV-2 microglial cell line, we confirmed the most potent compounds in primary cultured neonatal microglia. To be able to perform a run with primary microglia, I again had to reduce the number of compounds to a total number of 32 compounds. This validation required an amount of 78.6 million primary microglia. The primary microglia were extracted and cultured from murine neonatal brains days before the assay. Despite the difference in the number of used cells, the protocol was carried out exactly as described for the BV-2 cell line. Figure 3.4 illustrates the impact on the NO release and the cytotoxic potential of the 32 tested compounds on primary microglia.

None of the tested compounds showed a dose dependent cytotoxicity, indicated by a reduction in the absolute AlamarBlue values. However, the AlamarBlue values are selectively reduced for several compounds. 0.625 µM of compound 202641 decreased the AlamarBlue value by half, but higher concentrations did not show this effect. A similar effect can be seen for compound 206830 and 211563, which show a decreased AlamarBlue value for 0.625 µM and 5 µM, and 0.0391 µM and 2.5 µM respectively. This drop in AlamarBlue might result from experimental errors in the dilution, pipetting or readout of the assay. Furthermore, the AlamarBlue values for the compounds 213475, 213512, and 215365 are decreased when 20 µM compound is applied. This might indicate a cytotoxic potential; however missing data of higher concentrations do not allow any further interpretation.

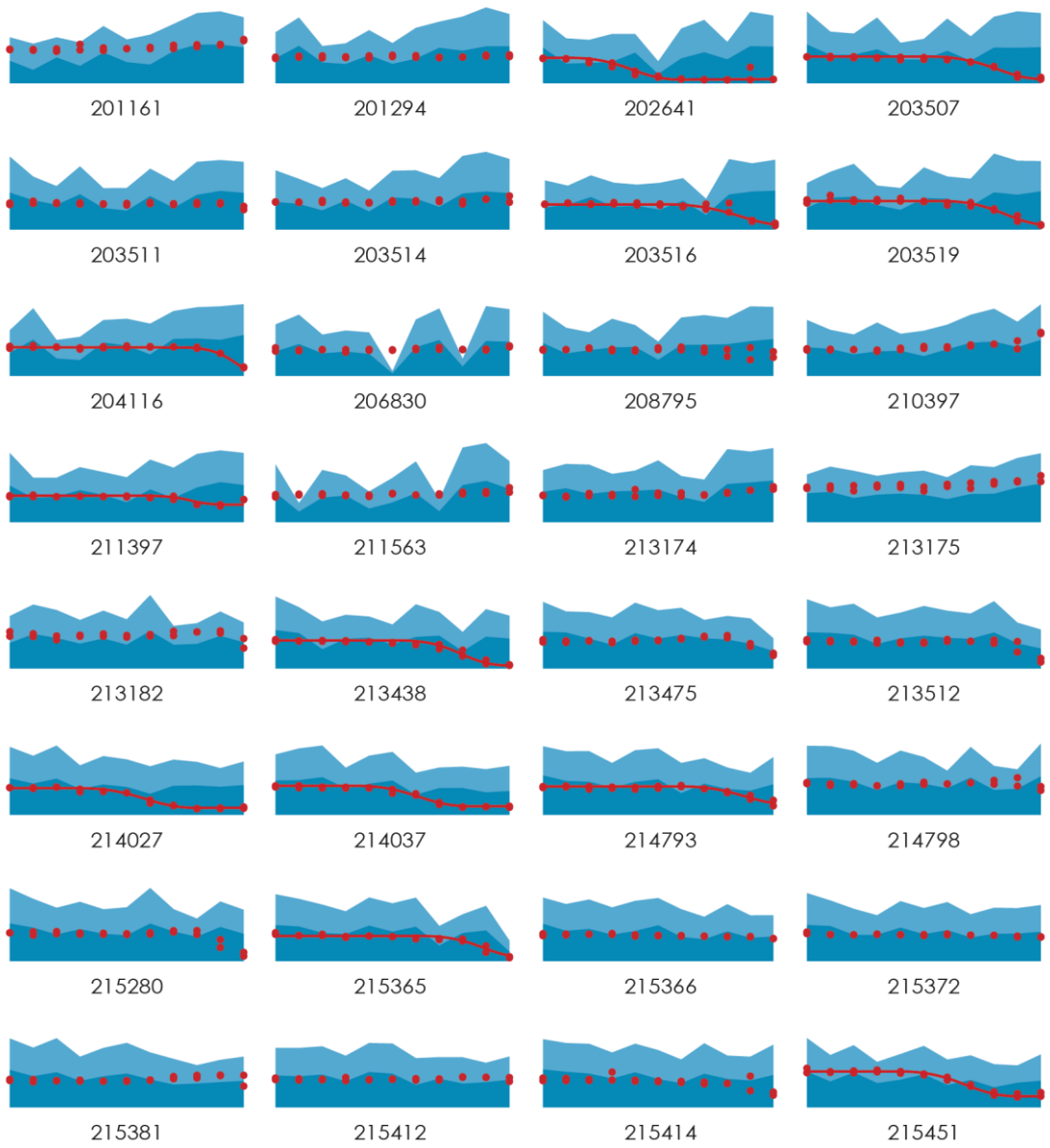

Figure 3.4: LPS induced nitric oxide release and metabolic activity in primary cultured neonatal microglia in the presence compounds.
NO was measured using the Griess assay (shown in red, normalised to the untreated LPS stimulated positive control), and the metabolic activity was measured using the AlamarBlue assay (shown in blue, absolute absorbance values are given). Calculated IC_{50} curves, as possible, are illustrated as a red line.

Although all tested compounds were positive for reducing the NO concentration in the BV-2 cell line, only 16 of those 32 compounds showed a reduction in primary microglia. An IC_{50} curve could be fitted for only 12 out of the 16 compounds. The 4 compounds, 213475, 213512, 215280, and 215414, which failed in calculating an IC_{50} curve, showed a reduction

in NO only for highest tested concentrations of 10 µM and 20 µM. 213512 and 215414 showed mixed results, as the 2 replicates of the NO readout vary a lot at a concentration of 10 µM (213512: t_1 = 55.36 %, t_2 = 91.05 %, 215414: t_1 = 56.07 %, t_2 = 105.51 %). The compound 213475 and 213512 showed a reduction in AlamarBlue as described above, therefore the reduction in NO concentration might be the result of cytotoxicity.

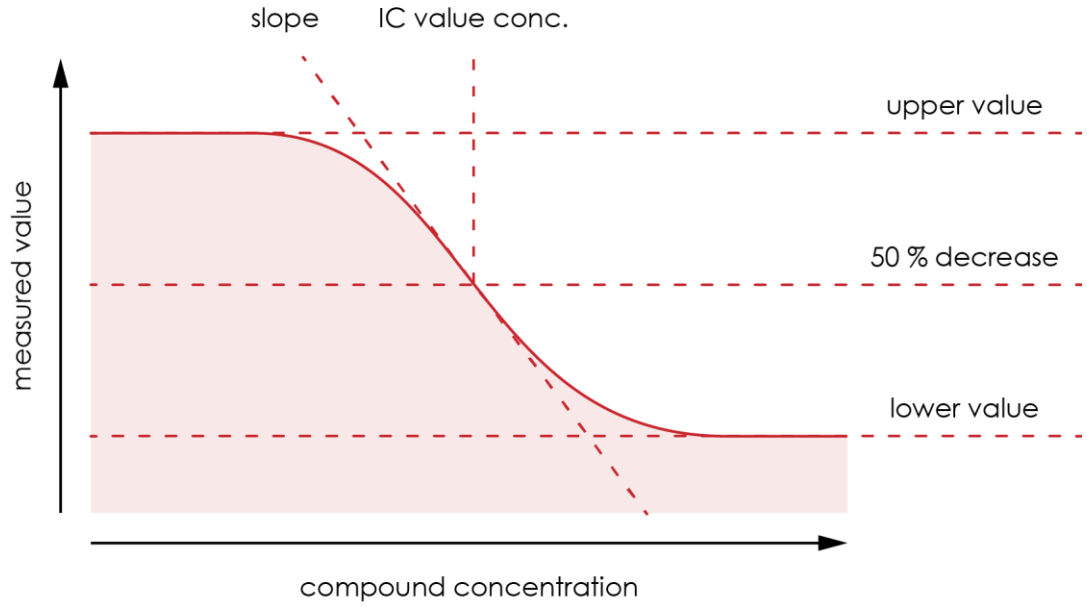

Figure 3.5: Illustration of an ideal IC_{50} curve.
An ideal IC_{50} curve (red solid line) is plotted as compound concentration (x-axis) against measured value (y-axis). The maximal and minimal possible values are given as dashed lines (upper values & lower value). The IC_{50} value is calculated from the given 50% decrease of the measured value. The steepness is defined by the Hill coefficient.

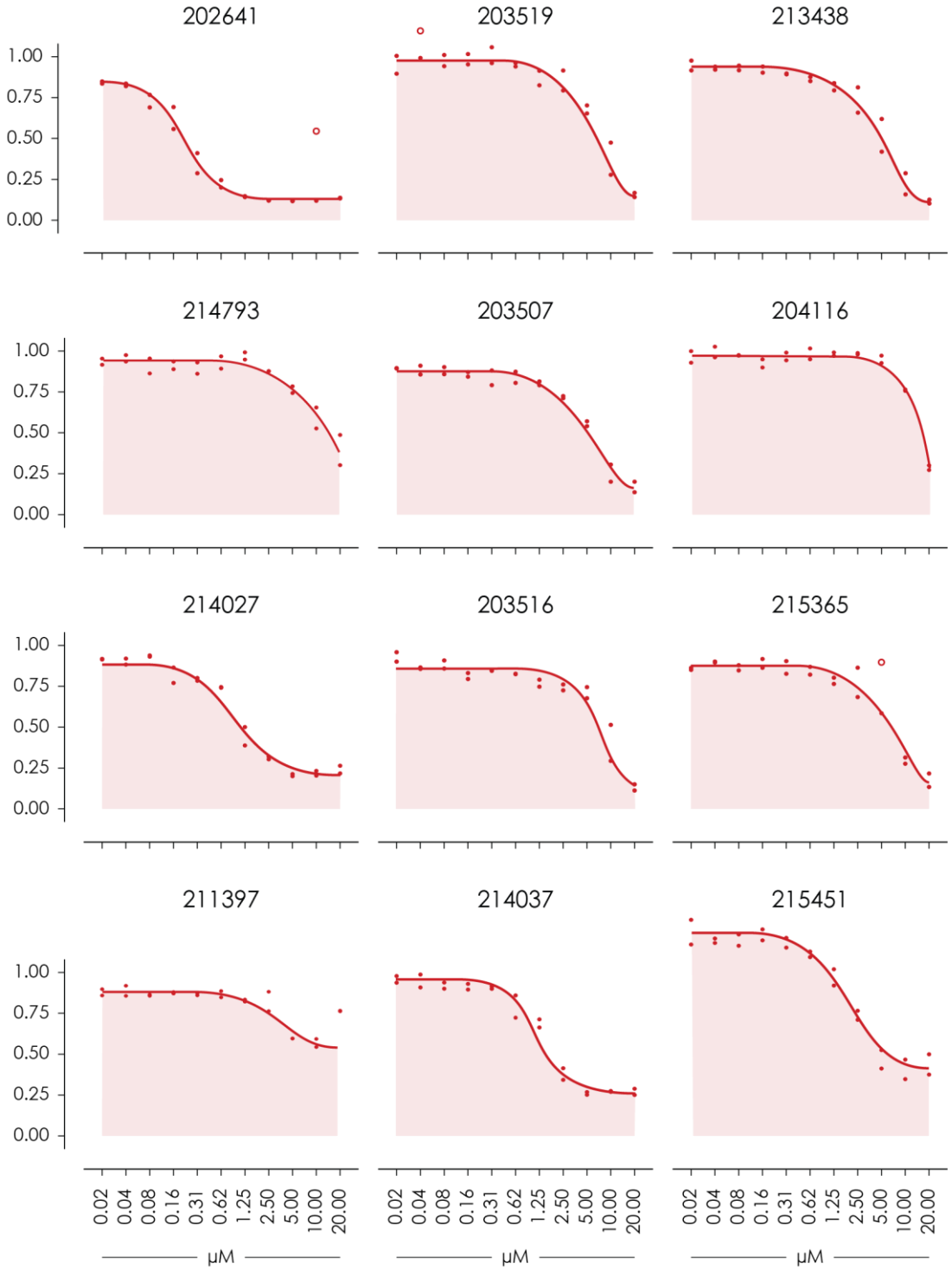

Figure 3.6: The dose dependent reduction of LPS induced NO in microglia
Out of 32 tested compounds, 16 showed a dose dependent decrease in NO concentration able to fit an IC_{50} curve. The measured values are given as red dots. Open dots were excluded from the fitting using a robust fit with outlier detection.

ID		value		std. error		p-value	
202641	lower Plateau	0.13062	%	0.01386	%	$3.6x10^{-08}$	****
	upper Plateau	1.94533	%	1.41690	%	0.18761	
	Hill coefficient	-0.06576		0.28847		0.82241	
	IC_{50} value	0.12511	µM	1.82800	µM	0.00309	**
203507	lower Plateau	0.15989	%	0.02609	%	$8.6x10^{-06}$	****
	upper Plateau	1.04172	%	0.09245	%	$1.3x10^{-09}$	****
	Hill coefficient	4.20059		0.71662		$1.5x10^{-05}$	****
	IC_{50} value	0.86050	µM	1.02995	µM	$7.6x10^{-05}$	****
203516	lower Plateau	0.16934	%	0.03498	%	0.0002	***
	upper Plateau	1.00427	%	0.09621	%	$8.2x10^{-09}$	****
	Hill coefficient	4.97996		0.93365		$5.4x10^{-05}$	****
	IC_{50} value	0.86270	µM	1.03679	µM	0.0008	***
203519	lower Plateau	0.12297	%	0.06617	%	0.0805	
	upper Plateau	1.26923	%	0.27893	%	0.0004	***
	Hill coefficient	4.68018		2.15670		0.0445	*
	IC_{50} value	0.90316	µM	1.03882	µM	0.0160	*
204116	lower Plateau	0.28158	%	0.02810	%	$8.6x10^{-09}$	****
	upper Plateau	0.97234	%	0.01023	%	$< 2x10^{-16}$	****
	Hill coefficient	11.43331		0.87970		$1.3x10^{-10}$	****
	IC_{50} value	0.78069	µM	1.14827	µM	0.0902	
211397	lower Plateau	0.64268	%	0.02577	%	$2x10^{-15}$	****
	upper Plateau	0.86663	%	0.01804	%	$< 2x10^{-16}$	****
	Hill coefficient	2.95672		3.34651		0.389	
	IC_{50} value	0.27818	µM	12266.28842	µM	0.893	
213438	lower Plateau	0.10345	%	0.04206	%	0.02427	*
	upper Plateau	1.28907	%	0.29344	%	0.00035	***
	Hill coefficient	2.82550		1.79972		0.13383	
	IC_{50} value	0.87976	µM	1.03892	µM	0.00353	**
214027	lower Plateau	0.22644	%	0.01772	%	$1.8x10^{-10}$	****
	upper Plateau	1.27851	%	0.31468	%	0.00073	***
	Hill coefficient	0.46224		0.45459		0.32272	
	IC_{50} value	0.53759	µM	1.18732	µM	0.00198	**
214037	lower Plateau	0.26651	%	0.01096	%	$1.2x10^{-14}$	****
	upper Plateau	1.01276	%	0.03414	%	$4.4x10^{-16}$	****

ID		value		std. error		p-value	
	Hill coefficient	1.41660		0.09410		$2.9x10^{-11}$	****
	IC_{50} value	0.49690	µM	1.09369	µM	$5.06E^{-07}$	****
214793	lower Plateau	0.37512	%	0.05983	%	$6.52E^{-06}$	****
	upper Plateau	1.01967	%	0.11324	%	$4.37E^{-08}$	****
	Hill coefficient	7.18445		1.55339		0.00021	***
	IC_{50} value	0.89200	µM	1.05510	µM	0.04716	*
215365	lower Plateau	0.05952	%	0.11725	%	0.61789	
	upper Plateau	1.04369	%	0.23435	%	0.00031	***
	Hill coefficient	7.25643		1.94524		0.001532	**
	IC_{50} value	0.91599	µM	1.04848	µM	0.080292	
215451	lower Plateau	0.41964	%	0.02649	%	5.16E-12	****
	upper Plateau	1.51906	%	0.24486	%	7.45E-06	****
	Hill coefficient	1.30398		0.64685		0.05899	
	IC_{50} value	0.71016	µM	1.10228	µM	0.00247	**

Table 3.1: Parameters and their significance of the calculated IC_{50} curve.

The 12 compounds that comply with the fitting of the IC_{50} curve are presented in Figure 3.6. The individual fitting parameters are presented in Table 3.1. 6 compounds show an IC_{50} value far above 20 µM. The 2 compounds, 211397 and 213438 have an intermediate IC_{50} value of 19.2 µM and 16.9 µM respectively. 4 compounds, 202641, 214027, 215451, and 214037, showed a reasonable IC_{50} value of below 5 µM, with a reduction in NO concentration by more than 50 %. Compound 202641 has an IC_{50} below 1 µM and is able to reduce the NO concentration to 13.1 % of the non-treated LPS stimulated positive control (= pos. ctrl.). Moreover, the Hill-coefficient, which defines the width of the dose dependent reduction, is -2.08 indicating a narrow width. Compound 214027 is less potent compared to 202641, reducing the NO concentration to only 22.6 % of the pos. ctrl. with an IC_{50} value of 1.6 µM. The compound acts on a much broader concentration, indicated by the Hill-coefficient of -0.62. Compound 215451 does reduce the NO concentration to only 42 % of the positive control. Its IC_{50} value is at 3.68 µM and the Hill-coefficient is even lower than the ones described before. Compound 214037 share a similar reduction in NO concentration (down to 26.7 %) and Hill-coefficient (-0.67). However, its IC_{50} value is more than doubled (4.12 µM).

We choose those 4 compounds for further validation. In the following, the compounds will be named numerically starting from C1.0 to C4.0. A list of translations can be found below in Table 3.2.

HTS	Laboratory
202641	C1.0
214027	C2.0
214037	C3.0
215451	C4.0

Table 3.2: Compound name translation.
The given compound name used in the HTS and the chosen name for experiments in laboratory scale.

3.2 Four compounds decrease the LPS induced NO release.

The previous experiments of the screen were run in a high-throughput setup using 386 well plates with 50 µL volumes and carried out by robots. These parameters might influence the outcome of the experiments, especially the small volume might interfere with the biological behaviour of the cells and the physical behaviour of the compounds. Therefore, I transferred the Griess and the AlamarBlue assay to 96 well plate setup run manually and repeated the experiments with the 4 compounds chosen beforehand. The transfer of the Griess and AlamarBlue assay were done previously and described in my master thesis. There, I demonstrated that the main parameters of the HTS, the incubation, treatment and stimulation time, as well as LPS concentration and the cell concentration could remain the same. In brief, 50000 primary microglia in 200 µL medium per well were seeded into a 96 well plate one day prior the experiment. The cells were treated with a defined concentration of the compounds, given below in Table 3.3. After 1 hour, LPS was added to reach a final concentration of 1 µg/mL and the cells were incubated for another 48 hours. The experiment was terminated by distributing the cell supernatant into 2 96 well plates, one was used immediately to determine the NO concentration in the supernatant, the remaining plate was stored at -20 °C for subsequent quantification of the secreted cytokines. The AlamarBlue assay was performed with the same cells. To do so, the initial 96

well plate containing the cells, was washed carefully and fresh medium containing the AlamarBlue solution was added. The plates were incubated for another 3 hours, afore the AlamarBlue turnover was measured.

Compound ID	Concentration			
	low	IC_{50} value	high	
C1.0	0.025	0.250	2.500	µM
C2.0	0.050	1.000	5.000	µM
C3.0	0.300	1.500	5.000	µM
C4.0	0.200	2.000	10.000	µM

Table 3.3: Compound concentrations.
The given concentrations were used throughout the whole study, if not stated otherwise. The concentrations were chosen by hand to represent a concentration of almost no effect (low), the calculated IC_{50} value (IC_{50} value), and a concentration of almost 100% activity (high).

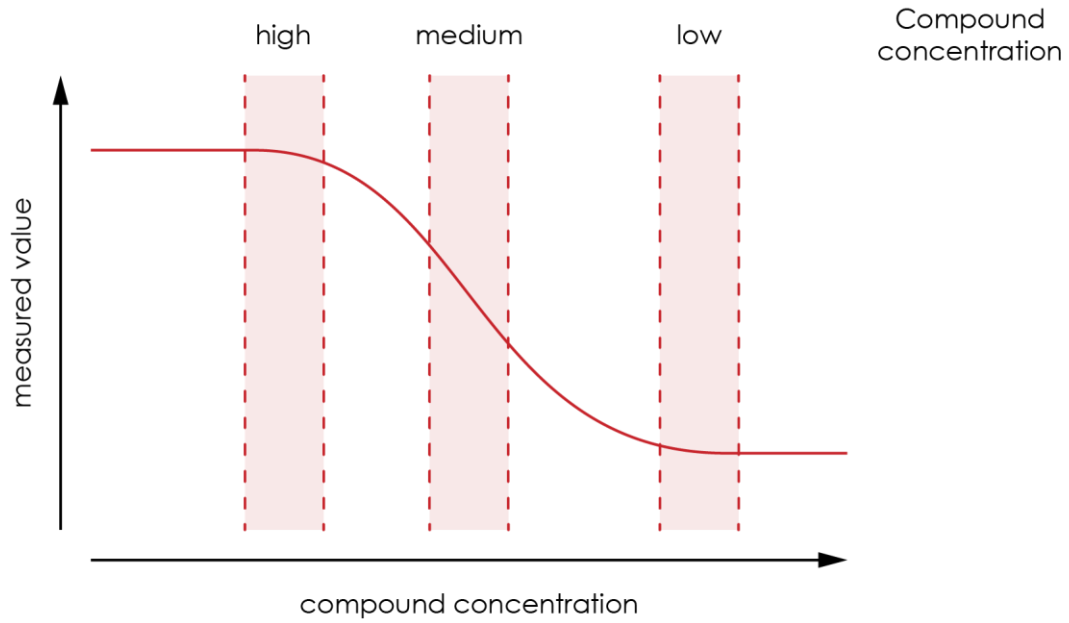

Figure 3.7: Illustration of the assignment of the compound concentrations.
The representation of an ideal IC_{50} curve (red solid line) and the three concentration ranges for low, IC_{50} value, and high (red dashed lines).

I tested 3 concentrations for each of the 4 compounds, one concentration close to the IC_{50} value, one high and one low concentration. The high and low concentration were chosen to be in the proximity of the IC_{50} value and reach almost 100 % or 0 % of the compound's potential. All concentrations where chosen by hand to ensure a feasible handling. The concentrations are illustrated in Figure 3.1 and are listed in Table 3.3.

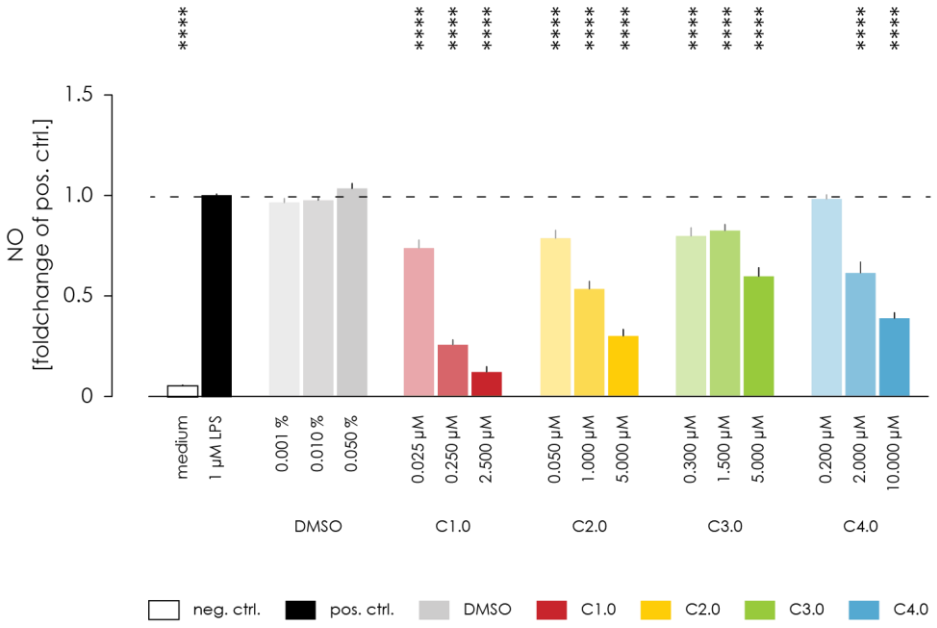

Figure 3.8: Validation of the dose dependent reduction of LPS induced microglial NO release scaled to a 96 well plate.
NO release measured using the Griess assay and normalised to the untreated LPS stimulated positive control. Microglia were treated 1 hour before stimulation for additional 48 hours. The solvent control containing only DMSO represent the 3 highest concentrations used. Data is shown as mean + SEM. Statistical significance is shown as * ≤ 0.05, ** ≤ 0.01,*** ≤ 0.001, **** ≤ 0.0001.

I could validate a dose dependent decrease in LPS induced NO release for all 4 compounds, illustrated in Figure 3.8. However, not all of them showed the same reduction as determined in the HTS (see Figure 3.4). In the highest tested concentration, the compounds C1.0, C2.0, and C4.0 reduced the NO concentration to the values calculated by the IC_{50} curve fitting: 2.5 µM of C1.0 reduced to 12.2 % of the pos. ctrl. (14.2 % std. error; calc.: 13 %, 1.3 % std. error, $p < 0.0001$), 5 µM of C2.0 reduced to 30 % of the pos. ctrl. (17.7 % std. error; calc.: 22.6 %, 1.7 % std. error, $p < 0.0001$), and 10 µM of C4.0 reduced to 38.7 % of the pos. ctrl. (14.8 % std. error; calc.: 42 %, 2.6 % std. error, $p < 0.0001$). C3.0 showed a reduction in the NO concentration to 59.5 % (23.1 % std. error) when 5 µM was applied but did not reach the values of the HTS (5 µM: 26 %, 0.83 % std. error) or the calculated lower plateau of the fitted curve (26.6 %, 1.1 % std. error, $p < 0.0001$). DMSO, the compounds solvent, did not show any effect on the NO concentration, preserving the NO level at 102.9 % (9.2 % std. error, $p > 0.9999$) when the highest used concentration of $5x10^{-4}$ v/v DMSO was applied.

C1.0 showed a significant reduction in the NO level for all tested concentration compared to the pos. ctrl.. 0.025 µM reduced the NO level to 73.6 % (21.6 % std. error, $p < 0.0001$), 0.25 µM to 25.6 % (13.5 % std. error, $p < 0.0001$), and as mentioned before 2.5 µM to 12.2 % (14.2 % std. error, $p < 0.0001$). The NO reduction in the presents of 2.5 µM showed no significant differences to the unstimulated control (5.6 %, 4.8 std. error, $p = 0.6944$).

Like compound C1.0, C2.0 and C3.0 do showed a significant reduction in the NO level for all tested concentration compared to the pos. ctrl.. 0.05 µM of C2.0 decreased the NO level to 78.4 % (21 % std. error, $p < 0.0001$), 1 µM to 53.3 % (20.1 % std. error, $p < 0.0001$), and 5 µM to 30 % (17.7 % std. error, $p < 0.0001$). 0.3 µM of C3.0 decreased the NO level to 79.4 % (22 % std. error, $p < 0.0001$), 1.5 µM to 82.2 % (14.8 % std. error, $p < 0.0001$), and 5 µM to 59.5 % (23.1 % std. error, $p < 0.0001$). None of the tested concentrations of both compounds were able to decrease the NO level indistinguishable to the neg. ctrl..

Other than the previous compounds, C4.0 decreased the NO level significantly only for 2 µM and 10 µM but not for 0.2 µM. 0.2 µM decreased the NO level to 97.8 % (10.8 % std. error, $p > 0.9999$) compared to the pos. ctrl., 2 µM to 61.2 % (29.2 % std. error, $p < 0.0001$), and 10 µM to 38.7 % (14.8 % std. error, $p < 0.0001$). All tested concentrations are significant above the neg. ctrl. ($p < 0.0001$).

In parallel to the validation of the compound's effect on LPS induced NO release, I assessed their impact on the metabolic activity by repeating the AlamarBlue assay, illustrated in Figure 3.9. All values were normalised to the LPS stimulated positive control (pos. ctrl.). Upon LPS stimulation the metabolic activity of primary microglia increases significantly by around 23.9 %, from 76.1 % (22.8 std. error) for the unstimulated control (neg. ctrl.) to 100 % for the pos. ctrl. (8.2 % std. error, $p < 0.0001$). With of drop of only 0.7 % to 99.3 % the DMSO control showed no effect on the metabolic activity of microglia (10.2 % std. error, $p > 0.9999$).

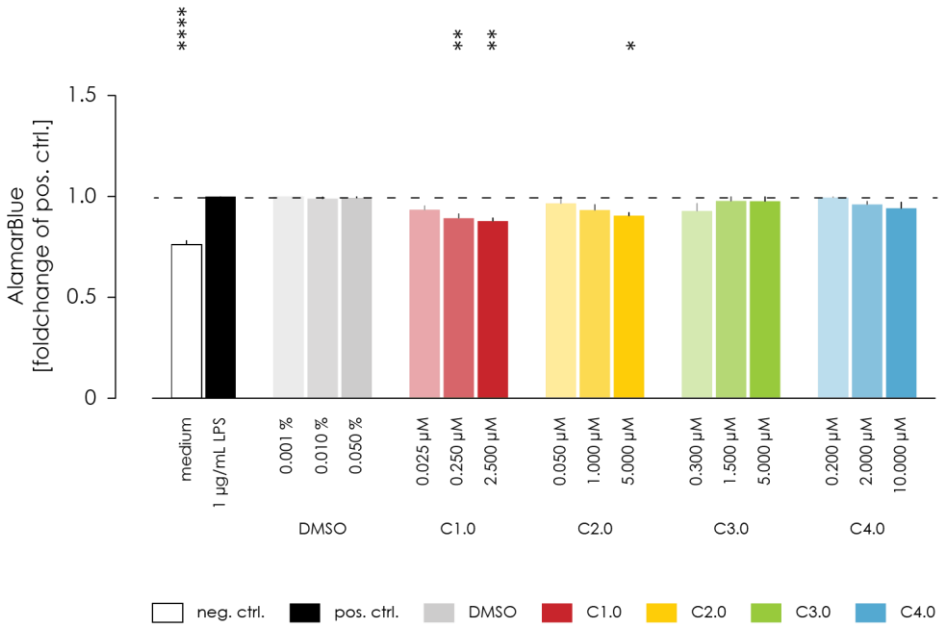

Figure 3.9: Validation of the dose dependent influence on LPS elevated microglial metabolic activity scaled to a 96 well plate.
Metabolic activity measured using the AlamarBlue assay and normalised to the untreated LPS stimulated positive control. Microglia were treated 1 hour before stimulation for additional 48 hours. Afterwards the AlamarBlue assay was performed for ca. 3 hours. The solvent control containing only DMSO represent the 3 highest concentrations used. Data is shown as mean + SEM. Statistical significance is shown as * ≤ 0.05, ** ≤ 0.01,*** ≤ 0.001, **** ≤ 0.0001.

C1.0 showed a dose dependent reduction in the metabolic activity, ranging from a decrease to 93.3 % for 0.025 µM (10.5 % std. error, $p < 0.9999$ compared to pos. ctrl.), and 89.2 % for 0.25 µM (11.1 % std. error, $p > 0.9999$ compared to pos. ctrl.), to 87.7 % for 2.5 µM (8.1 % std. error). The decrease caused by a concentration of 2.5 µM is significant different compared to the LPS stimulated control ($p = 0.0122$), but remains above the unstimulated control (76.1 %, $p = 0.0251$).

C2.0, C3.0, and C4.0 did not show any significant decrease in the metabolic activity. C2.0 reduced the metabolic activity to a maximum of 10 %. 0.05 µM showed a decrease to 96.5 % (20.2 % std. error, $p = 0.9996$), 1 µM to 93.2 % (14.1 % std. error, $p = 0.7391$), and 5 µM to 90.4 % (8.2 %, std. error, $p = 0.1689$). C3.0 reduced the metabolic activity by a maximum of 7.2 %. 0.3 µM showed a decrease to 92.8 % (19.4 std. error, $p = 0.6605$), 1.5 µM to 97.7 % (16.3 std. error, $p > 0.9999$), and 5 µM to 97.6 % (14.9 % std. error, $p > 0.9999$). C4.0 showed the least amount of impact on the metabolic activity, with a reduction to 99.4 %

for 0.2 μM (9.0 % std. error, p > 0.9999), 96.0 % for 2 μM (6.5 % std. error, p = 0.9996), and 94.1 % for 10 μM (14.1 % std. error, p = 0.9553).

3.3 The NO release is regulated independently from the pro-inflammatory stimulus.

To study whether the effect on the NO release is LPS dependent, I repeated the previous assays with different stimulation, namely IFNγ and polyIC. The effect on IFNγ induced microglial NO release was tested using a similar protocol as for LPS induced NO release. I used the same schedule stimulating the microglia with 100 ng/ml IFNγ for 48 hours, illustrated in Figure 3.10. In order to assess the effect on polyIC induced NO release, I reduced the stimulation duration to 24 hours, which lead to a larger difference between unstimulated negative control (neg. ctrl.) and the 100 μg/mL polyIC stimulated positive control (pos. ctrl.), illustrated in Figure 3.11. The time dependent NO production of primary microglia with IFNγ and polyIC was assessed previously in my master thesis.

3.3.1 IFNγ induced NO release is regulated in a dose dependent manner in primary microglia

Upon IFNγ stimulation the NO concentration increases significantly by almost 10-fold, from 13.2 % (8.0 % std. error) under unstimulated conditions (neg. ctrl.) to 100 % (20.1 % std. error, p < 0.0001) after IFNγ stimulation. All four compounds, C1.0, C2.0, C3.0, and C4.0, reduced this IFNγ induced NO release in a dose dependent manner; all to a different extent. C1.0 showed the most potent decrease to 21.9 % (19.1 % std. error). 0.025 μM of C1.0 reduced the NO level in a non-significant manner to 84.2 % (28.8 std. error, p = 0.3357), already 0.25 μM reduced the NO level significantly to 41.3 % (14.8 % std. error, p < 0.0001), and 2.5 μM reduced it significantly to 21.9 % (19.1 % std. error). This concentration of C1.0 was statistically not different from the neg. ctrl. with an p value of 0.9907. C2.0 showed a similar result, reducing the NO level non-significantly to 85.1 % (30.4 % std. error, p = 0.8231) when 0.05 μM were applied, 1 μM reduced the NO level significantly

to 63.7 % (23.9 % std. Error, $p = 0.0001$) and 5 µM significantly to 26.8 % (6.1 % std. error, $p < 0.0001$). Moreover, did this concentration not show a statistically difference compared to the neg. ctrl. ($p = 0.9214$). C3.0 is less potent than the previous compounds, reducing the NO level non-significantly to 87.0 % (32.9% std. error, $p = 0.9459$) when 0.3 µM were applied, 1.5 µM reduced the NO level non-significantly to 74.5 % (22.9 std. error, $p = 0.0574$) and 5 µM reduced it significantly to 63.1 & (25.8 % std. error, $p < 0.0001$). 0.2 µM of C4.0 reduced the NO level non-significantly to 85.0 % (45.6 % std. error, $p = 0.4358$), 2 µM significantly to 64.0 % (18.1 % std. error, $p < 0.0001$), and 10 µM to 55.1 % (28.0 % std. error, $p < 0.0001$). Interestingly, $5x10^{-4}$ v/v DMSO alone did decrease the NO level significantly to 69.6 % (18.4 % std. error, $p = 0.0009$). Therefore, I tested the dose dependent effect on DMSO using a broad range of DMSO concentration (Figure 3.10), $1x10^{-5}$ v/v = 0.02 µM compound, $1x10^{-4}$ v/v = 2 µM compound, and 0.05 % = 10 µM compound. Those tested concentrations did decrease the NO level significantly but did not show a dose dependent decrease in the NO level as seen for the compounds. Contrariwise, the NO concentration increased in parallel with the increase of the DMSO concentration. 0.001 % with rose Moreover but not in a dose dependent manner. $1x10^{-5}$ v/v DMSO decreased the NO level to 56.2 % (12.5 % std. error, $p < 0.0001$), $1x10^{-4}$ v/v DMSO to 61.8 % (8.6 % std. error, $p < 0.0001$), and $5x10^{-4}$ v/v DMSO to 69.6 % (18.4 % std. error, $p = 0.0009$).

Figure 3.10: IFNγ induced NO release in microglia and the reduction by the compounds.
NO release measured using the Griess assay and normalised to the untreated IFNγ stimulated positive control. Microglia were treated 1 hour before stimulation for additional 48 hours. The solvent control containing only DMSO represent the 3 highest concentrations used. Data is shown as mean + SEM. Statistical significance is shown as * ≤ 0.05, ** ≤ 0.01,*** ≤ 0.001, **** ≤ 0.0001.

3.3.2 PolyIC induced NO release is regulated in a dose dependent manner in primary microglia.

Stimulating primary microglia with 100 µg/ml polyIC increased the detected NO concentration in the supernatant significantly, from 49.2 % (39.3 % std. error) under unstimulated conditions (neg. ctrl.) to 100 % (22.4 % std. error, $p < 0.0001$) under stimulated conditions. All 4 compounds decreased the NO release in a dose dependent manner. C1.0 showed a stronger reducing effect compared to the stimulations with LPS or IFNγ. 0.025 µM decreased the NO level significantly to 66.1 % (27.9 % std. error) compared to the pos. ctrl. ($p < 0.0001$). This reduction in the NO level is statistically not significantly different compared to the neg. ctrl. ($p = 0.2732$). 0.25 µM decreased the NO level below the neg. ctrl. to 29.1 % (14.9 % std. error), significantly different compared to the pos. ctrl. ($p < 0.0001$) but not significantly different to the neg. ctrl. ($p = 0.0803$). 2.5 µM of C1.0 decreased the NO level to 24.7 % (24.5 % std. error), significantly different compared to the

pos. ctrl. ($p < 0.0001$) and compared to the neg. ctrl. ($p = 0.0048$). C2.0 showed a similar reduction in the NO level. 0.05 µM reduced the NO concentration significantly to 62.8 % (15.2 % std. error, $p = 0.0017$), 1 µM to 38.6 % (20.0 % std. error, $p < 0.0001$), and 5 µM 26.2 % (19.9 % std. error, $p < 0.0001$). None of those concentrations were significantly different to the neg. ctrl. (0.05 µM: $p = 0.9763$, 1 µM: $p = 0.9980$, 5 µM: $p = 0.3601$). C3.0 decreased the NO level to a far less extent compared to C1.0 and C2.0. 0.3 µM did not show any effect on the NO level (101.3 %, 14.0 % std. error, $p > 0.9999$), 1.5 µM decreased the NO level non-significantly to 80.7 % (58.6 % std. error, $p = 0.6712$) and 5 µM showed a significant decrease to 62.9 % (19.8 % std. error, $p = 0.0018$). C4.0 showed a significant decrease for all tested concentrations. 0.2 µM decrease the NO level to 80.6 % (16.0 % std. error, $p = 0.0190$), 2 µM to 43.5 % (25.9 % std. error, $p < 0.0001$), and 10 µM to 46.3 % (24.1 % std. error, $p < 0.0001$). Both 2 µM and 10 µM did not show a significant difference compared to the neg. ctrl. $p = 0.9993$, and $p > 0.9999$ respectively. DMSO did not show any effect on the NO level. Here I tested the highest applied concentration of DMOS 0.05 %, equal to 10 µM compound concentration, which resulted in a reduction to a slight but not significant reduction to 89.0 % (12.7 % std. error, $p = 0.9891$).

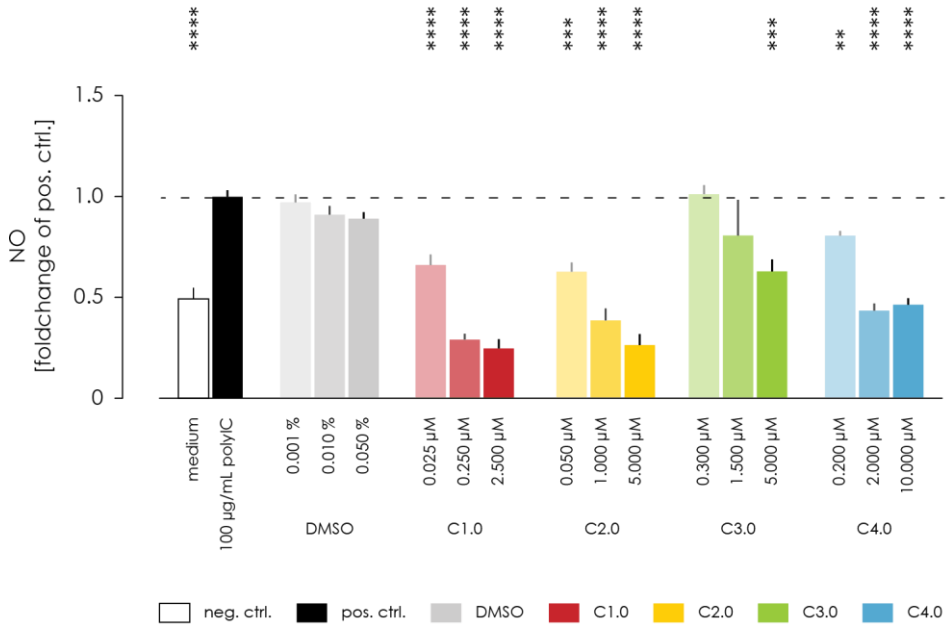

Figure 3.11: The reduction of polyIC induced NO release in microglia by the 4 compounds.
NO release measured using the Griess assay and normalised to the untreated polyIC stimulated positive control. Microglia were treated 1 hour before stimulation for additional 24 hours. The solvent control containing only DMSO represent the 3 highest concentrations used. Data is shown as mean + SEM. Statistical significance is shown as * ≤ 0.05, ** ≤ 0.01,*** ≤ 0.001, **** ≤ 0.0001.

3.4 Selective regulation of LPS induced, IL1ß, IL6, and TNFα release in primary microglia.

Beside the production of NO, microglia do release proinflammatory cytokines upon stimulation with LPS. To study the influence of the compounds on the cytokine release, I treated stimulated microglia as described previously in chapter 3.2 (on page 43) with 1 µg/mL for 48 hours and measured the concentration of the proinflammatory cytokines IL1ß, IL6, and TNFα. All data were normalised to the LPS stimulated positive control (pos. ctrl.).

3.4.1 Selective inhibition of LPS induced release of IL1ß in primary microglia.

Stimulating primary microglia with 1 µg/mL LPS increased the IL1ß release significantly by around 10-fold, from 11.7 % (1.1 % SEM) under unstimulated conditions, to 100 % (16.6 % SEM, $p < 0.0001$) (Figure 3.12). $5x10^{-4}$ v/v DMSO alone did not have a significant effect reducing the IL1ß concentration to 82.4 % (6.3 % SEM, $p = 0.0924$). C1.0 did increase the IL1ß level up to 143.6 % dose dependently. 0.025 µM induced a significant increase of IL1ß to 122.9% (6.1 % SEM, $p = 0.0115$) compared to the pos. ctrl.. With an increased concentration of C1.0 to 0.25 µM the level of IL1ß increased in parallel to 143.6 % (7.3 % SEM, $p < 0.0001$). A further increase to 2.5 µM did not change his elevated IL1ß concentration (142.5 %, 6.1 % SEM, $p < 0.0001$). C2.0 increased the IL1ß level similar to C1.0. 0.05 µM evoked an increase by 5.1 % to 105.1 % (2.1 % SEM, $p > 0.9999$), 1 µM by 14.8 % (114.8 %, 4.6 % SEM, $p = 0.4407$), and 5 µM increased the level of IL1ß even more to 126.0 % (8.8 % SEM, $p = 0.0014$). C3.0 and C4.0 decreased the IL1ß level in a dose dependent manner. While 0.3 µM of C3.0 increased the IL1ß level to 110.5 % (2.7 % SEM, $p = 0.9153$), 1.5 µM keep it at the entry level (99.0 %, 3.8 % SEM, $p > 0.9999$), and 5 µM reduced it to 83.1 % (2.6 % SEM, $p = 0.2431$). None of these values reached significance compared to the pos. ctrl.. C4.0 showed the most potent effect reducing the level of IL1ß, whereas 0.2 µM did alter the IL1ß concentration not significantly (106.4 %, 2.3 % SEM, $p = 0.9998$), 2 µM decreased the IL1ßß level to 86.7 % (2.6 % SEM, $p = 0.7608$) non-significantly, and 10 µM decreased it significantly to 55.5 % (2.6 % SEM, $p < 0.0001$).

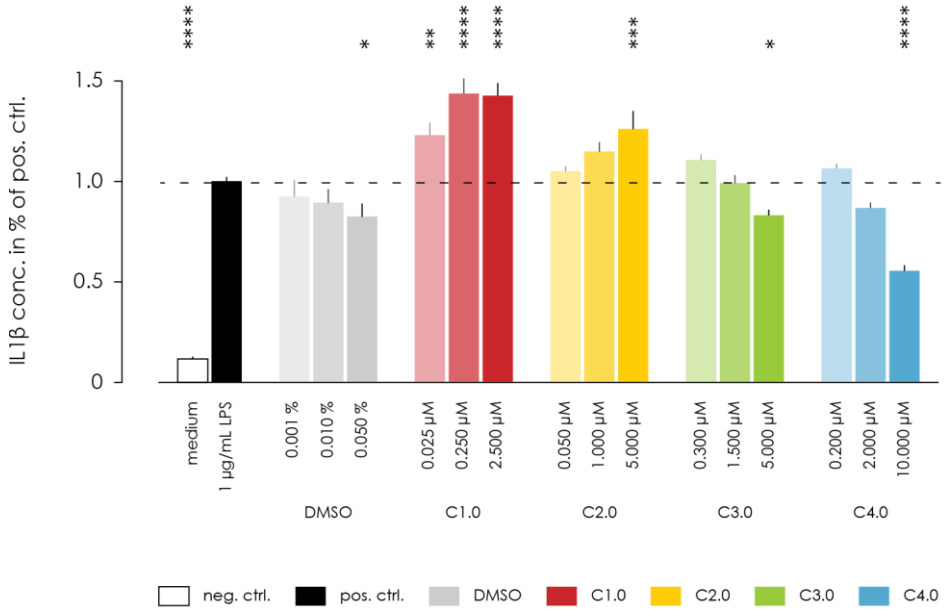

Figure 3.12: Dose dependent influence on LPS induced IL1β release in microglia.
IL1ß release measured using ELISA and normalised to the untreated LPS stimulated positive control. Microglia were treated 1 hour before stimulation for additional 48 hours. The solvent control containing only DMSO represent the 3 highest concentrations used. Data is shown as mean + SEM. Statistical significance is shown as * ≤ 0.05, ** ≤ 0.01,*** ≤ 0.001, **** ≤ 0.0001.

3.4.2 Selective inhibition of LPS induce release of IL6 in primary microglia

In unstimulated conditions the level of IL6 produced by primary microglia is hardly detectable. Stimulating primary microglia with 1 µg/mL increased the IL6 level from 0.9 % (neg. ctrl., 0.1 % SEM) to 100 % (pos. ctrl., 0.7 % SEM, $p < 0.0001$) (Figure 3.13). Treatment with $5x10^{-4}$ v/v DMSO did not influence the increase in IL6 concentration, and remained at 102.8 % (5.8 % SEM, $p > 0.9999$). C1.0 did not show any influence on the induced IL6 production (0.025 µM: 99.5 %, 1.5 % SEM, $p > 0.9999$; 0.25 µM: 100.9 %, 2.7 % SEM, $p > 0.9999$; and 2.5 µM: 98.7 %, 2.22 % SEM, $p > 0.9999$). C2.0 did show a significant dose dependent increase in the IL6 level starting with a concentration of 1 µM. 0.05 µM of C2.0 did not alter the IL6 concentration significantly (100.8 %, 2.65 % SEM, $p > 0.9999$), 1 µM increased the IL6 level significantly by 13.0 % (113.0, 3.5 % SEM, $p = 0.0147$), and 5 µM by 32.8 % (132.8 %, 5.2 % SEM, $p < 0.0001$). C3.0 did show a slight non-significant dose

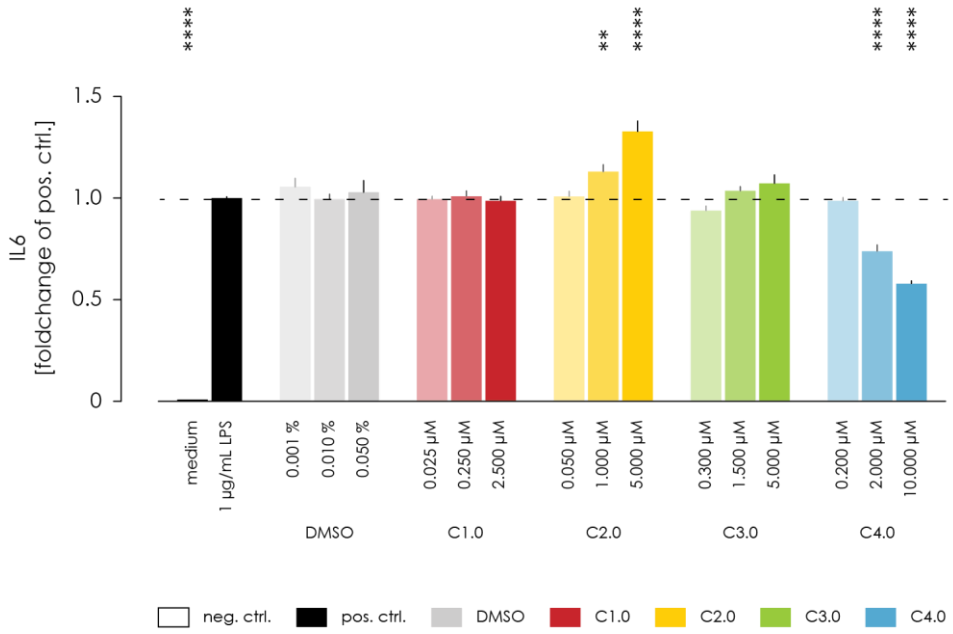

Figure 3.13: Dose dependent influence on LPS induced IL6 release in microglia.
IL6 release measured using ELISA and normalised to the untreated LPS stimulated positive control. Microglia were treated 1 hour before stimulation for additional 48 hours. The solvent control containing only DMSO represent the 3 highest concentrations used. Data is shown as mean + SEM. Statistical significance is shown as * ≤ 0.05, ** ≤ 0.01,*** ≤ 0.001, **** ≤ 0.0001.

dependent increase in the IL6 level (0.3 µM: 93.9 %, 2.3 % SEM, $p > 0.9999$; 1.5 µM: 103.6 %, 2.1 % SEM, $p > 0.9999$; and 5 µM: 107.2 %, 4.3 % SEM, $p > 0.9999$). Out of the 4 tested compounds, only C4.0 decreased the IL6 level significantly in a dose dependent manner. 0.2 µM did not affected the IL6 level significantly (98.7 %, 1.6 % SEM, $p > 0.9999$). However, 2 µM decreased it significantly to 73.9 % (3.2 % SEM, $p < 0.0001$), and 10 µM to 57.9 % (1.4 % SEM, $p < 0.0001$).

3.4.3 Selective inhibition of LPS induce release of TNFα in primary microglia

Upon LPS stimulation microglia increased the production of TNFα significantly from 7.3 % (0.8 % SEM) in unstimulated conditions (neg. ctrl.) to 100 % (1.2 % SEM, $p < 0.0001$). Treatment with $5x10^{-4}$ v/v DMSO alone did not influence the TNFα level significantly (96.7

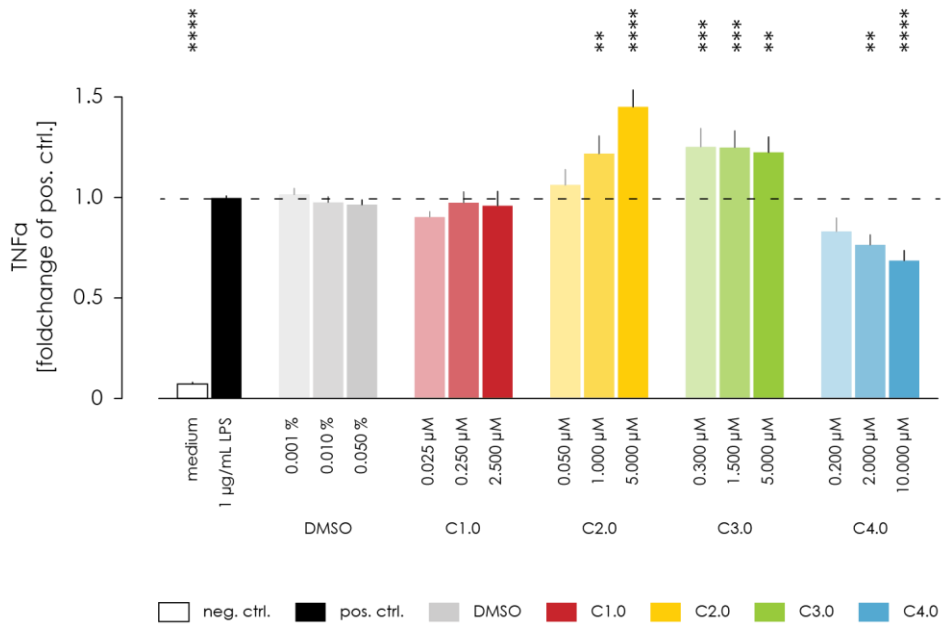

Figure 3.14: Dose dependent influence on LPS induced TNFα release in microglia.
TNFα release measured using ELISA and normalised to the untreated LPS stimulated positive control. Microglia were treated 1 hour before stimulation for additional 48 hours. The solvent control containing only DMSO represent the 3 highest concentrations used. Data is shown as mean + SEM. Statistical significance is shown as * ≤ 0.05, ** ≤ 0.01,*** ≤ 0.001, **** ≤ 0.0001.

%, 2.5 % SEM, p > 0.9999) (Figure 3.14). C1.0 did not show a dose dependent effect on the level of TNFα. The concentration remained above 90 % of the pos. ctrl. 0.025 µM did decreased it to 90.5 % (2.7 % SEM, p = 0.9801), 0.25 µM to 97.6 % (5.5 % SEM, p > 0.9999), and 2.5 µM to 96.1 % (7.2 % SEM, p > 0.9999). C2.0 did increase the TNFα level dependently, starting a non-significant increase to 106.5 % (7.8 % SEM, p = 0.9996) by 0.05 µM treatment, 1 µM increased it significantly to 122.1 % (8.9 % SEM, p = 0.0238), and 5 µM increased it significantly to 145.4 % (8.5 % SEM, p < 0.0001). C3.0 showed a significant increase in the TNFα level compared to the pos. ctrl., but no dose dependent correlation within the tested concentration range. 0.3 µM increased the TNFα level to 125.5 % (0.92 % SEM, p = 0.0027), 1.5 µM to 125.2 % (8.4 % SEM, p = 0.0035), and 5 µM to 122.7 % (7.8 % SEM, p = 0.0168). As already shown for the other two cytokines IL1ß and IL6, C4.0 reduced the TNFα level in a dose dependent manner, significantly. 0.2 µM of C4.0 reduced the TNFα level to 83.3 % (6.7 % SEM, p = 0.2914) non-significantly, 2 µM reduced it significantly to 76.6 % (5.1 % SEM, p = 0.0154), and 10 µM significantly to 68.7 % (5.1 % SEM, p = 0.0001).

For further experiments, I reduced the number of compounds to C1.0 and C4.0. C1.0 was chosen because of the low IC_{50} value of only 252 nM, and its exclusive impact on the induced NO release by LPS, polyIC, and IFNγ while showing no effect on the LPS induced release of the pro-inflammatory cytokines, IL1ß, IL6, TNFα. C4.0 was chosen due to its reducing effect on NO as well as the pro-inflammatory cytokines IL1ß, IL6, and TNFα. C2.0 and C3.0 were excluded because of their high IC_{50} and their negative undetermined impact on the cytokine release.

3.5 The compounds show an analogous effect on primary macrophages as they show on microglia.

Microglia and macrophages share similar activation and regulation pattern. Both upregulate their NO and cytokine production upon a proinflammatory stimulus. I have shown in the previous experiments, that C1.0 decreases the induced NO but not cytokines release in a dose dependent manner, and that C4.0 decrease induced NO and cytokine in primary microg. Here, I evaluate the effect of the compounds on the induced NO and cytokine release in primary cultured derived macrophages. I evaluated the NO release after stimulation with 1 µg/mL LPS or 100 ng/ml IFNγ for 48 hours, or 100 µg/mL polyIC for 24 hours. The release of the cytokines IL1ß, IL6, and TNFα was evaluated after the stimulation with 1 µg/mL LPS for 48 hours. The protocol used for macrophages and microglia differed only in the number of seeded cells (100.000 microglia/well, 50.000 macrophages/well). 50 000 macrophages per well were seeded 1 day prior to the start of the assay. The cells were treated with defined concentrations of DMSO, C1.0, or C4.0 for one hour, followed by an additional stimulation for 24/48 hours.

3.5.1 LPS induced NO release is reduced by compound C1.0 and C4.0 in a dose depended manner.

Upon 1 µg/mL LPS stimulation for 48 hours the NO concentration in the supernatant of macrophages increased significantly from 6.0 % (0.6 % SEM) to 100 % (1.3 % SEM, $p < 0.0001$). A concentration of $5x10^{-4}$ v/v DMSO did not change the increased NO level significantly (93.0 %, 2.2 % SEM, $p = 0.6969$). Treatment with compound C1.0 decreased the NO level significantly in a dose dependent manner. 0.025 µM C1.0 did not show a significant decrease in the NO level (93.6 %, 4.5 % SEM, $p = 0.8123$), however 0.25 µM reduced the NO level significantly to 44.4 % (4.6 % SEM, $p < 0.0001$). 2.5 µM of C1.0 reduced the NO level below the neg. ctrl. of 6.0 % to only 4.9 % (0.7 % SEM). This reduction is significantly different to the pos. ctrl. ($p < 0.0001$), but not to the neg. ctrl. ($p > 0.9999$). The treatment with compound C4.0 showed again a dose dependent reduction of the NO concentration, but far less potent than compound C1.0. 0.2 µM C4.0 did not show a significant influence on the NO level (89.4 %, 3.8 % SEM, $p = 0.1208$). 2 µM reduced the NO level significantly to 70.8 % (3.0 % SEM, $p < 0.0001$) and 10 µM to 48.9 % (3.7 % SEM, $p < 0.0001$).

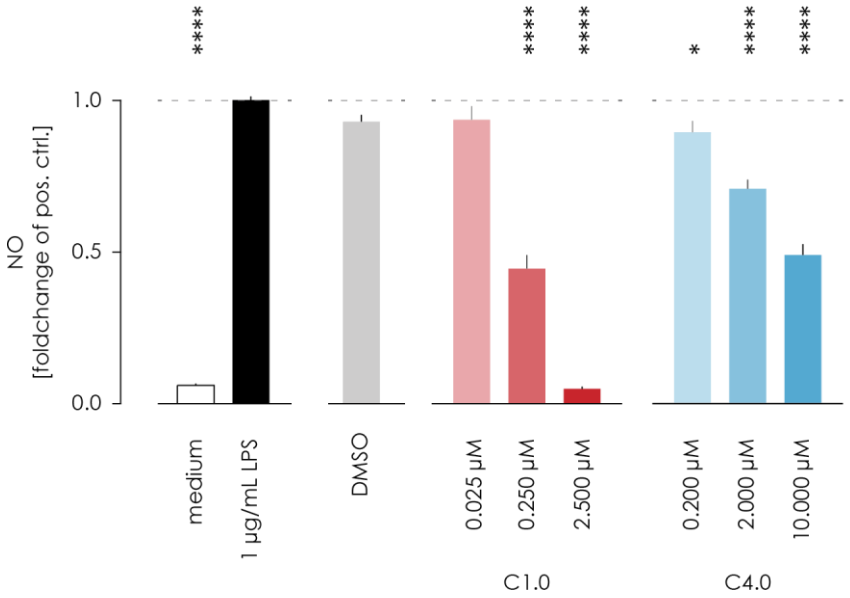

Figure 3.15: Dose dependent reduction of LPS induced NO release in macrophages.
NO release measured using the Griess assay and normalised to the untreated LPS stimulated positive control. Macrophages were treated 1 hour before stimulation for additional 48 hours. Data is shown as mean + SEM. Statistical significance is shown as * ≤ 0.05, ** ≤ 0.01,*** ≤ 0.001, **** ≤ 0.0001. All data are normalised to the pos. ctrl.

3.5.2 C1.0 and C4.0 do not interfere with metabolic activity in LPS stimulated macrophages.

In parallel to the evaluation of influence on the NO level, I assessed the compounds impact on macrophages metabolic activity using the AlamarBlue assay. In contrast to microglia, the metabolic activity of macrophages does not significantly increase upon LPS stimulation. Under unstimulated conditions the metabolic activity remained at 89.5 % (4.7 % SEM), compared to 100 % (0.9 % SEM, p = 0.8822) after LPS stimulation. DMSO did not affect the metabolic activity of activated macrophages (87.5 %, 4.0 % SEM, p = 0.8090). Treatment with compound C1.0 did selectivity decrease the metabolic activity in a significant manner but did not show a dose dependency. 0.025 µM decreased significantly to 69.2 % (8.4 % SEM, p = 0.0013), 0.25 µM non-significantly to 78.5 % (7.1 % SEM, p = 0.0878), and 2.5 µM again significantly to 66.5 % (7.6 % SEM, p = 0.0005). Compound C4.0 did show a similar impact on the metabolic activity of macrophages, 0.2 µM decreased it to 79.8 % (5.9 % SEM, p = 0.1556) in a non-significant manner, 2 µM in a significant

manner to 71.6 % (4.2 % SEM, p = 0.0037), and 10 µM also significantly to 73.2 % (4.0 % SEM, p = 0.0126).

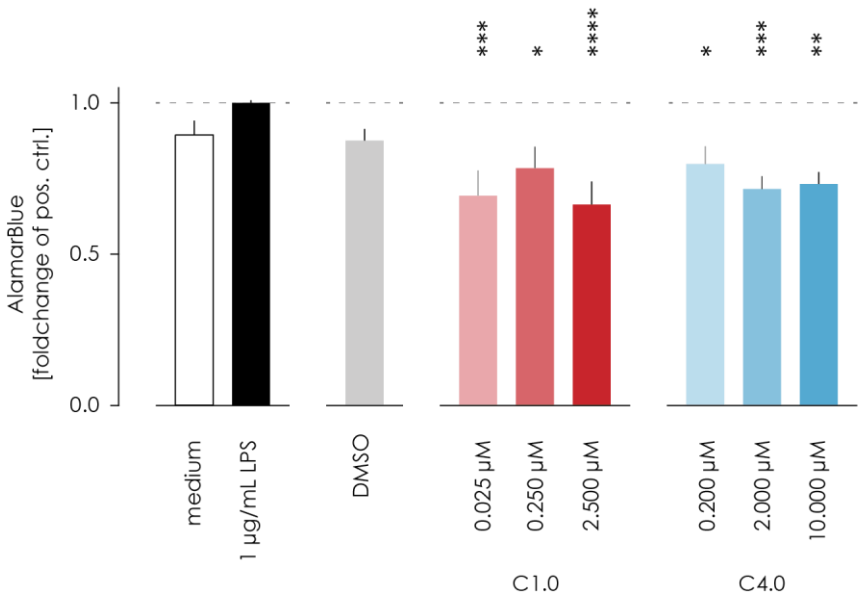

Figure 3.16: Dose dependent influence on LPS elevated macrophages metabolic activity.
Macrophages metabolic activity measured using the AlamarBlue assay and normalised to the untreated LPS stimulated positive control. Macrophages were treated 1 hour before stimulation for additional 48 hours. Afterwards the AlamarBlue assay was carried out for ca. 3 hours. Data is shown as mean + SEM. Statistical significance is shown as * ≤ 0.05, ** ≤ 0.01,*** ≤ 0.001, **** ≤ 0.0001. All data are normalised to the pos. ctrl.

3.5.3 IFNγ induced NO release in primary macrophages is regulated in a dose dependent manner.

Upon stimulation with 100 ng/mL IFNγ the NO concentration increased significantly from 28.8 % (1.6 % SEM) under unstimulated conditions to 100 % (2.5 % SEM, p < 0.0001). $5x10^{-4}$ v/v of DMSO alone decreased the NO level to 84.5 % (2.6 % SEM) significantly (p = 0.0096). To evaluate weather this effect is dose dependent, I repeated the assay with a concentration of $1x10^{-5}$ v/v and $1x10^{-4}$ v/v DMSO. Both concentration of DMSO showed a

similar reduction in the NO concentration, indicating a dose independent effect on the IFNγ induced NO release ($1x10^{-5}$ v/v DMSO: 84.5 %, 2.6 % SEM, $p = 0.0090$, $1x10^{-4}$ v/v DMSO: 83.5 %, 2.8 % SEM, $p = 0.0034$). Compound C1.0 did decrease the NO level in a dose dependent manner, starting with a reduction to 78.6 % (3.9 % SEM, $p < 0.0001$) with a concentration of 0.025 µM applied. This reduction is significantly different to the pos. ctrl. ($p < 0.0001$) but not the DMSO control ($p = 0.9520$). 0.25 µM decreased the NO level significantly to 46.0 % (3.6 % SEM) compared to the pos. ctrl. ($p < 0.0001$) and the DMSO ($p < 0.0001$). And 2.5 µM reduced it below the neg. ctrl. to 18.4 % (2.2 % SEM). This reduction is significantly different to the pos. ctrl ($p < 0.0001$) and DMSO ($p < 0.0001$), but not significantly different to the neg. ctrl. ($p = 0.2146$). The dose dependent reduction of compound C4.0 is less potent compared to compound C1.0. 0.2 µM. 0.2 µM of compound C4.0 reduced the NO level to 75.9 % (4.2 % SEM) significantly different to the pos. ctrl. ($p < 0.0001$) but not to DMSO ($p = 0.6018$). 2 µM reduced the NO level significantly different to pos. ctrl. ($p < 0.0001$) and DMSO ($p < 0.0001$) to 52.3 % (3.4 % SEM), and 10 µM reduced the NO level to 40.1 % (3.8 % SEM) significantly different to pos. ctrl. ($p < 0.0001$) and DMSO ($p < 0.0001$) but not to the neg. ctrl. ($p = 0.2782$).

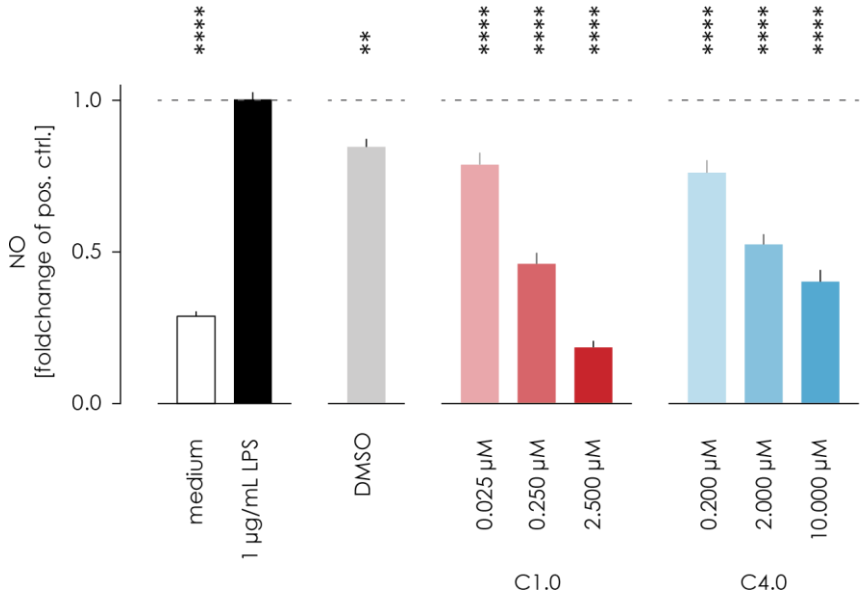

Figure 3.17: Dose dependent reduction of IFNγ induced NO release in macrophages.
NO release measured using the Griess assay and normalised to the untreated IFNγ stimulated positive control. Macrophages were treated 1 hour before stimulation for additional 48 hours. Data is shown as mean + SEM. Statistical significance is shown as * ≤ 0.05, ** ≤ 0.01,*** ≤ 0.001, **** ≤ 0.0001. All data are normalised to the pos. ctrl.

3.5.4 PolyIC induced NO release in primary macrophages is regulated in a dose dependent manner.

Stimulating macrophages with 100 µg/mL polyIC for 24 hours results in a similar outcome as described for the stimulation with LPS and IFNγ. Upon stimulation with polyIC the NO concentration increased significantly from 24.3 % (2.4 % SEM) to 100 % (3.1 % SEM, $p < 0.0001$). DMSO did not show any significant effect on the NO level (94.2 %, 3.5 % SEM, $p = 0.9217$). As shown for the other stimulations, compound C1.0 decreased the NO concentration in a dose dependent manner. 0.025 µM did not show a significant effect on the NO level (99.3 %, 5.1 % SEM, $p > 0.9999$), 0.25 µM decreased the NO level to 38.7 % (3.4 % SEM), significantly different to the pos. ctrl. ($p < 0.0001$) but not to the neg. ctrl. ($p = 0.2582$), and 2.5 µM reduced the NO level below neg. ctrl. to only 15.0 % (1.8 % SEM) significantly different to the pos. ctrl. ($p < 0.0001$) but not the neg. ctrl. ($p = 0.7708$). Compound C4.0 showed a similar pattern, decreasing the NO level to 82.9 % (3.8 % SEM)

significantly different compared to pos. ctrl. (p = 0.0111) but not DMSO (p = 0.4890) when concentration of 0.2 µM was applied. A concentration of 2 µM decreased the NO level significantly to 61.9 % (3.4 % SEM, p < 0.0001), and 10 µM to 40.9 % (5.0 % SEM, p < 0.0001). The reduction caused by any concentration of C4.0 were significantly higher than the neg. ctrl..

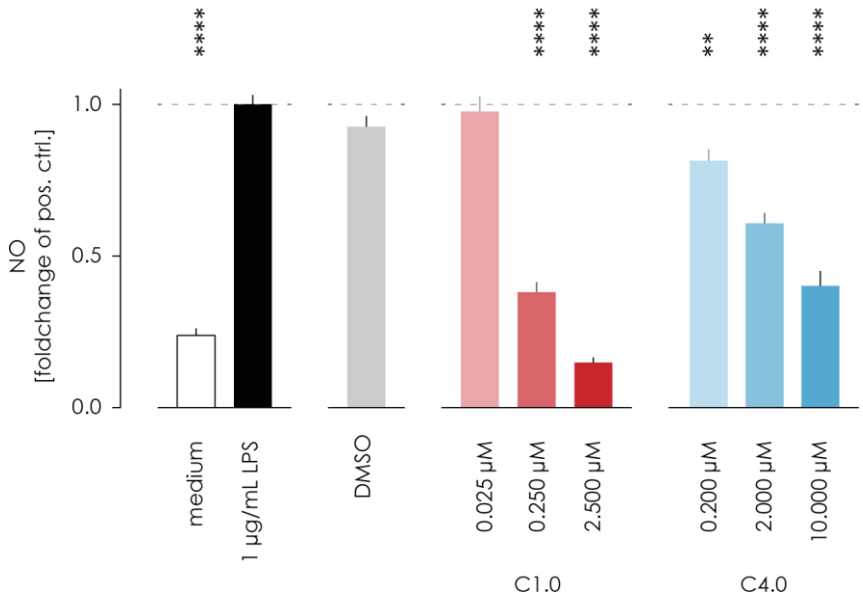

Figure 3.18: Dose dependent reduction of polyIC induced NO release in macrophages.
NO release measured using the Griess assay and normalised to the untreated polyIC stimulated positive control. Macrophages were treated 1 hour before stimulation for additional 48 hours. Data is shown as mean + SEM. Statistical significance is shown as * ≤ 0.05, ** ≤ 0.01,*** ≤ 0.001, **** ≤ 0.0001. All data are normalised to the pos. ctrl.

3.6 The different regulation of LPS induced pro-inflammatory cytokines release in primary macrophages.

The compounds do influence the LPS induced cytokine release in macrophages in an analogous way as they do in microglial. LPS (1 µg/mL) stimulation upregulate the release of

IL1ß, IL6, and TNFα more than 10-fold. Compound C1.0 does not show a reducing effect on any of tested cytokines, whereas compound C4.0 reduces the induced cytokine release in a dose dependent manner.

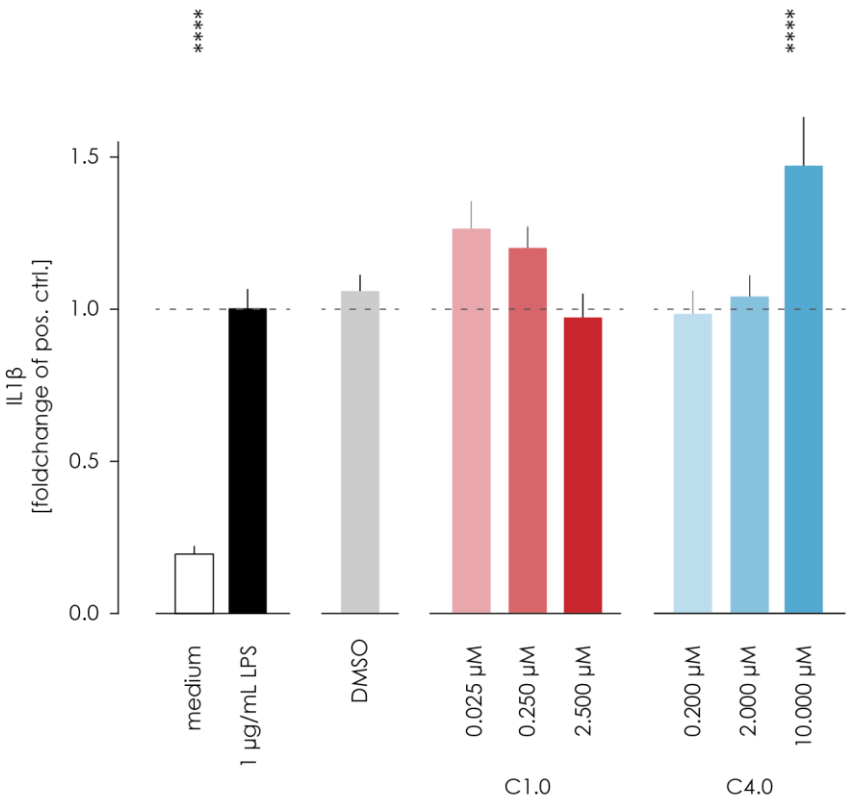

Figure 3.19: Dose dependent influence on LPS induced IL1β release in macrophages.
IL1ß release measured using ELISA and normalised to the untreated LPS stimulated positive control. Macrophages were treated 1 hour before stimulation for additional 48 hours. Data is shown as mean + SEM. Statistical significance is shown as * ≤ 0.05, ** ≤ 0.01,*** ≤ 0.001, **** ≤ 0.0001. All data are normalised to the pos. ctrl.

IL1ß is upregulated significantly upon stimulation from 19.7 % (2.5 % SEM) to 100 % (6.4 % SEM, $p < 0.0001$). DMSO did not influence this upregulation (105.8 %, 5.3 % SEM, $p > 0.9999$). In contrast to the effect on microglia, compound C1.0 did not overshoot LPS induced the IL1ß release. All applied concentrations of compound C1.0 are not significantly different from the pos. ctrl. and DMSO. 0.025 µM caused an slight increase to 126.3 % (9.0 % SEM, $p = 0.5858$), 0.25 µM to 120.0 % (7.0 % SEM, $p = 0.8561$), and 2.5 µM to 97.1 % (7.8 % SEM, $p > 0.9999$). Also compound C4.0 did act differently on macrophages than it did on microglia. 0.2 µM and 2 µM of compound C4.0 did not have a significant effect on

the IL1ß level (0.2 µM: 98.3 %, 7.6 % SEM, p > 0.9999; 2 µM 104 %, 7.1 % SEM, p > 0.9999), and 10 µM overshoot the LPS induced IL1ß release significantly, increasing the level to 146.9 % (16.0 % SEM, p = 0.0048).

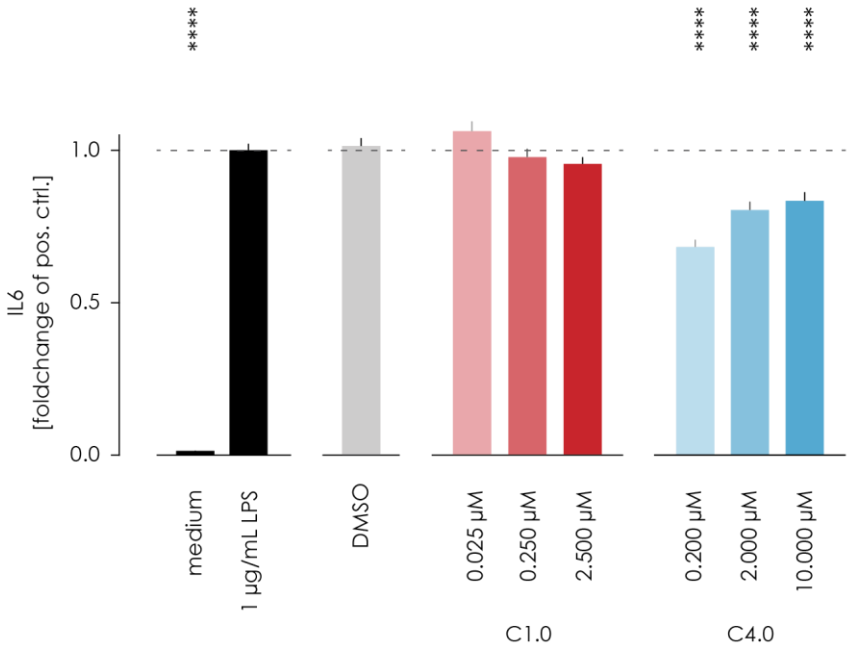

Figure 3.20: Dose dependent influence on LPS induced IL6 release in macrophages.
IL6 release measured using ELISA and normalised to the untreated LPS stimulated positive control. Macrophages were treated 1 hour before stimulation for additional 48 hours. Data is shown as mean + SEM. Statistical significance is shown as * ≤ 0.05, ** ≤ 0.01,*** ≤ 0.001, **** ≤ 0.0001. All data are normalised to the pos. ctrl.

Upon LPS stimulation the release of IL6 is increased from 1.4 % (0.2 % SEM) to 100 % (2.1 % SEM, p < 0.0001). DMSO alone did not influence this increase keeping the untreated stimulated IL6 level (101.3 %, 2.7 % SEM, p > 0.9999). Compound C1.0 remained the IL6 concentration at above 95 % independent from the applied concentration (0.025 µM: 106.2 %, 3.3 % SEM, p = 0.7096; 0.25 µM: 97.7 %, 2.7 % SEM, p = 0.9998; 2.5 µM: 95.4 %, 2.3 % SEM, p = 0.9428). Compound C4.0 showed an increase in IL6 with an increase in the applied concentration. This increase started and ended significantly below the pos. ctrl.. 0.2 µM decreased the IL6 level significantly compared to the pos. ctrl. to 68.2 % (2.3 % SEM, p < 0.0001), 2 µM to 80.5 % (2.7 % SEM, p < 0.0001), and 10 µM to 83.3 % (2.9 % SEM, < 0.0001).

The TNFα is increased from 2.8 % (0.4 % SEM) to 100 % (1.7 % SEM, $p < 0.0001$) upon LPS stimulation. DMSO did not affect this increase, keeping the IL1ß level at 96.5 % (2.2 % SEM, $p > 0.9999$). The treatment with compound C1.0 did not change the level of TNFα significantly, keeping the values above 90 % (0.025 µM: 94.3 %, 2.3 % SEM, $p = 0.6557$; 0.25 µM: 95.1%, 2.5 % SEM, $p = 0.8701$; 2.5 µM: 91.0 %, 1.8 % SEM, $p = 0.1141$). Compound C4.0 effected the TNFα release similar as described for IL6. Low concentrations of C4.0 decreased the TNFα level more than high concentrations. 0.2 µM reduced the level significantly to 87.5 % (2.6 % SEM, $p = 0.0008$), 2 µM significantly to 87.0 % (2.7 % SEM, $p = 0.0005$, and 10 µM non-significantly to 95.0 % (2.5 % SEM, $p = 0.8073$).

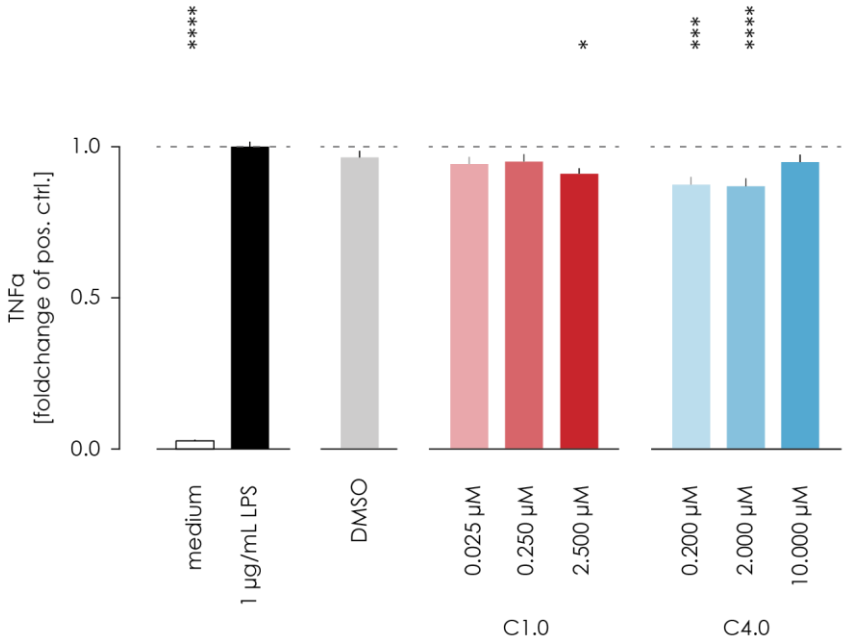

Figure 3.21: Dose dependent influence on LPS induced TNFα release in macrophages.
TNFα release measured using ELISA and normalised to the untreated LPS stimulated positive control. Macrophages were treated 1 hour before stimulation for additional 48 hours. Data is shown as mean + SEM. Statistical significance is shown as * ≤ 0.05, ** ≤ 0.01,*** ≤ 0.001, **** ≤ 0.0001. All data are normalised to the pos. ctrl.

3.7 Compound C1.0 and C4.0 do influence the AlamarBlue, PI and NO readout in high concentrations.

To study the direct influence of the compound 1 and 4 on the AlamarBlue assay, the PI driven Dead-or-Alive assay and the nitric oxide assay I conducted those assays without the presence of cells. I prepared a concentration series of the compound 1 and 4 starting from 2 µM and reaching up to 4 mM (2, 4, 20, 40, 200, 400, 2000, 4000 µM) diluted in plain cell culture medium. In parallel I diluted the solvent DMSO in the corresponding concentration of the compound, reaching from $1x10^{-4}$ up to $2x10^{-1}$ v/v ($1x10^{-4}$, $2x10^{-4}$, $1x10^{-3}$, $2x10^{-3}$, $1x10^{-2}$, $2x10^{-2}$, $1x10^{-1}$, $2x10^{-1}$ v/v). Those concentrations were plated into the same 96-well plates as used for the cell-based assays, and the assays specific wavelength were measured. Plain cell culture medium served as the negative control and was subtracted from all measured values.

3.7.1 High doses of C1.0, C4.0, and DMSO increase the measured values of nitric oxide.

Figure 3.22 illustrates the dose dependent influence on Griess assay relevant wavelength of 550 nm. The data was assessed using the identical plate reader and program as for the cell-based assay, 550 nm wavelength with a bandwidth of 9 nm and 3 repeated flashes. All applied substances influenced the readout in a positive linear fashion. DMSO showed a slight but significant dose dependent increase with a linear regression defined by a slope of $2.023\ 10^{-5}$ ($\pm 6.786\ 10^{-6}$) and an interception of $-8.732\ 10^{--4}$ (± 0.01078, $R^2 = 0.5971$, $p = 0.0246$). Compound 1.0 showed a steeper significant increase with a linear regression defined by a slope of $4.284\ 10^{-4}$ ($\pm 2.492\ 10^{-5}$) and an interception of $-3.496\ 10^{-2}$ ($\pm 3.96\ 10^{-2}$, $R^2 = 0.9801$, $p < 0.0001$). Compound 4.0 showed similar significant result as compound 1.0 resulting in a linear regression defined by a slope $3.197\ 10^{-4}$ ($\pm 1.135\ 10^{-5}$) of and an interception of $-9.928\ 10^{-3}$ ($\pm 1.804\ 10^{-2}$, $R^2 = 0.9925$, $p < 0.0001$).

DMSO and the compounds artificially increase the calculated NO concentration by directly interfering with the measured wavelength. This increase acts contrary to the detected decrease in NO (see Figure 3.6, Figure 3.10, Figure 3.11, Figure 3.15, Figure 3.17, and Figure 3.18), and therefore cannot be the reason for the observed reducing effect.

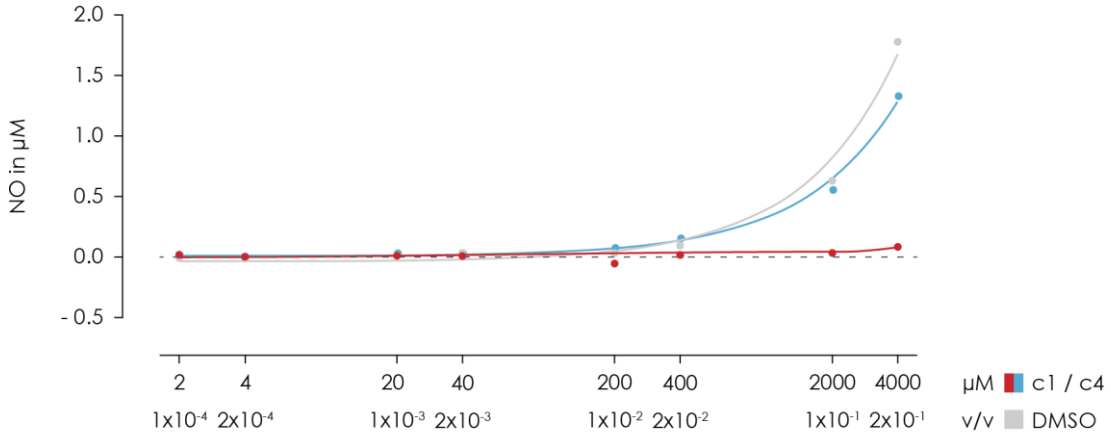

Figure 3.22: Direct dose dependent influence on the read out of the Griess assay.
Different compound concentrations ranging from 2 µM to 4 mM were incubated with the Griess reagents and their influence on the Griess assay read out was measured. DMSO concentration ranged from 0.0001 to 0.2 v/v.

Treatment		Values	95 % confidence interval			different from zero	
DMSO	slope	2x10-5 µM	0.00000363	to	3.68E-05	0.0246	*
	intercept	-9x20-4 µM	-0.02726	to	0.02551		
C1.0	slope	4x10-4 µM	0.0003674	to	0.000489	< 0.0001	****
	intercept	-3x10-2 µM	-0.1319	to	0.06194		
C4.0	slope	3x10-4 µM	0.000292	to	0.000348	< 0.0001	****
	intercept	1x10-2 µM	-0.03422	to	0.05408		

Table 3.4: Description of the linear regression curves of the compounds influence the Griess assay.

3.7.2 The AlamarBlue readout is affected by C1.0, C4.0, and DMSO.

The effect on the measurement wavelength of 570 nm and a reference wavelength of 600 nm are illustrated in Figure 3.23. Both wavelengths were measured the same way as the

cell-based assay was performed. The applied substances showed a similar effect on the measurement and reference wavelength of the AlamarBlue assay as they have shown for the nitric oxide assay. DMSO, compound 1.0 and 4.0 did increase the readout significantly and dose dependently in a linear fashion. The data for the linear regressions are shown in Table 3.5. For a precise calculation of the AlamarBlue assay, the reference wavelength is subtracted from the measurement wavelength. However, this calculation did not prevent an influence of the compounds 1.0 and 4.0 on the AlamarBlue readout, as shown in Figure 3.23 and the corresponding Table 3.5.

DMSO and the compounds artificially increased the calculated metabolic activity detected by the AlamarBlue by interfering with both the measurement and reference wavelength. This might counteract a negative effect of the compounds on the metabolic activity of primary microglia, shown in Figure 3.9 and Figure 3.16. However, below a concentration of 40 µM the maximal interference was 0.023, whereas the absorbance of LPS stimulated microglia were 0.258 (0.0224 SEM), resulting in an interference of 9.22 % and are smaller than the SEM of the positive ctrl.

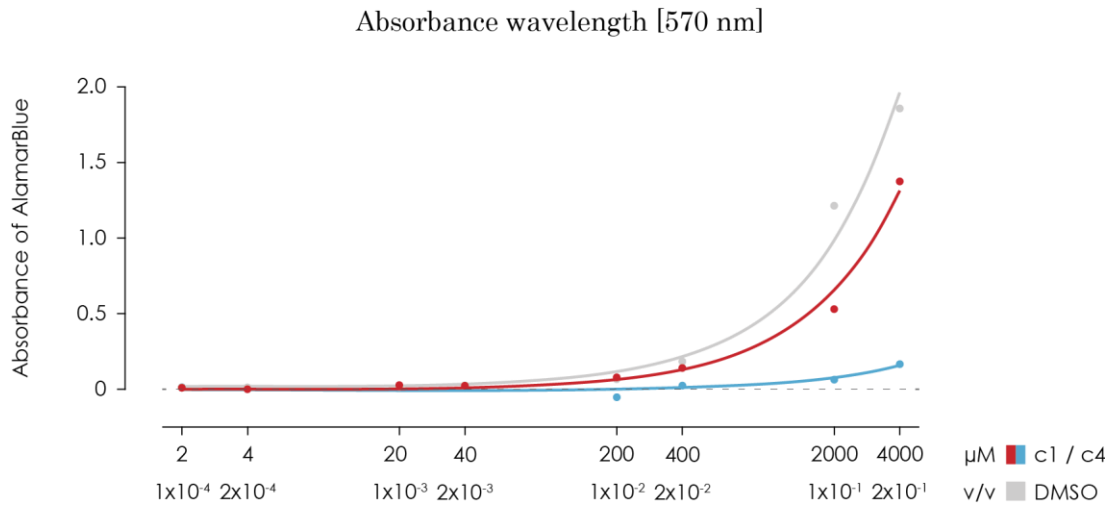
Absorbance wavelength [570 nm]
Absorbance of AlamarBlue
2.0
1.5
1.0
0.5
0
2 4 20 40 200 400 2000 4000
1x10-4 2x10-4 1x10-3 2x10-3 1x10-2 2x10-2 1x10-1 2x10-1
µM c1 / c4
v/v DMSO

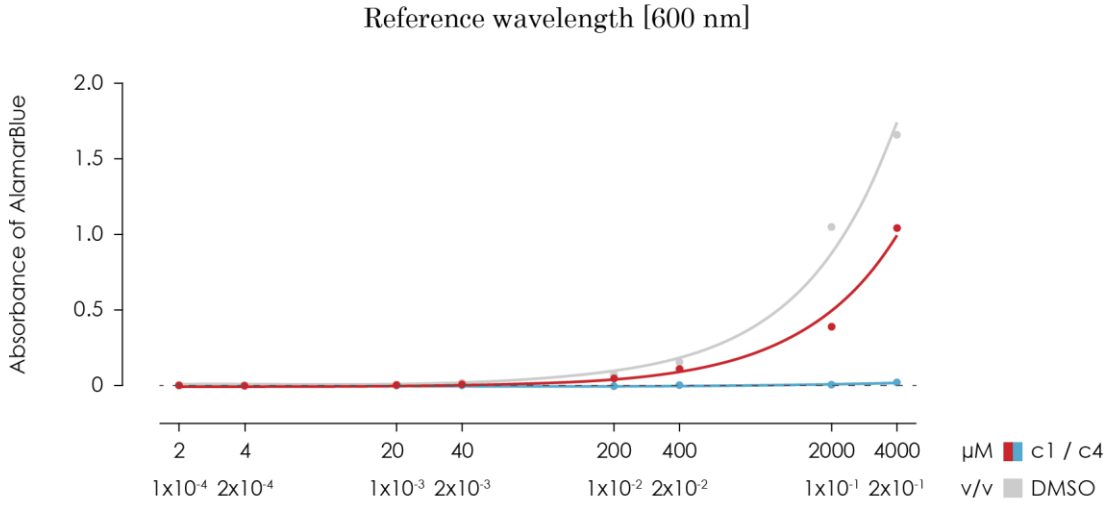
Reference wavelength [600 nm]
Absorbance of AlamarBlue
2.0
1.5
1.0
0.5
0
2 4 20 40 200 400 2000 4000
1x10-4 2x10-4 1x10-3 2x10-3 1x10-2 2x10-2 1x10-1 2x10-1
µM c1 / c4
v/v DMSO

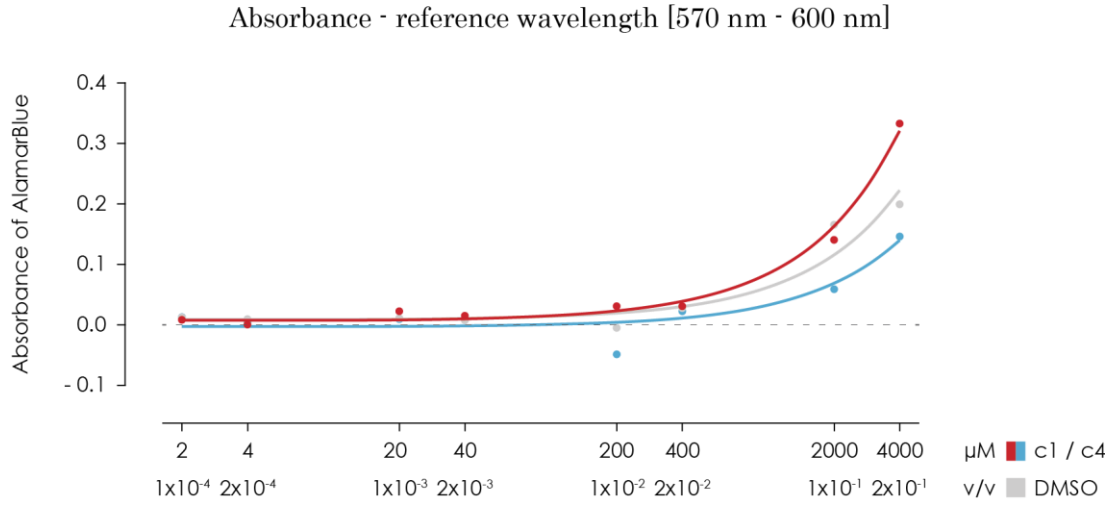
Absorbance - reference wavelength [570 nm - 600 nm]
Absorbance of AlamarBlue
0.4
0.3
0.2
0.1
0.0
- 0.1
2 4 20 40 200 400 2000 4000
1x10-4 2x10-4 1x10-3 2x10-3 1x10-2 2x10-2 1x10-1 2x10-1
µM c1 / c4
v/v DMSO

Figure 3.23: Direct dose dependent influence on the readout of the AlamarBlue assay.
Different compound concentrations ranging from 2 µM to 4 mM were incubated with the Griess reagents and their influence on the Griess assay read out was measured. DMSO concentration ranged from 0.0001 to 0.2 v/v.

Treatment		Value	95 % confidence interval			different from zero	
DMSO	slope	$2x10^{-5}$ µM	$3.6x10^{-6}$	to	$3.6 x10^{-5}$	0.0013	**
	intercept	$-9x10^{-4}$ µM	-0.02726	to	0.02551		
C1.0	slope	$4x10^{-4}$ µM	0.00037	to	0.000489	< 0.0001	****
	intercept	$-3x10^{-2}$ µM	-0.1319	to	0.06194		
C4.0	slope	$3x10^{-4}$ µM	0.00029	to	0.000348	< 0.0001	****
	intercept	$1x10^{-2}$ µM	-0.03422	to	0.05408		

Table 3.5: Description of the linear regression curves of the compounds influence the AlamarBlue assay.

3.7.3 The readout of PI is shifted by high concentrations of C1.0, C4.0, and DMSO.

The influence of DMSO, compound 1.0 and 4.0 on the PI driven Dead-or-Alive assay are illustrated in Figure 3.24. DMSO, compound 1.0 and 4.0 did show a dose-dependent effect on the readout in a linear fashion, significantly different from the zero. The single values of the linear regression defining the increase are given in Table 3.6.

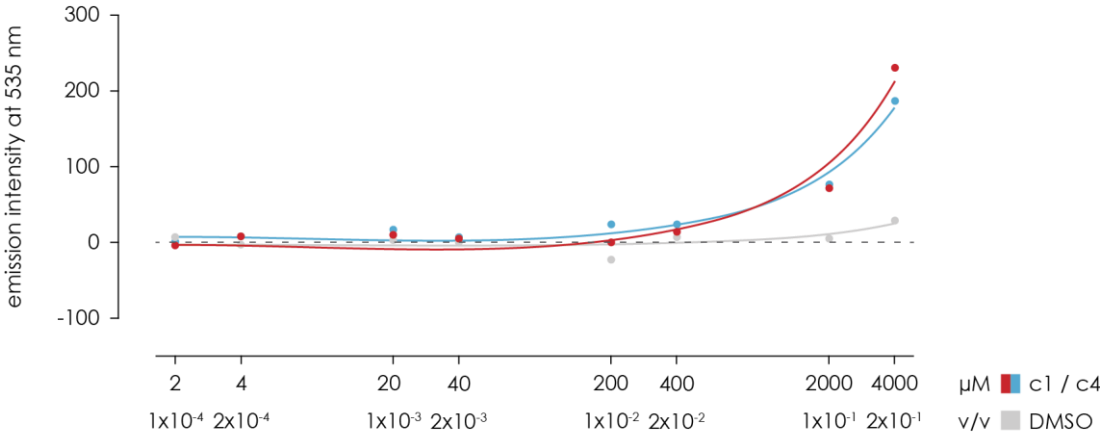

Figure 3.24: Direct dose dependent influence on the read out of the PI-based proliferation and cell death assay.
Different compound concentrations ranging from 2 µM to 4 mM were incubated with the Griess reagents and their influence on the Griess assay read out was measured. DMSO concentration ranged from 0.0001 to 0.2 v/v.

Treatment		value	95 % confidence interval			different from zero	
DMSO	slope	0.007 µM	0.000143	to	0.01398	0.0467	*
	intercept	-2.759 µM	-13.75	to	8.235		
C1.0	slope	0.054 µM	0.04328	to	0.06557	< 0.0001	****
	intercept	-3.226 µM	-20.94	to	14.48		
C4.0	slope	0.043 µM	0.03719	to	0.04921	< 0.0001	****
	intercept	7.255 µM	-2.293	to	16.8		

Table 3.6: Description of the linear regression curves of the compounds influence on the PI-based proliferation and cell death assay.

3.7.4 Compound C1.0 and C4.0 are soluble in the used concentration range but precipitate in high concentrations.

Next, I studied the solubility of compound 1.0 and 4.0 in plain cell culture medium (DMEM) to ensure that the full potential of the applied concentration can be utilized.

Moreover, crystals or other solid forms of the compound can trigger unwanted side-effects, as activation of microglia. I used the same concentration range dissolved in DMEM as described in chapter 3.7, ranging from 2 µM up to 4 mM for the compounds and $1x10^{-4}$ up to $2x10^{-1}$ v/v for DMSO. 200 µL of those were plated into a clear bottom 96-well plate, sealed with a PCR-foil to prevent a change in concentration due to evaporation and incubated for 48 hours under cell culture conditions to maintain the previous assay conditions. Afterwards, a picture of each well was taken using a 40x fold brightfield microscope. The results are shown in Figure 3.25 below. Due to handling process small irritations, like linear and doted scratches, could not be prevented, as they can be seen in the DMEM control conditions. DMSO alone does not show any dose dependent formations of crystals or other solid aggregations. Compound 1.0 showed white milky visual contaminations starting from 20 µM up to 40 µM. An increase in compounds concentration was accompanied by an enlargement of the visual contaminations. From a concentration 200 µM on, a clear formation of crystals could be observed, starting with a small white rod like crystals in a high density at 200 µM. Those crystals grew in size and decreased in number with in an increase in compound concentration. Compound 4.0 did show visual contaminations starting from 200 µM, indicated by a white milky colouring. With an increase in concentrations, these milky colouring changed from transparent to opaque. No discrete crystals could be seen for compound 4.0 in any concentration. The observed visual contaminations appeared in parallel with the previously reported influence on the readout of the NO, the AlamarBlue and the PI based Dead-Or-Alive assay. The visual contaminations arose in concentrations that are at least 8-fold higher (for compound 1.0, and 20-fold for compound 4.0) than the applied concentrations.

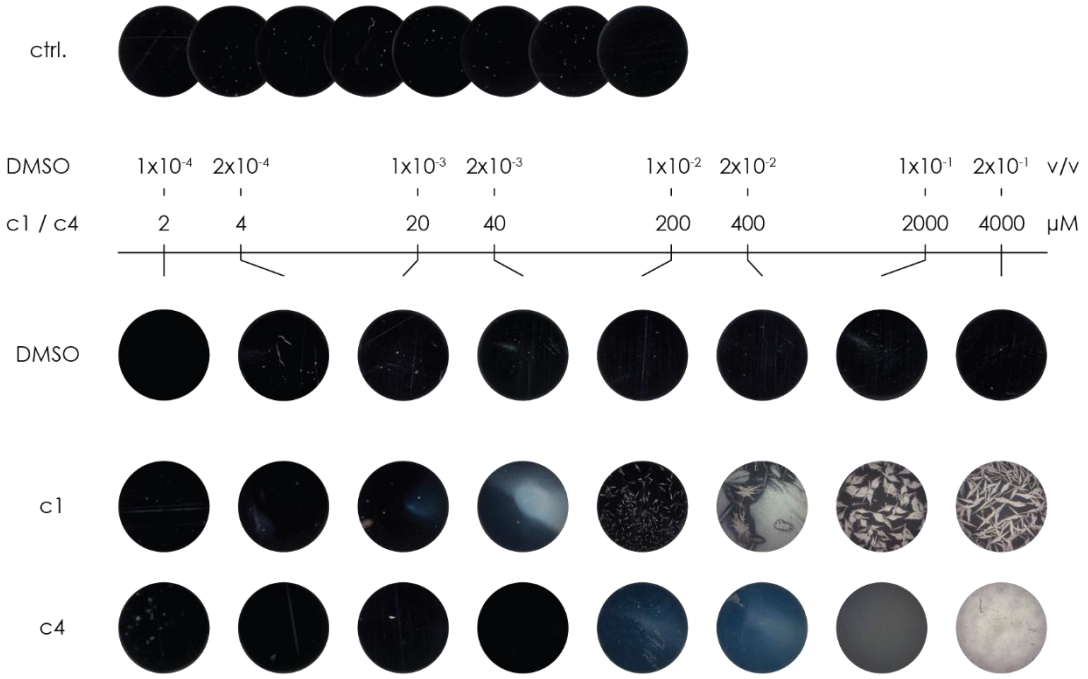

Figure 3.25: Solubility the compounds in PBS.
Images of compounds and DMSO dissolved in PBS and incubated for 48 hours in a sealed 96 well plate.

3.7.5 C1.0 and C4.0 do not act as a NO-Scavenger.

I have excluded an effect of the compound C1.0 and C4.0, as well as DMSO on the readout of the NO assay, and the AlamarBlue and PI based Dead-Or-Alive assay. Next, I reviewed the effect NO itself, testing if the compounds are able to clear it directly from the cell culture medium. Therefore, I harvested NO enriched medium from LPS stimulated primary microglia (1 µg/mL LPS stimulation for 48 h). I transferred this enriched medium into a new 96-well plate and added a defined concentration of DMSO or the compounds. For the compounds I used a concentration range representing the previous used concentration, starting from 0.002 µM up to 20 µM (0.002, 0.01, 0.02, 0.1, 0.2, 1, 2, 10, and 20 µM). The corresponding DMSO concentration range started at $1x10^{-7}$ % up to $1x10^{-3}$ v/v. The enriched medium was incubated with the compounds or DMSO overnight and the NO concentration was measured using the Griess assay. As a positive control untreated NO

enriched medium was used and as negative control the supernatant of unstimulated primary microglia was used. All values were normalised to positive control. The results illustrated in Figure 3.26 did not show a dose dependent reduction in measured NO level. Fitting the values with the previous used IC_{50} curve was not convergent, however, a fitting with linear regression resulted in a function with a slope that is not significantly different from a horizontal line, indicating no dose dependent increase or decrease in NO. Singular values of compound 1.0 show a significant decrease compared to the positive control, 0.1 µM with p = 0.0095, and 1 µM with p = 0.0007. Only 0.1 µM of compound 1.0 was significant different to DMOS control (p = 0.0157).

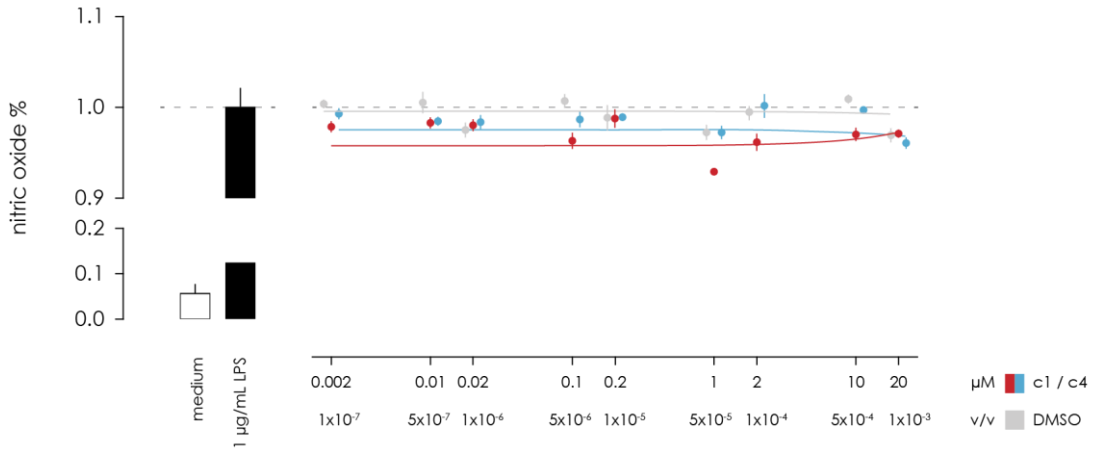

Figure 3.26: Compounds dose dependent NO savaging ability.
NO enriched medium from LPS stimulated microglia were mixed with the given DMSO or compound concentration, ranging from 1x10-7 to 1x10-3 v/v or 0.002 to 20 µM respectively, for 24 hours. The NO concentration was measured using the Griess assay and normalised to untreated stimulated positive control.

Treatment		Value	95 % confidence interval			different from zero	
DMSO	slope	-3x10-4	-0.00216	to	0.001557	0.7442	ns
	intercept	0.9915	0.9774	to	1.006		
C1.0	slope	1x10-3	-0.00036	to	0.002761	0.1281	ns
	intercept	9.526	0.9406	to	0.9645		
C4.0	slope	-5x10-4	-0.00204	to	0.000885	0.4298	ns
	intercept	0.9808	0.9698	to	0.9917		

Table 3.7: Description of the linear regression curve of the compounds NO scavenging ability.

3.8 The compounds effect on microglial phagocytosis and migration.

Microglia cells, as part of the innate immune system, are capable of increasing their motility, chemotaxis and phagocytic activity upon a pro-inflammatory stimulus [41,172]. In the following, I assessed the influence of C1.0 and C4.0, as well as the solvent DMSO on microglial migration and phagocytosis.

3.8.1 Neither compound C1.0 nor C4.0 shows an effect on the basal and stimulated microglial phagocytosis.

To study the influence of the compounds on the phagocytic activity, I quantified the uptake of FCS coated bright-blue fluorescent microspheres under unstimulated control conditions and LPS stimulated conditions. Primary microglia were treated with 2.5 µM of C1.0, 10 µM of C4.0 or $5x10^{-4}$ DMSO one hour prior 1 µg/mL LPS was added in addition and incubated for another 24 hours, or the cells were incubated without stimulation. Afterwards, the cells were exposed to the microspheres for 30 minutes, the cells were harvested, and the phagocytic uptake was quantified using flow cytometry. All values were normalised to the unstimulated untreated negative control. Under unstimulated conditions neither of the applied substances showed a significant effect on the phagocytic activity (DMSO: 119.9

%, 14.8 % SEM, p = 0.9673; C1.0: 98.6 % 4.0 % SEM, p > 0.9999; C4.0: 82%, 8.8 % SEM, p = 0.9813). Upon LPS stimulation microglia increased the phagocytic activity significantly up to 170.8 % (17.9 % SEM, p = 0.0048). Treatment with DMSO, C1.0, or C4.0 did not change the increased phagocytic rate significantly (DMSO: 162.7 %, 7.7 % SEM, p = 0.9929; C1.0: 139.5 % 10.7 % SEM, p = 0.6915; C4.0: 145.6%, 24.8 % SEM, p = 0.6998).

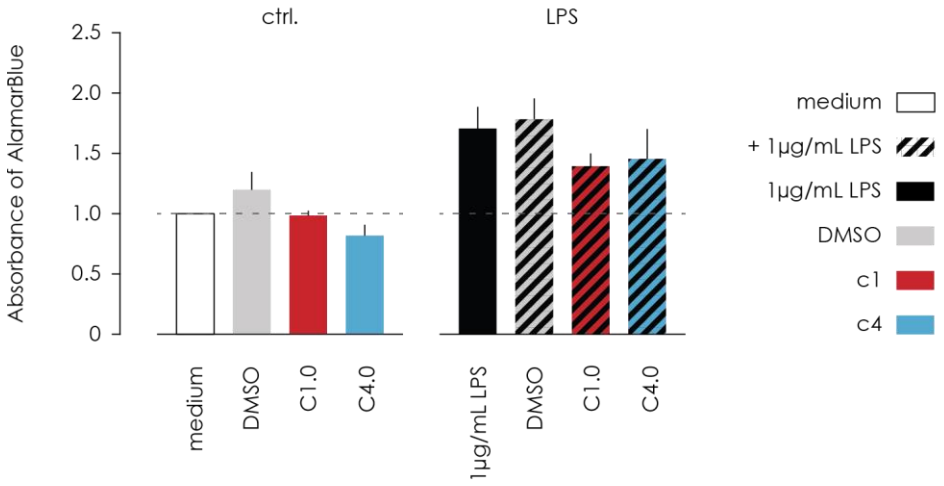

Figure 3.27: Modulation of the basal and LPS stimulated phagocytosis in microglia.
Microglia phagocytosis of FCS coated beads with and without 24 hour LPS pre-stimulation and compound treatment.

	medium.		DMSO	
medium			0.7838	ns
DMSO	0.7838	ns		
C1.0	> 0.9999	ns	0.8305	ns
C4.0	0.8303	ns	0.2892	ns

Table 3.8: Statistical comparison of the basal phagocytosis.

	medium		DMSO	
medium			0.9833	ns
DMSO	0.9833	ns		
C1.0	0.5964	ns	0.409	ns
C4.0	0.6328	ns	0.4099	ns

Table 3.9: Statistical comparison of the LPS induced phagocytosis.

3.8.2 C1.0 and C4.0 show a diverse effect on the microglial migration.

To assess the influence on microglial chemotaxis and motility I used the Boyden-chamber assay, which allows both measurements in parallel. In the present of the gradient, the chemotactic properties can be assessed, missing a gradient of the substance of interest the effect on the microglial motility can be assessed. Here, I tested the chemotactic and motility properties of the compound C1.0 and C4.0, and their modulatory effect on the ATP induces chemotaxis and motility. Primary microglia were directly seeded into the Boyden-chamber in the present of the given stimulus or treatment, as stated below, and incubated for 6 hours under cell culture conditions. All values were normalised to the positive control (pos. ctrl.) of ATP driven chemotaxis. Untreated motility was used as a negative control (neg. ctrl.).

To evaluate chemotactic properties of the compound, I applied 2.5 µM C1.0, 10 µM C4.0 or $5x10^{-4}$ DMSO in the lower compartment of the Boyden-chamber and primary microglia in the upper compartment. DMSO alone did not influence the microglial chemotaxis compared to the neg. ctrl. (18.2 %, 3.2 % SEM, $p = 0.7947$). However, compound C1.0 increased the chemotactic migration significantly from 26.0 % (2.4 % SEM) to 47.4 % (6.9 % SEM, $p = 0.189$) compared to the neg. ctrl. Compound C4.0 induced a significant chemotactic increase to 61.2 % (12.8 % SEM, $p < 0.0001$).

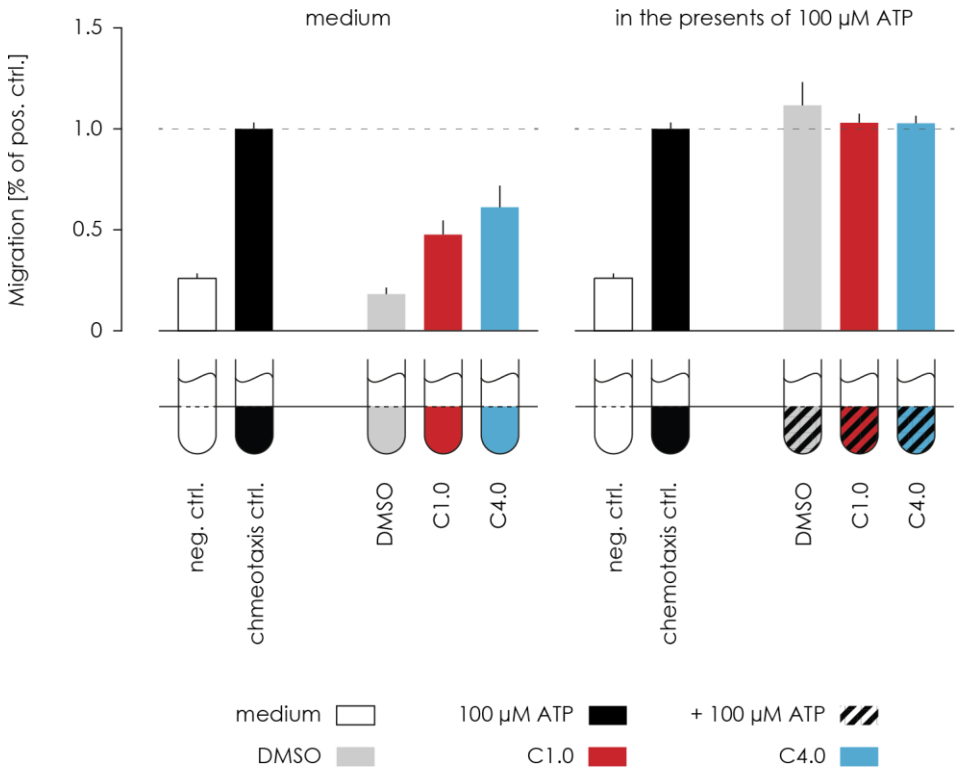

Figure 3.28: Modulation of microglial chemotaxis by compound C1.0 and C4.0. Microglial chemotaxis towards the compounds and DMSO and the modulation effect of the compounds and DMSO on the chemotaxis towards 100 µM ATP. Migration was assessed using the Boyden Chamber. All values were normalised to the ATP induced chemotaxis positive control.

	Chemotaxis ctrl.		**Neg. ctrl.**		**DMSO**	
Neg. ctrl.	< 0.0001	****			0.7947	ns
DMSO	< 0.0001	****	0.7947	ns		
C1.0	< 0.0001	****	0.0189	*	0.0079	**
C4.0	< 0.0001	****	< 0.0001	****	< 0.0001	****

Table 3.10: Statistical comparison of the compound induced chemotaxis.

	Chemotaxis ctrl.		Neg. ctrl.		DMSO	
Neg. ctrl.	< 0.0001	****			< 0.0001	****
DMSO	0.5395	ns	< 0.0001	****		
C1.0	0.9757	ns	< 0.0001	****	0.8126	ns
C4.0	0.9841	ns	< 0.0001	****	0.7881	ns

Table 3.11: Statistical comparison of ATP induced chemotaxis in the presents of the compound.

The compounds effect on microglial motility was assessed by applying 2.5 µM C1.0, 10 µM C4.0 or $5x10^{-4}$ DMSO in the lower and together with the primary microglial in the upper compartment of the Boyden-chamber. DMSO alone did not change the microglial motility significantly (9.9 %, 2.3 % SEM, p = 0.1411). In the presents of compound C1.0, the microglial motility decreased significantly to 1.2 % (0.7 % SEM, p = 0.0018) compared to the neg. ctrl. (24.2 %, 2.1 % SEM). Compound C4.0 did not show any effect on microglial motility (11.1 %, 3.5 %, p = 0.2381).

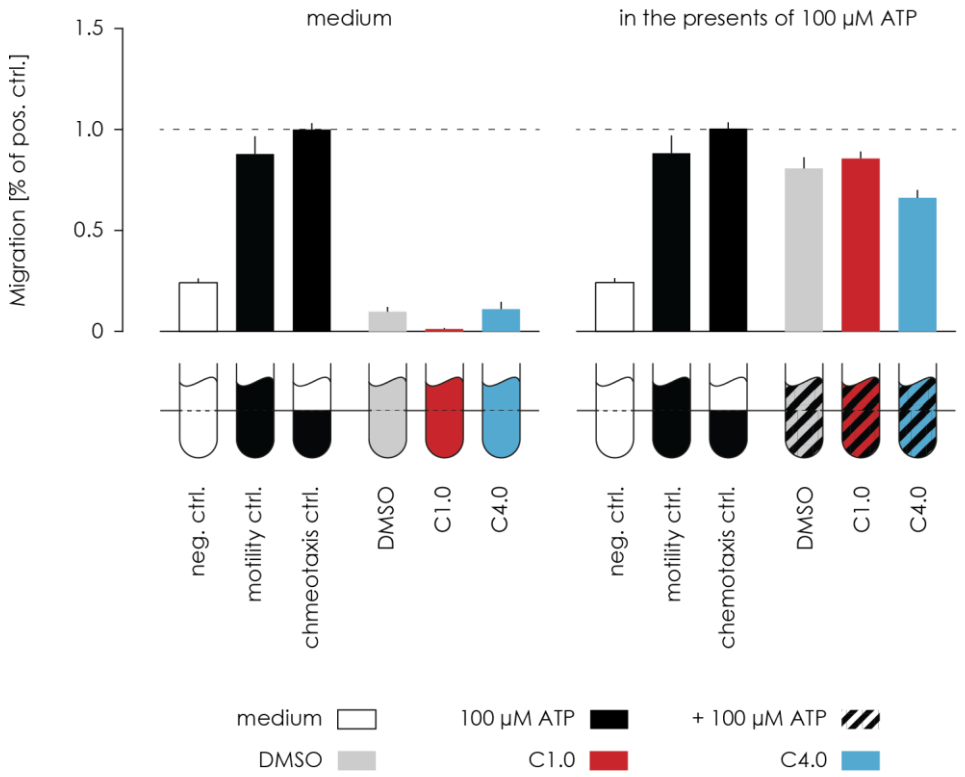

Figure 3.29: Modulation of microglial motility by compound C1.0 and C4.0.
Microglial motility in the presence of the compounds and DMSO and the modulation effect of the compounds and DMSO on the motility in the presence of 100 µM ATP. Migration was assessed using the Boyden Chamber. All values were normalised to the ATP induced chemotaxis positive control.

	Chemotaxis Ctrl.		**Neg. Ctrl.**		**DMSO**	
Neg. Ctrl.	< 0.0001	****			0.1411	ns
Chemotaxis ctrl.	0.3021	ns	< 0.0001	****	< 0.0001	****
DMSO	< 0.0001	****	0.1411	ns		
C1.0	< 0.0001	****	0.0018	**	0.8496	ns
C4.0	< 0.0001	****	0.2381	ns	> 0.9999	ns

Table 3.12: Statistical comparison of the compound modified motility.

	Chemotaxis ctrl.		Neg. Ctrl.		DMSO	
Neg. Ctrl.	< 0.0001				< 0.0001	****
Chemotaxis ctrl.	0.5829	****	< 0.0001	****	0.9287	ns
DMSO	0.0025	ns	< 0.0001	****		
C1.0	0.051	ns	< 0.0001	****	0.9513	ns
C4.0	< 0.0001	ns	< 0.0001	****	0.0907	ns

Table 3.13: Statistical comparison of the ATP induced motility in the presents of the compound.

The modulating effect of the compounds on ATP induced chemotaxis was evaluated applying 2.5 µM C1.0, 10 µM C4.0 or $5x10^{-4}$ DMSO in the upper and lower compartment of the Boyden-chamber and in addition 100 µM ATP in the lower compartment. Neither DMSO nor the compounds C1.0 and C4.0 did change the ATP induced chemotaxis significantly. DMSO increased the microglial chemotaxis slightly to 111.7 % (11.6 % SEM, p = 0.5395), whereas C1.0 and C4.0 showed almost no modulating effect (C1.0: 103.1 %, 4.5 % SEM, p = 0.9757; C4.0: 102.8 %, 3.8 % SEM, p = 0.9841).

In the presents of ATP microglia increase their motility activity significantly from 24.2 % (2.1 % SEM) to 87.9 % (8.8 % SEM, p < 0.0001). I evaluated the effect of compound C1.0 and C4.0, and DMSO applying them in a non-gradual fashion to the upper and lower compartment together with 100 µM ATP. DMSO alone and compound C1.0 did not change the microglial motility significantly (DMSO: 80.5 %, 45.1 % SEM, p = 0.9287; C1.0: 85.4 %, 3.5 % SEM, p = 0.9994). However, compound C4.0 reduced the ATP induced motility significantly to 66.0 % (3.8 % SEM, p = 0.0496).

3.9 The compounds interference with the metabolism, cell death, and cell number of cells of the healthy brain.

One goal of this work is to find a compound which can be administered to a healthy animal. I could show that the compounds do not interfere with the metabolic activity of pro-inflammatory stimulated microglia and macrophages. To evaluate the effect on a healthy

brain I measured the metabolic activity of unstimulated microglia, astrocytes, neurons, and oligodendrocytes. In addition, I quantified the impact of the compound on the cell number and cell death. The metabolic activity was measured using the AlamarBlue assay, the cell number and cell death were assessed using the PI based Dead-Or-Alive assay. The cells were seeded into a 96-well plate 1 day before the assay started. The cells were treated with either 2.5 µM C1.0, 10 µM C4.0, or the corresponding dose of DMSO ($5x10^{-4}$ = 10 µM compound) for 48 hours. Afterwards, the desired assay was performed. All data were normalised to the control condition of plain medium.

3.9.1 The positive effect of the compounds on microglial metabolic activity.

DMSO, C1.0, and C4.0 showed no effect on the metabolic activity in neurons and microglia. However, compound C4.0 showed a reducing effect on the metabolic activity of astrocytes compared to the DMSO control ($p = 0.0068$), and in oligodendrocytes compared to the control condition ($p = 0.0306$).

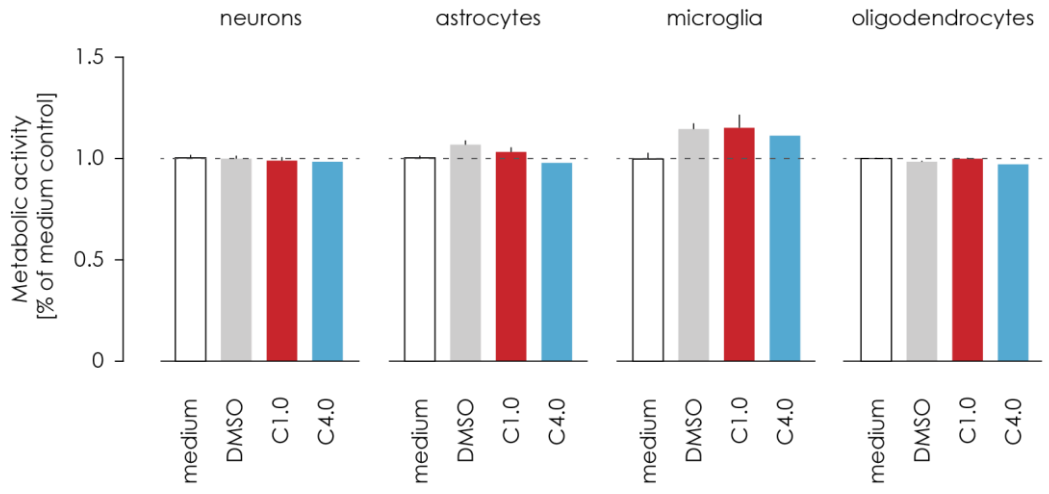

Figure 3.30: Compounds influence on the metabolic activity of non-stimulated neurons, astrocytes, microglia, and oligodendrocytes.
Different cells of the brain were treated for 24 hours with the either the compound or DMSO. The effect on the metabolic activity was measured using the AlamarBlue assay. C4.0 decrease the metabolic activity of astrocytes and oligodendrocytes significantly. All values were normalised to the medium control.

		medium		DMSO	
microglia	medium			0.3021	ns
	DMSO	0.3021	ns		
	C1.0	0.2894	ns	0.9999	ns
	C4.0	0.5409	ns	0.9811	ns
neurons	medium			0.9992	ns
	DMSO	0.9992	ns		
	C1.0	0.9476	ns	0.9729	ns
	C4.0	0.8502	ns	0.8955	ns
oligodendrocytes	medium			0.4214	ns
	DMSO	0.4214	ns		
	C1.0	> 0.9999	ns	0.1261	ns
	C4.0	0.0306	*	0.2751	ns
astrocytes	medium			0.0789	ns
	DMSO	0.0789	ns		
	C1.0	0.7004	ns	0.5578	ns
	C4.0	0.8123	ns	0.0068	**

Table 3.14: Statistical analysis of the compounds influence on the metabolic activity of non-stimulated neurons, astrocytes, microglia, and oligodendrocytes.

3.9.2 The compounds positive effect on the cell number of astrocytes and microglia.

The cell number of oligodendrocytes did not change by any of the applied substances. Compound C1.0 increase the cell number of microglia significantly compared to control condition ($p = 0.0371$) and the DMSO control ($p = 0.0002$). Here, compound C4.0 showed a reducing effect on the number of microglia compared to the DMSO control ($p = 0.0206$). However, C4.0 increased the cell number in astrocytes significantly compared to the control conditions ($p = 0.0012$). DMSO, but not the compounds had a significant increasing effect on the cell number of neurons compared to the control condition ($p = 0.0112$). The compounds C1.0 and C4.0 counteracted this increase, reducing the cell number compared to the DMSO control significantly (C1.0: $p = 0.0335$; C4.0: $p = 0.0267$) but not compared to the control condition.

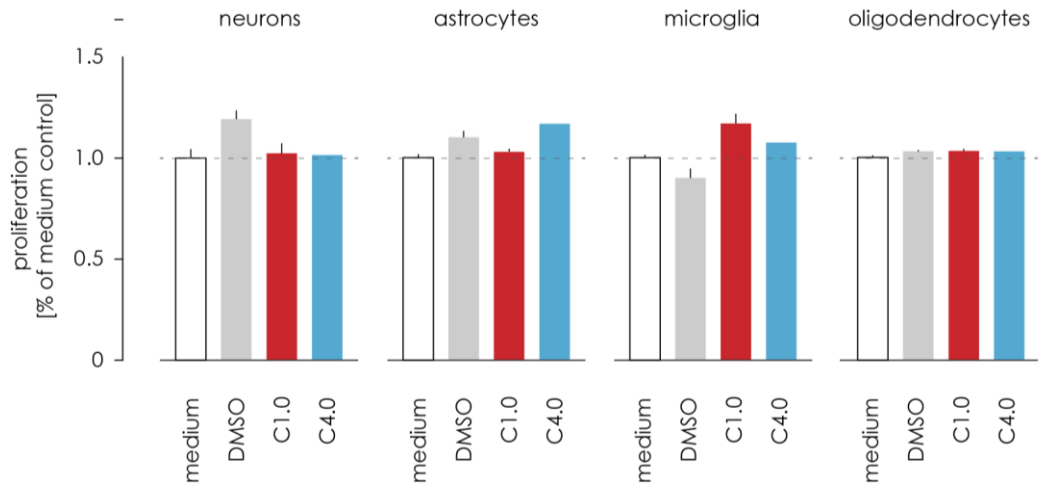

Figure 3.31: Compounds influence on the proliferation of non-stimulated neurons, astrocytes, microglia, and oligodendrocytes.
Different cells of the brain were treated for 24 hours with the either the compound or DMSO. The effect on the cell number was measured using a propidium iodide assay. All values were normalised to the medium control.

		medium		DMSO	
microglia	medium			0.3571	ns
	DMSO	0.3571	ns		
	C1.0	0.0371	*	0.0002	***
	C4.0	0.6053	ns	0.0206	*
neurons	medium			0.0112	*
	DMSO	0.0112	*		
	C1.0	0.9777	ns	0.0335	*
	C4.0	0.9939	ns	0.0267	*
oligodendrocytes	medium			0.1695	ns
	DMSO	0.1695	ns		
	C1.0	0.1119	ns	0.9974	ns
	C4.0	0.1575	ns	> 0.9999	ns
astrocytes	medium			0.1123	ns
	DMSO	0.1123	ns		
	C1.0	0.9237	ns	0.392	ns
	C4.0	0.0012	**	0.4207	ns

Table 3.15: Statistical analysis of the compounds influence on the proliferation of non-stimulated neurons, astrocytes, microglia, and oligodendrocytes.

3.9.3 Compound C1.0 and C4.0 show no effect on the cell death.

The cell death of astrocytes, oligodendrocytes, and neurons was not significantly altered by the compounds or DMSO. In microglia, DMSO increased the cell death significantly compared to the control condition ($p = 0.0256$). However, no significant difference between the compounds and the control condition or the DMSO control could be detected.

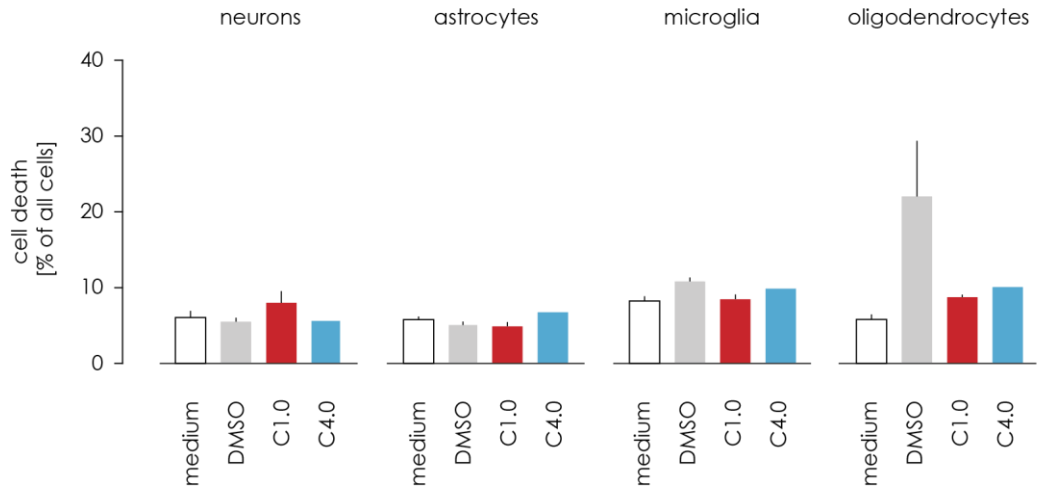

Figure 3.32: Compounds influence on the cell death of non-stimulated neurons, astrocytes, microglia, and oligodendrocytes.
Different cells of the brain were treated for 24 hours with the either the compound or DMSO. The effect on the cell death was measured using a propidium iodide assay. All values were normalised to the total number of cells.

		medium		DMSO	
microglia	medium			0.0258	*
	DMSO	0.0258	*		
	C1.0	0.994	ns	0.0622	ns
	C4.0	0.2356	ns	0.7244	ns
neurons	medium			0.9738	ns
	DMSO	0.9738	ns		
	C1.0	0.5178	ns	0.2724	ns
	C4.0	0.9849	ns	0.9999	ns
oligodendrocytes	medium			0.2624	ns
	DMSO	0.2624	ns		
	C1.0	0.9877	ns	0.1634	ns
	C4.0	0.963	ns	0.2292	ns
astrocytes	medium			0.7589	ns
	DMSO	0.7589	ns		
	C1.0	0.6204	ns	0.9962	ns
	C4.0	0.5276	ns	0.0908	ns

Table 3.16: Statistical analysis of the compounds influence on the cell death of non-stimulated neurons, astrocytes, microglia, and oligodendrocytes.

3.10 Structure action relationship analysis (SAR) of compound C4.0 reveal an inconsistent mode of action.

In the previous experiments compound C4.0 showed a reducing effect on NO and some cytokines (Il1ß, IL6, and TNFα), no effect on the phagocytosis and some specific effects on microglial migration. To analysis the relationship of the compounds structure to its action and to determine a chemical lead structure, I performed a structure action relationship (SAR) analysis. The compound was altered at three positions resulting 19 structural different compounds named C4.1 to 4.20 (4.3 is missing due to supply difficulties). The proposed lead structure left untouched. Alterations of the structure included the addition and

subtraction of polar groups (carbonyl acid, hydroxymethyl, halogens, etc.) changing the number of H-acceptors and H-donors, the alteration of the occupied space of some groups (from a trifluoromethyl group to a fluoride group), changing the linker length between some groups, or removing them completely. The chemical analysis and recommended alterations of the lead structure were done by Edgar Specker from the FMP. I tested all compounds on their effect on LPS induced NO, IL1ß, Il6, and TNFα release, as well as on the metabolic activity in primary cultured neonatal microglia. The assays were performed in parallel as described above and the previously established compound concentrations were used (0.2 µM, 2 µM, and 10 µM).

Beside the initial compound C4.0, no compound showed a dose dependent decrease in NO, IL1ß, Il6, and a slight decrease in TNFα, while showing no effect on the metabolic activity. The treatment with some compounds led to a decrease in the metabolic activity, indicating a cytotoxic property: C4.1, C4.2, C4.3, C4.9, C4.10, C4.12, C4.14, C4.15, C4.16, and C4.18. Another group of compounds decreased the cytokines independently of the used concentration: C4.10, C4.11, and C4.12. Only a few compounds reduced the LPS induced NO release significantly: C4.2, C4.4, C4.9, C4.10, C4.12, and C4.18. Compound C4.6, C4.15, C4.16, C4.17, C4.18, and C4.20 did increase the LPS induced TNFα release even more.

Due to the complex antagonistic result of the SAR, I excluded compound C4.0 from further analysis.

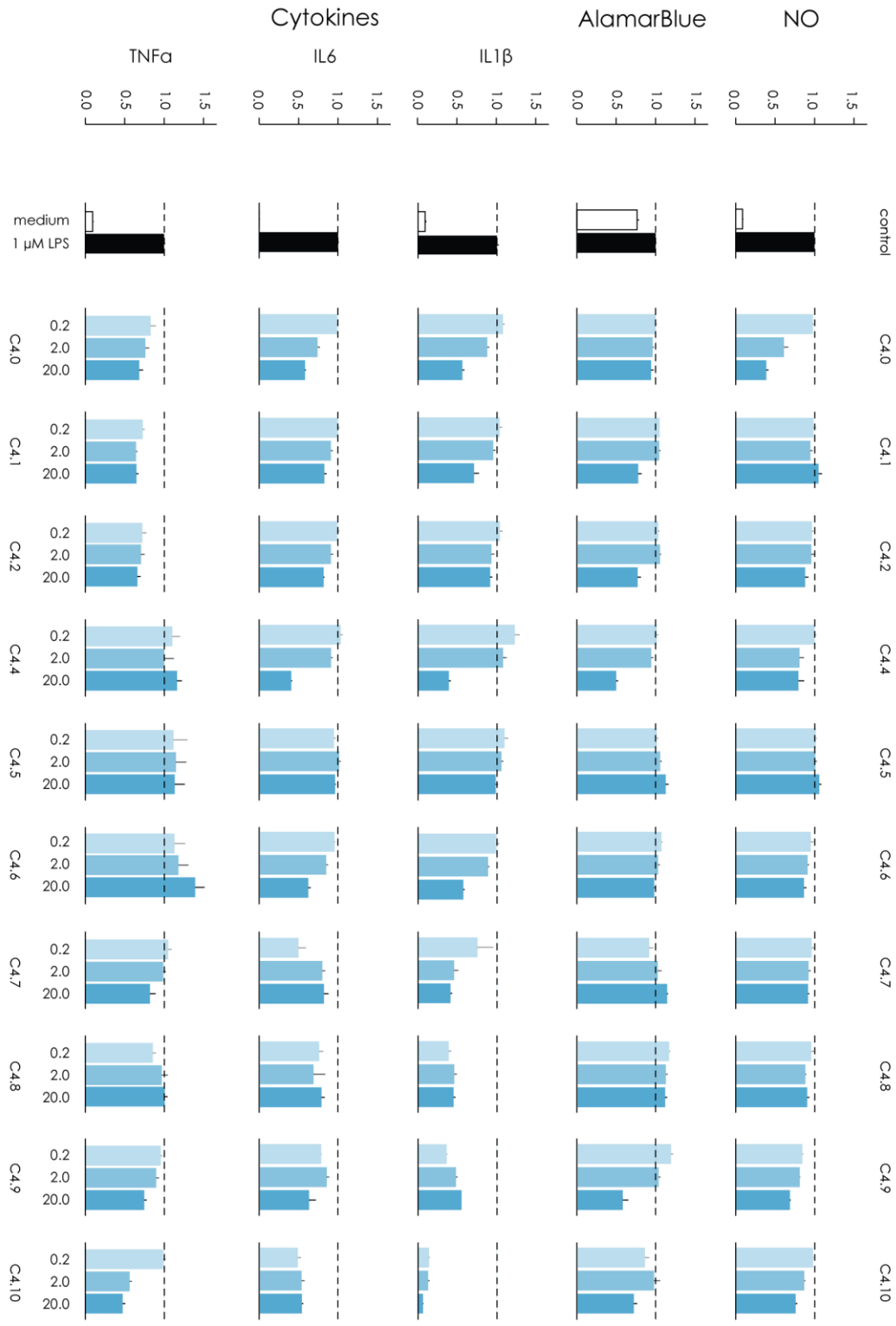
Cytokines
AlamarBlue
NO
TNFa
IL6
IL1β
0.0
0.5
1.0
1.5
medium
1 µM LPS
control
C4.0
C4.1
C4.2
C4.4
C4.5
C4.6
C4.7
C4.8
C4.9
C4.10
0.2
2.0
20.0

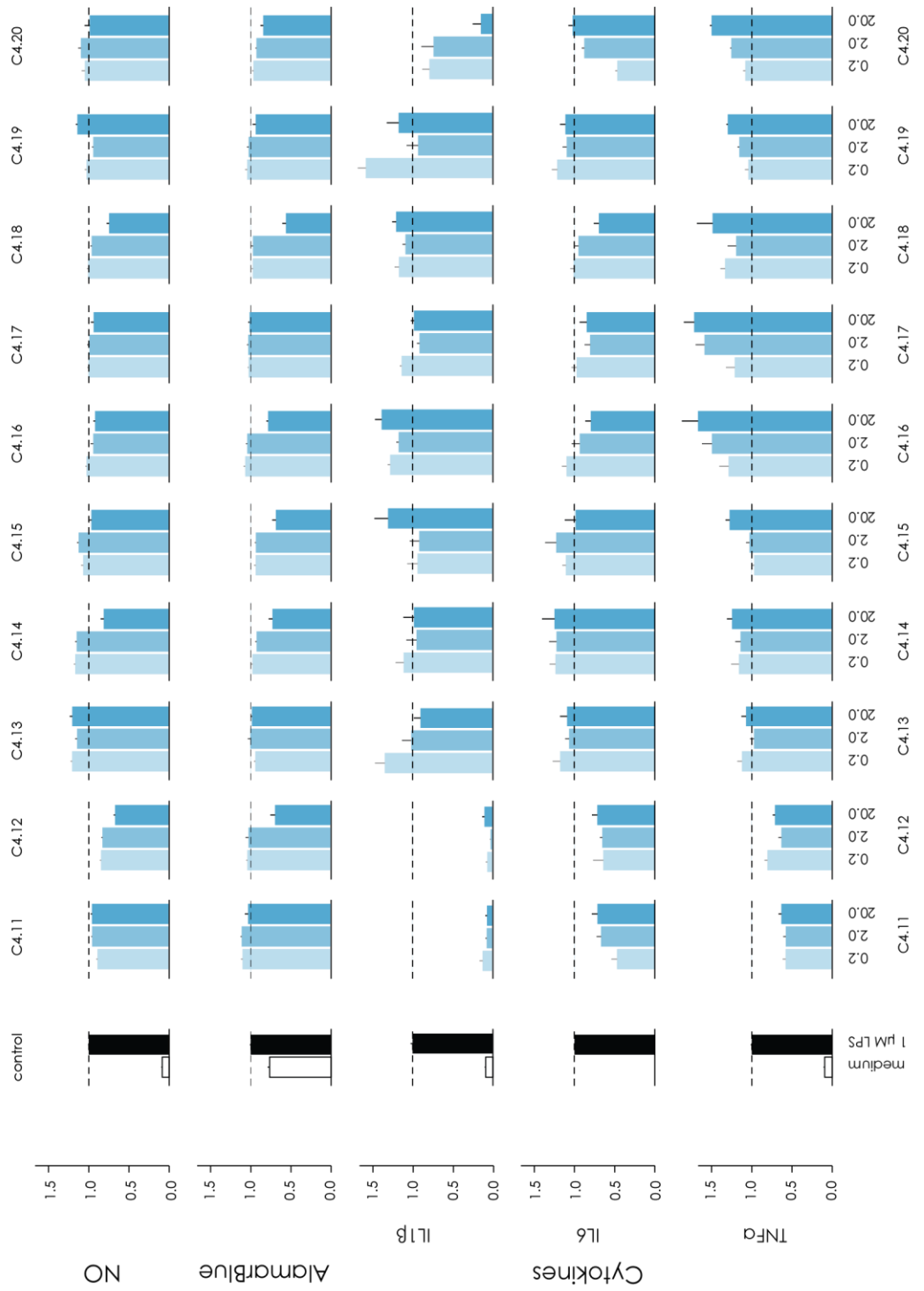

Figure 3.33: Structure action relationship analysis of compound C4.0.
The LPS induced release of NO, IL1ß, IL6, and TNFα in microglia and their modulation through the different variations of compound C4.0. The compounds influence on the metabolic activity measured using AlamarBlue.

3.11 C1.0 is able to reduce the NO release of previously activated microglia.

In the previous experiments, microglia and macrophages were pre-treated for 1 hour prior to the pro-inflammatory stimulation. This setup was used to assess the total effect of the compound on the induced NO and cytokine release. However, this approach does not represent the situation in a therapeutic use. To mimic a situation closer to the therapeutic use, I applied C1.0 or DMSO on already activated microglia. Microglia were stimulated in a 96-well plate with 1 µg/mL LPS for 24 hours, afterwards, the supernatant was discarded, and the cells were washed carefully with warm PBS. Next, fresh cell culture medium was applied containing 2.5 µM C1.0, the corresponding concentration of $125x10^{-5}$ v/v DMSO, or no additional substance. The NO release was measured after 2, 4, 6, 8 hours and 12, 24, 36, 48, 60 hours. Under control conditions with no additional substance applied, the NO concentration increased in a linear fashion reaching 28.7 µM (1.036 µM SEM). This linear increase is defined by a slope of 0.4597 µM/h (0.00957 µM/h SEM), a y-interception of 0.7832 µM (0.2507 µM SEM) with an R^2 of 0.9412. DMSO does not change this linear increase in NO significantly compared to the control condition ($p < 0.9999$), reaching 29.2 µM (1.119 µM SEM) after 60 hours. The linear increase is defined by a slope of 0.6443 µM/h and a y-interception of 0.4640 with an R^2 of 0.9612. Treatment of already activated microglia reduces the NO release significantly over time. After 60 hours the NO concentration reaches only 7.256 µM (0.6127 µM SEM) and is significantly different compared to the medium and DMSO control (both $p < 0.0001$). From 8 hours on after medium change the NO concentration is significantly reduced compared the control condition and from 12 hours on compared to the DMSO control, too. The change in NO concentration shifted from a linear increase to an increase defined by a one-phase association, described by a start value (= y-interception) of 1.054 µM (CI 95 % from 0.3759 to 1.732 µM), an end plateau of 7.063 µM (CI 95 % from 5.999 to 8.127), and tau of 19.87 (CI 95 % from 13.13 to 40.79).

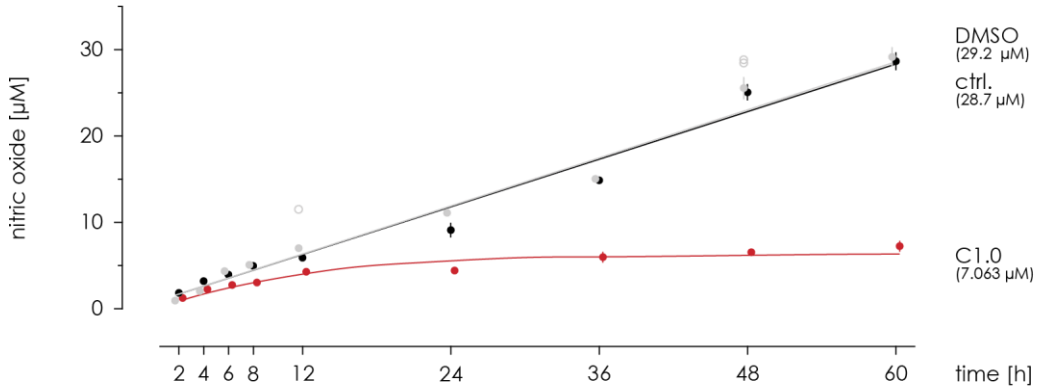

Figure 3.34: Impact of compound C1.0 on the NO release of pre-stimulated microglia.
Microglia were stimulated for 24 hours prior compound treatment. The amount NO was measured afterwards using the Griess assay.

	Time in hours								
	2 h	**4 h**	**6 h**	**8 h**	**12 h**	**24 h**	**36 h**	**48 h**	**60 h**
ctrl. vs. DMSO	0.9182	0.4825	> 0.9999	> 0.9999	0.7931	0.0489	> 0.9999	> 0.9999	> 0.9999
	ns	ns	ns	ns	ns	*	ns	ns	ns
C1.0 vs. ctrl.	0.9999	0.8306	0.436	0.006	0.0416	< 0.0001	< 0.0001	< 0.0001	< 0.0001
	ns	ns	ns	**	*	****	****	****	****
C1.0 vs. DMSO	> 0.9999	> 0.9999	0.0539	0.0755	< 0.0001	< 0.0001	< 0.0001	< 0.0001	< 0.0001
	ns	ns	ns	ns	****	****	****	****	****

Table 3.17: Statistical analysis of the compound's impact on the NO release of pre-stimulated microglia.

3.12 Compound C1.0 includes two distinct two diastereomers.

Compound C1.0's structure contains 2 stereo centres. Both are located in the backbone of the peptide bonds, one in the amino acid proline, the other in the amino acid like structure

of tyrosine. The stereo centre in the amino acid proline is defined in its *S* conformation. The stereo centre in the amino acid like structure of tyrosine occurs in both *S* and *R* conformation. In the previous experiments, a diastereomeric mixture of the *S* and *R* conformation of compound C1.0 was used. To evaluate the composition of this mixture, I separated both diastereomers using HPLC with a chiral column. The experiments were conducted in the facilities of the FMP with the help of Dr. Edgar Specker setting them up. The final experiments were executed by me. The separation with the HPLC showed two distinct peaks, with the first peak starting after 7:15 min and ending at around 8:45, and the second peak starting at around 9:30 min and ending at around 11:45 min. The area under the curve (AUC), determine a relative amount of the diastereomer of 43 % for the first peak and 57 % for the second peak. In the following, the isolated diastereomers will be named C1.0a and C1.0b by the order of their appearance in the HPLC.

The chiral centers in compound C1.0

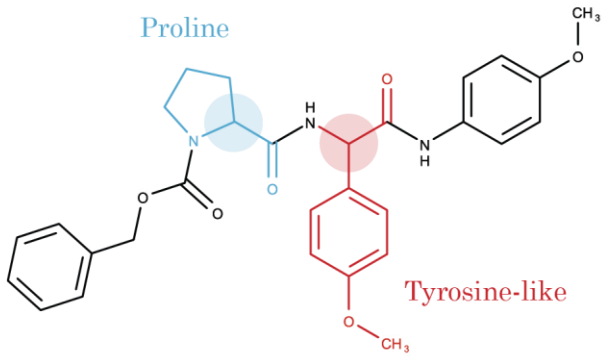

The four distereomers of C1.0

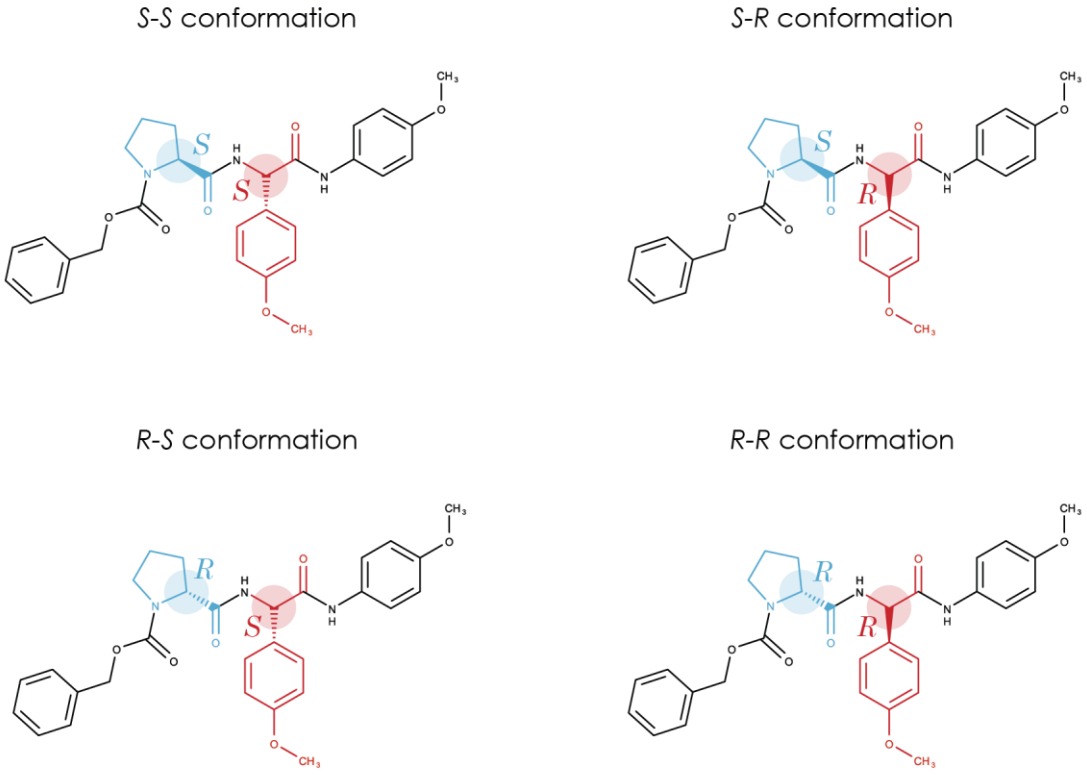

Figure 3.35: Possible chiral structure of compound C1.0.

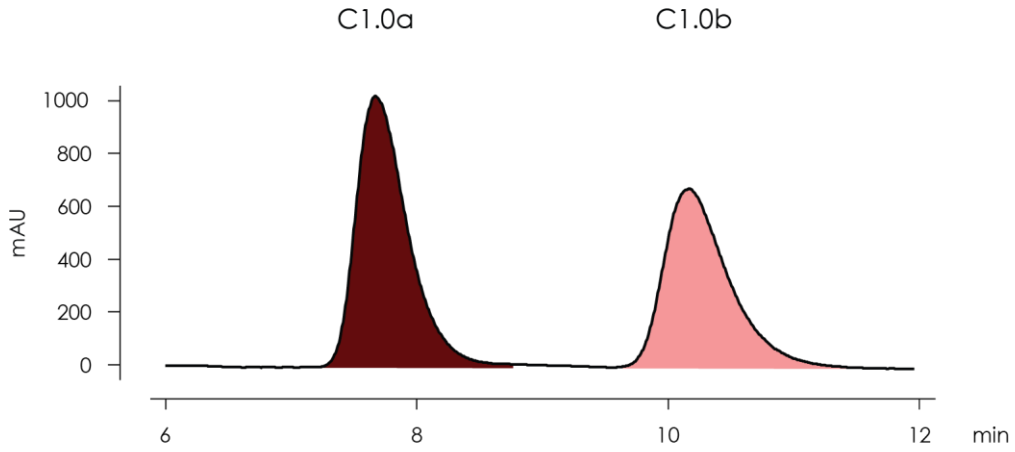

Figure 3.36: HPLC chiral separation of C1.0.
Exemplary curve of the chiral HPLC of the diastereomeric mixture C1.0 shows the separation into 2 defined peaks. mAU = milli Absorbance Unit.

I evaluated the potential in reducing the LPS induced NO release in microglia of both isolated diastereomers. Therefore, I repeated the NO assay described in chapter 3.2 (on page 43). The treatment with the compound C1.0a and C1.0b was initiated 1 hour prior to the stimulation with 1 µg/mL LPS for additional 48 hours. The compounds were applied in the same dose range used before: 0.025 µM, 0.25 µM, and 2.5 µM. Non-treated primary microglia served as a negative control (unstimulated) and as a positive control when stimulated with LPS. In addition, I tested the initial diastereomeric mixture of compound C1.0. The negative and positive control, as well as the diastereomeric mixture of compound C1.0, showed the same results as described beforehand in 3.2 (on page 43). The first fraction, C1.0a, showed an even stronger reduction of the induced NO release compared to the previous tested diastereomeric mixture C1.0, whereupon the second fraction, C1.0b, showed a significant reduction only in the highest applied concentration (2.5 µM). C1.0a reduced the NO release significantly in a dose depended manner, starting at the concentration of 0.025 µM by reducing the NO concentration to 88.36 % (1.234 % SEM, $p < 0.0001$) of the pos. ctrl.. 0.25 µM reduced the NO concentration to 28.56 % (2.566 % SEM, $p < 0.0001$), and 2.5 µM to 2.60 % (0.0079 % SEM, $p < 0.0001$). Compared to the diastereomeric mixture C1.0, C1.0a showed a larger decrease in every applied concentration (0.025 µM: C1.0 = 93.93%, C1.0a = 88.36 %; 0.25 µM: C1.0 = 50.84 %, C1.0a =28.56 %; 2.5 µM: C1.0 = 3.66 %, C1.0a = 2.60 %) reaching significance for 0.25 µM ($p < 0.0001$). Fraction

C1.0b showed no dose dependent reduction within the tested concentration range. Treatment with 0.025 µM C1.0b showed now significant reduction (96.85 %, 1.426 % SEM, p = 0.9027), with 0.25 µM the NO concentration remained at 100.9 % (1.019 % SEM, p > 0.9999), only 2.5 µM reduced the NO concentration significantly to 88.69 % (1.283 % SEM, p < 0.0001).

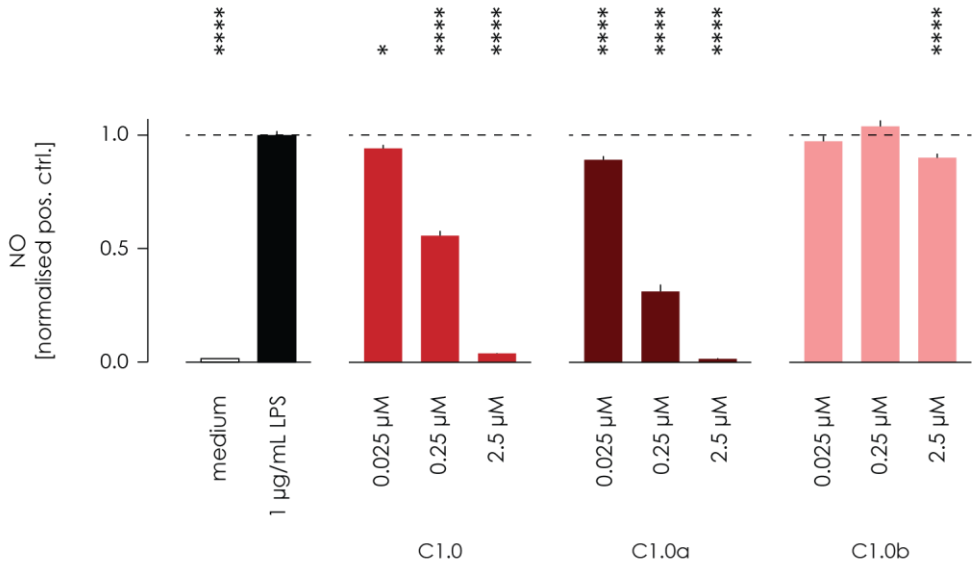

Figure 3.37: Dose dependent influence of the two separated fractions on the LPS induced NO release in microglia.
NO release measured using the Griess assay and normalised to the untreated LPS stimulated positive control. Microglia were treated 1 hour before stimulation for additional 48 hours. Data is shown as mean + SEM. Statistical significance is shown as * ≤ 0.05, ** ≤ 0.01,*** ≤ 0.001, **** ≤ 0.0001.

3.12.1 S-S is the active conformation of compound C1.0

In the previous HPLC fractioning I could show that compound C1.0 exists in an active (C1.0a) and in an inactive (C1.0b) conformation. However, the allocation of the active form to the conformation is missing. To determine the conformation of the active form, both the *S-S* and the *S-R* was synthesised by Keven Malow in the FMP. An HPLC with a chiral column was run with the same setting used before in chapter 3.12 (page 92) to verify the purity of the synthesised compounds and to allocate the structure to a particular peak. Both conformations and their allocation to the corresponding HPLC peak are illustrated in Figure 3.38. The first fraction, C1.0a, contains the *S-S* conformation, the second peak, C1.0b, contains the S-R conformation of the compound.

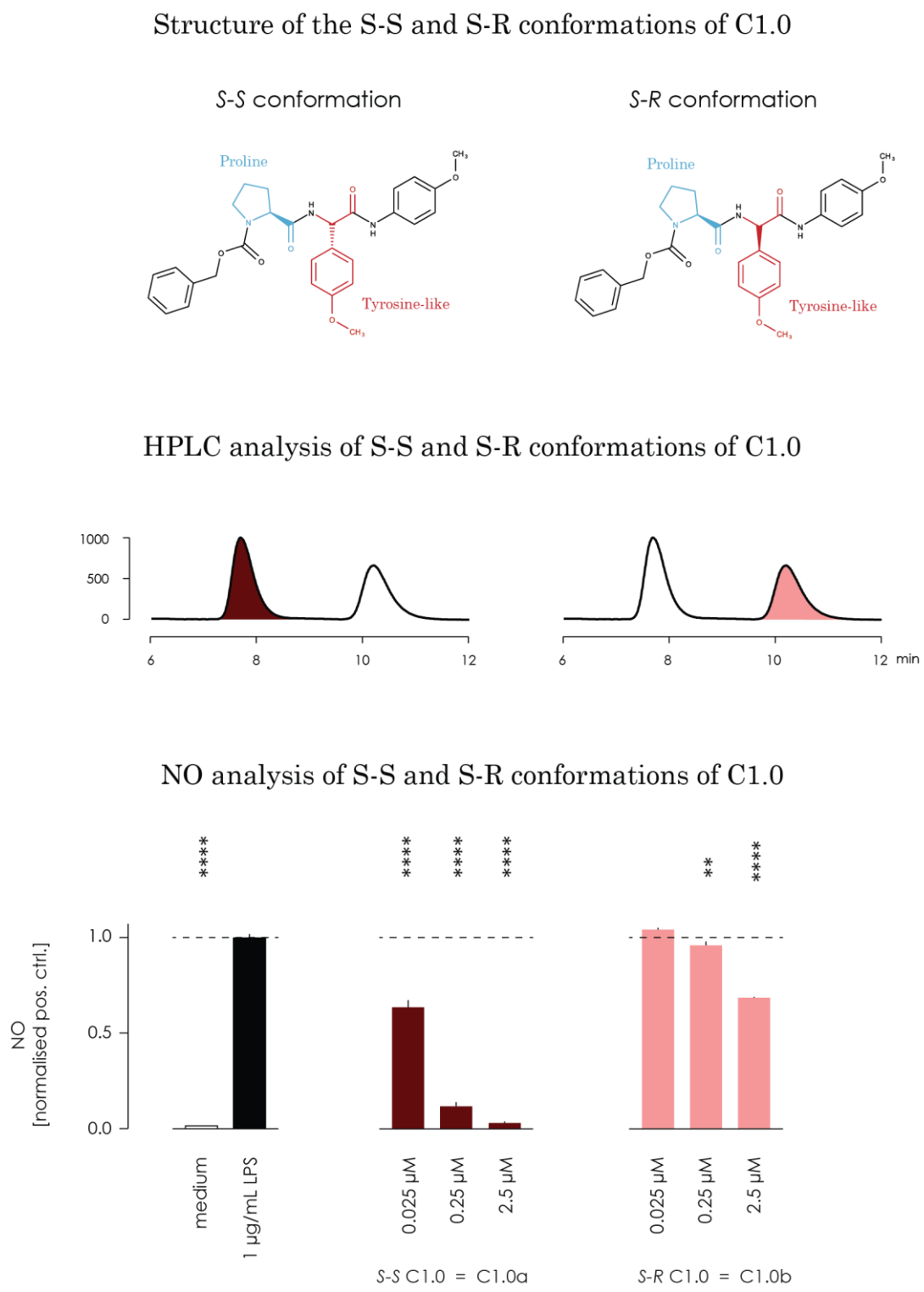

Figure 3.38: Identification of the chiral structure of compound C1.0
The chemical structures of compound C1.0a and C1.0b (top), the corresponding peak in the HPLC analysis (middle), and the effect on the LPS induced NO release in microglia (bottom). Data is shown as mean + SEM. Statistical significance is shown as * ≤ 0.05, ** ≤ 0.01,*** ≤ 0.001, **** ≤ 0.0001. All data are normalised to the pos. ctrl.

In addition, I tested both formations C1.0a and C1.0b in the above described NO assay to

confirm the allocation and the activity of the in-house synthesized molecules. The LPS stimulation of the primary microglia showed the expected increase in NO release in primary microglia (neg. ctrl.: 1.88 %, 0.589 % SEM; pos. ctrl.: 100 %, 6.52 % SEM). The *S-S* conformation showed a significant dose dependent decrease on the NO release: 0.025 µM decreased the NO concentration to 61.30 % (3.60 % SEM, $p < 0.0001$), 0.25 µM to 11.61 % (2.14 % SEM, $p < 0.0001$), and 0.025 µM to 3.13 % (0.92 % SEM, $p < 0.0001$). The *S-R* conformation, too, showed a dose dependent decrease of the NO release, however to far less extend, compared to the *S-S* conformation. Treatment with 0.025 µM *S-R* conformation did not change the NO concentration (100.30 %, 0.92 % SEM, $p > 0.9999$), 0.25 µM reduced the NO concentration slightly but significant to 92.48 % (2.01 % SEM, $p = 0.0049$), and 2.5 µM to 66.16 % (0.41 % SEM, $p < 0.0001$). Both data confirm the allocation made with the HPLC experiment, C1.0a is the *S-S* conformation, and C1.0b is the *S-R* conformation.

3.12.2 The IC50 value of the active *S-S* conformation C1.0a is 104 nM.

I could show that the compound C1.0 is a diastereomeric mixture of *S-S* and *S-R* conformation. Next, I assessed the IC_{50} value of both conformations in reducing the LPS induced NO release in primary microglia. Complied with the previous experiments, primary cultured neonatal microglia were seeded into a 96 well plate on the day before the assay started. The microglia were treated with the fraction C1.0a or C1.0b. As a control, the mixture of both conformations (= C1.0), which was used in previous experiments, or the corresponding concentration of the solvent DMSO was used. The concentrations range for the compounds started at 2 nM and ended at 20 µM (2, 10, 20, 100, 200 nM, 1, 2, 10, 20 µM), and for DMSO started at $2.5x10^{-7}$ v/v and ended at $2.5x10^{-3}$ v/v ($2.5x10^{-7}$, $5x10^{-7}$, $2.5x10^{-6}$, $5x10^{-6}$, $2.5x10^{-5}$, $5x10^{-5}$, $2.5x10^{-4}$, $5x10^{-4}$ v/v). DMSO itself showed no dose dependent effect on the LPS induced NO release in microglia. The highest reduction in NO concentration was measured at a concentration of 5×10^{-5} (= 2 µM compound, 87.36 %). Higher concentration of DMSO increased the detected NO concentrations again up to 94.17 % ($5x10^{-4}$ v/v = 20 µM compound). None of the tested concentrations did decrease the NO concentration in a significant manner compared to the non-treated stimulated pos. ctrl.. The diastereomeric mixture of both conformations showed a dose dependent decrease, reaching a significance reduction compared to the non-treated stimulated pos. ctrl. starting with a concentration of 100 nM (70.49 %, 5.67 % SEM, $p < 0.0001$). Concentrations

above 1 µM evoked a reduction in the NO concentration that does not show a significant difference to the non-treated unstimulated neg. ctrl. ($p = 0.1378$). The calculated IC_{50} of C1.0 is 252 nM (95% CI = 0.2069 to 0.3234), confirming the IC_{50} of the HTS (Figure 3.6). C1.0a showed a more potent dose dependent decrease in the NO concentration. A concentration of 20 nM did already reduce the NO level significantly to 79.76 % (1.47 % SEM, $p < 0.0001$). Similar to C1.0, C1.0a showed no significant difference compared to the neg. ctrl. starting at a concentration above 1 µM. The calculated IC_{50} value is 104 nM (95% CI = 0,09491 to 0,1152), which fits with the distribution in the diastereomeric mixture C1.0 (43 % C1.0a, 57 % C1.0b, 252 nM x 43 % = 108.36 nM). C1.0b showed a significant decrease starting from 2 µM (89.23 %, 2.93 % SEM, $p = 0.0036$), a concentration in which C1.0 and C1.0a already reached a level similar to the neg. ctrl.. Within the tested concentration range, a treatment with C1.0b did not reach NO level significantly different to the neg. ctrl. The calculated IC_{50} value is 43.29 µM. It has huge variance with a 95 % confidence interval from 8,841 to +infinity and is outside the tested concentration range.

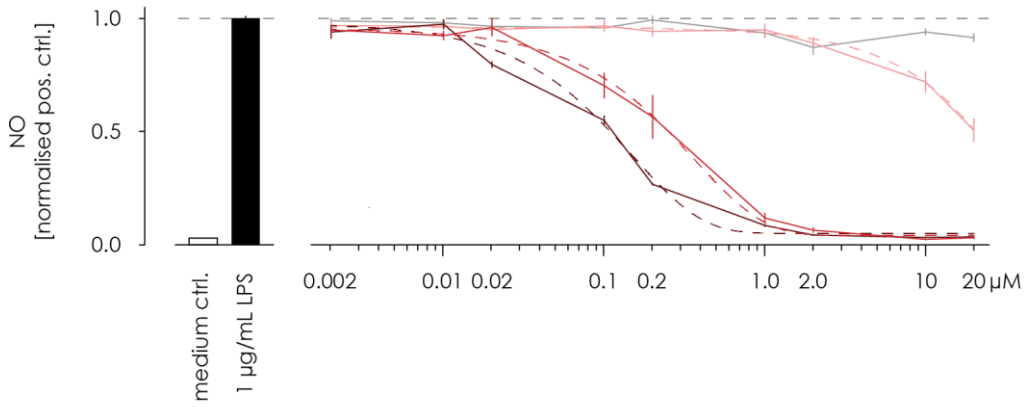

Figure 3.39: Dose dependent reduction of LPS induced NO release in microglia of compound C1.0, C1.0a, and C1.0b.
Microglia pre-treated with a given compound concentration or the corresponding DMSO concentration, and subsequently LPS stimulation for 48 hours. The NO concentration was measured using the Griess assay. All data are normalised to the pos. ctrl.

µM	ctrl. vs. DMSO	ctrl. vs. C1.0		ctrl. vs. C1.0a		ctrl. vs. C1.0b	
0.002	> 0,9999	0.9181		0.615		> 0,9999	
0.010	> 0,9999	0.0893		> 0,9999		> 0,9999	
0.020	> 0,9999	> 0,9999		< 0,0001	****	0.575	
0.100	> 0,9999	< 0,0001	****	< 0,0001	****	> 0,9999	
0.200	> 0,9999	< 0,0001	****	< 0,0001	****	0.3836	
1.000	0.8799	< 0,0001	****	< 0,0001	****	0.4967	
2.000	0.0510	< 0,0001	****	< 0,0001	****	0.0049	**
10.000	> 0,9999	< 0,0001	****	< 0,0001	****	< 0,0001	****
20.000	0.4865	< 0,0001	****	< 0,0001	****	< 0,0001	****

Table 3.18: Statistical analysis of the NO dose response curve using a 2-way ANOVA

In parallel to the NO concentration, I measured the effect on the metabolic activity of primary microglia. The experiment was performed as described previously (chapter 3.2) with the same concentration used above. Across the whole concentration range, all tested substances (DMSO, C1.0, C1.0a, C1.0b) showed a significant decrease in microglial metabolic activity in singular concentrations. However, this decrease did neither follow a dose dependent pattern nor did it dropped below the metabolic activity of non-treated unstimulated microglia (68.64 %, 2.47 % SEM), indicating no effect on microglial viability.

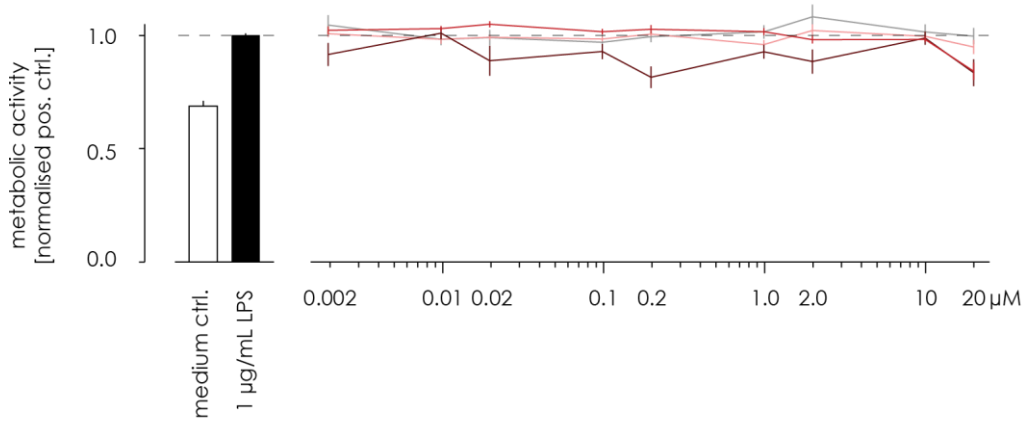

Figure 3.40: Dose dependent scavenging effect on NO by compound C1.0, C1.0a, and C1.0b
Microglia pre-treated with a given compound concentration or the corresponding DMSO concentration, and subsequently LPS stimulation for 48 hours. The metabolic activity was measured using the AlamarBlue assay. All data are normalised to the pos. ctrl.

µM	ctrl. vs. DMSO		ctrl. vs. C1.0		ctrl. vs. C1.0a		ctrl. vs. C1.0b	
0.002	0.3114		0.799		< 0,0001	****	> 0,9999	
0.010	> 0,9999		0.1545		> 0,9999		0.6457	
0.020	> 0,9999		0.0039	**	< 0,0001	****	> 0,9999	
0.100	0.5959		> 0,9999		< 0,0001	****	0.905	
0.200	> 0,9999		0.3551		< 0,0001	****	> 0,9999	
1.000	> 0,9999		> 0,9999		< 0,0001	****	0.0188	*
2.000	0.0037	**	0.422		< 0,0001	****	> 0,9999	
10.000	> 0,9999		0.372		> 0,9999		> 0,9999	
20.000	> 0,9999		< 0,0001	****	< 0,0001	****	0.0023	**

Table 3.19: Statistical analysis of the metabolic activity dose response curve using a 2-way ANOVA

To test whether C1.0a or C1.0b does react with NO directly, I repeated the assay described in chapter "3.7.5 C1.0 and C4.0 do not act as a NO-Scavenger" (page 74) with the complete concentration range used above. None of the tested substance decreased the NO concentration in dose dependent manner. Interestingly, C1.0, but not C1.0a or C1.0b, did increase the measured NO level significantly for singular concentrations (10 nM: 107.75 %, 1.31 % SEM, p = 0.0338 ; 200 nM: 107.18 %, 1.39 % SEM, p = 0.0117 ; 10 µM: 108.43 %, 1.26 % SEM, p = 0.0169 ; and 20 µM: 108.59 %, 0.76 % SEM, p = 0.0143).

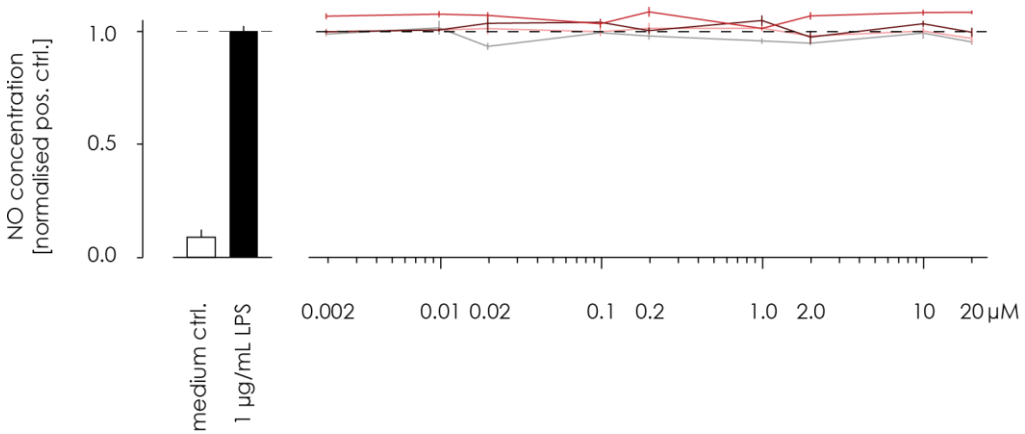

Figure 3.41: Dose dependent scavenging influence of the NO concentration of NO enriched medium of compound C1.0, C1.0a, and C1.0b.
NO enriched medium from LPS stimulated microglia were incubated with a given compound concentration or the corresponding DMSO concentration and incubated for 48 hours. All data are normalised to the pos. ctrl.

	ctrl. vs. DMSO	ctrl. vs. C1.0		ctrl. vs. C1.0a	ctrl. vs. C1.0b
0.002	> 0,9999	0.0807		> 0,9999	> 0,9999
0.010	> 0,9999	0.0338	*	> 0,9999	> 0,9999
0.020	0.1026	0.0582		0.8362	> 0,9999
0.100	> 0,9999	> 0,9999		0.623	> 0,9999
0.200	> 0,9999	0.0117	*	> 0,9999	> 0,9999
1.000	0.6301	> 0,9999		0.3748	> 0,9999
2.000	0.0981	0.0706		> 0,9999	> 0,9999
10.000	> 0,9999	0.0169	*	0.9179	> 0,9999
20.000	0.4666	0.0143	*	> 0,9999	> 0,9999

Table 3.20: Statistical analysis of the scavenger dose response curve using a 2-way ANOVA

3.13 Treatment with C1.0, C1.0a, or C1.0b does not modify the iNOS's mRNA regulation.

In microglia and macrophages, NO is produced by the inducible isoform of the nitric oxide synthase (iNOS). It is known that iNOS is regulated on the transcriptional level[54]. Under physiological conditions, iNOS's mRNA is barely detectable, while upon a pro-inflammatory stimulus, like LPS, the transcription of iNOS's mRNA is upregulated. Thus, I further investigated whether the induction of iNOS's mRNA is affected by the treatment with a diastereomer mixture of C1.0, or the pure diastereomers C1.0a, and C1.0b. 1 10^6 Microglia were seeded into a 6 cm petri dish 1 day before the assay started. Afterwards, the cells were pre-treated for 1 hour with 2.5 µM of C1.0, C1.0a, C1.0b or the corresponding DMSO concentration of $125x10^{-5}$ v/v, followed by an additional 24 hours incubation with or without LPS. The amount of mRNA was quantified using qRT-PCR, and all values were normalised to untreated LPS stimulated medium control. Upon stimulation, with 1 µg/mL LPS the mRNA level increased significantly more than 5000-fold ($p < 0.0001$). Treatment with DMSO or the compounds did not change this behaviour. Under unstimulated conditions, the iNOS mRNA level remained below 0.0195 %, with no significant change compared to the medium control or DMSO treatment (see Table 3.21). Under LPS stimulated

conditions the iNOS mRNA stayed in between 61.7 % and 104.0 %, showing no significant difference compared to the LPS stimulated medium control and the stimulated DMSO control (see Table 3.22). The difference between the unstimulated and stimulated condition within each treatment are significant (ctrl., DMSO, C1.0, and C1.0b: $p < 0.0001$, C1.0a = 0.0236).

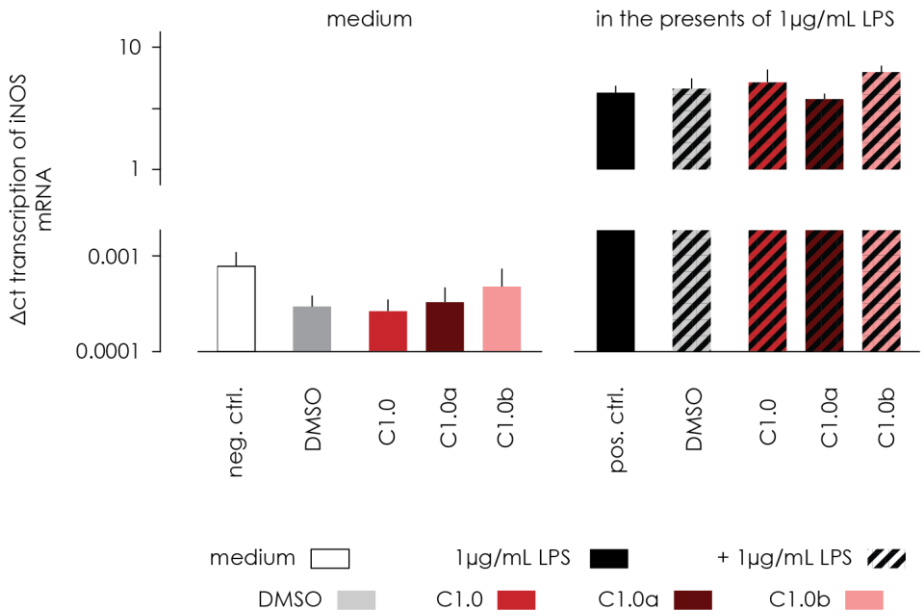

Figure 3.42: Compounds influence on the LPS stimulated and non-stimulated iNOS mRNA transcription in microglia.
Microglia treated with the compounds or DMSO and subsequently stimulated with or without LPS. mRNA was asses 24 hours after stimulation using qRT-PCR.

	Neg. ctrl.	DMSO	C1.0	C1.0a
DMSO	ns (0.9974)			
C1.0	ns (0.7717)	ns (0.9683)		
C1.0a	ns (0.9810)	ns (0.9333)	ns (0.4995)	
C1.0b	ns (0.1469)	ns (0.429)	ns (0.6701)	ns (0.0736)

Table 3.21: Statistical analysis of the compounds influence on the non-stimulated iNOS mRNA transcription in microglia.

	Neg. ctrl.	DMSO	C1.0	C1.0a
DMSO	ns (>0.9999)			
C1.0	ns (>0.9999)	ns (>0.9999)		
C1.0a	ns (>0.9999)	ns (>0.9999)	ns (>0.9999)	
C1.0b	ns (>0.9999)	ns (>0.9999)	ns (>0.9999)	ns (>0.9999)

Table 3.22: Statistical analysis of the compounds influence on the LPS stimulated iNOS mRNA transcription in microglia.

3.14 C1.0a does not directly regulate the NO-Synthesis iNOS, eNOS, or nNOS

In mammalians, NO is produced by the three isoforms of NOS: iNOS, eNOS, and nNOS. To evaluate the direct influence of C1.0a on the different isoforms of NOS, an enzyme activity assay was conducted by the company Eurofins. The experiments were carried out as following: C1.0a was mixed with the enzyme buffer, which included co-factors and substrates, by adding the enzyme the reaction was initiated. After 30 min, the reaction was stopped, and NO concentration was measured. The results are normalised to the positive control performed without any additional compounds and are presented as a percentage in inhibition. The known inhibitors W1400 for iNOS (Figure 3.44, in black), L-NMMA for eNOS (Figure 3.43, in black), and S-Methylisothiourea for nNOS (Figure 3.45, in black) were used as a reference. To evaluate the compound's effect on iNOS a concentration range from 1 pM up to 5 µM were applied (1, 10, 100 pM, 1, 10, 100 nM, 1, and 5 µM). The steps were chosen to incorporate the previous in house tested concentrations between 10 nM and 5 µM, and to account for the fact that I switch from a cell-based assay to an enzyme-based assay. Since I do not have any data on the effectiveness of the compound on eNOS and nNOS, I chose a high (1 µM) and low (1 nM) concentration. The known inhibitors reduced the enzyme activity of all tested synthases as predicted. However, C1.0a did not show any regulatory impact on the enzyme activity of any of the three NOS isoforms within the tested concentrations range. The impact on iNOS remain within a range of 4.3 % (1.7 % SEM) and 0.9 % (1.4 % SEM) stimulation. A fitted linear regression showed no significant in- or decrease in NO concentration. The slope was not significantly different to zero ($p = 0.2628$). The impact on eNOS remained within a range of 5.5 % (2.5 % SEM)

inhibition and 7.5 % (16.45 % SEM) stimulation, and on nNOS within a range of 10.05 % (1.85 % SEM) and 14.45 % (4.45 % SEM). Inhibitions or stimulations above 50 % are considered as significant (personal correspondence with Eurofins).

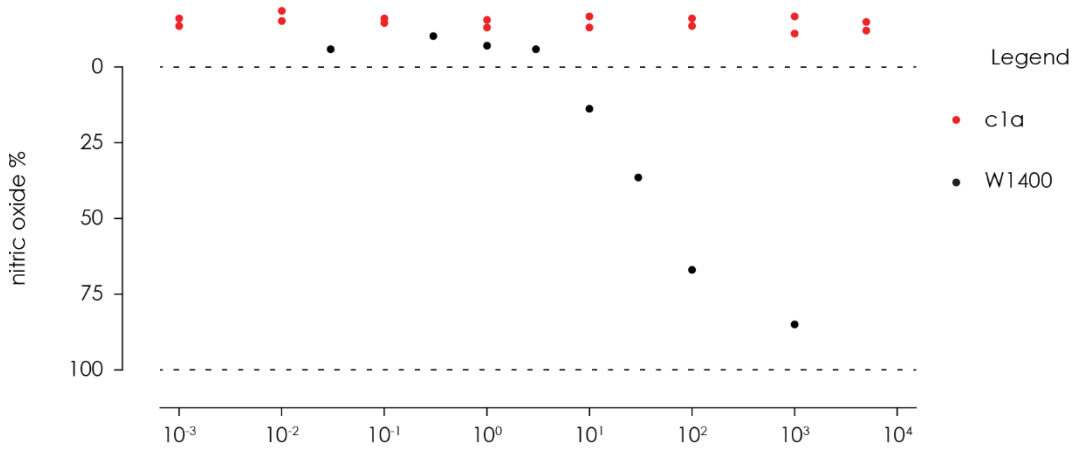

Figure 3.44: Modulation the iNOS enzyme activity by compound C1.0a

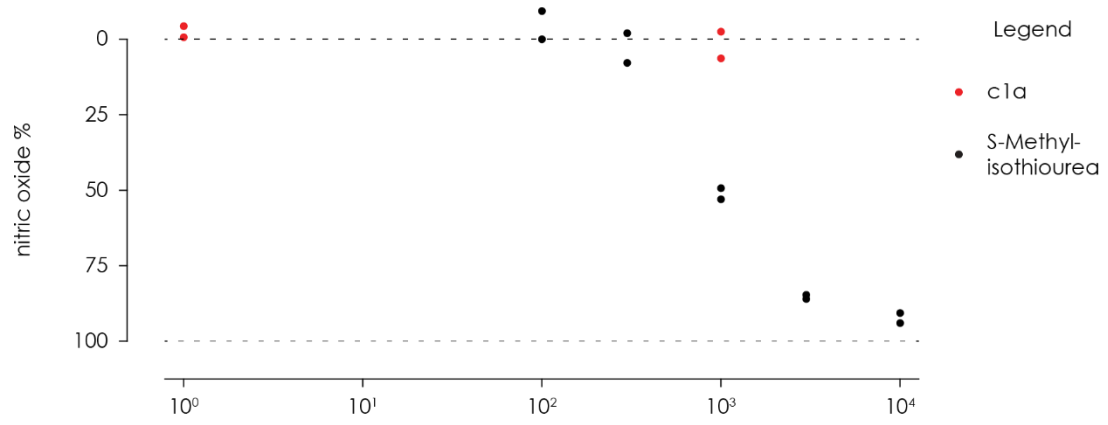

Figure 3.43: Modulation of the eNOS enzyme activity by compound C1.0a

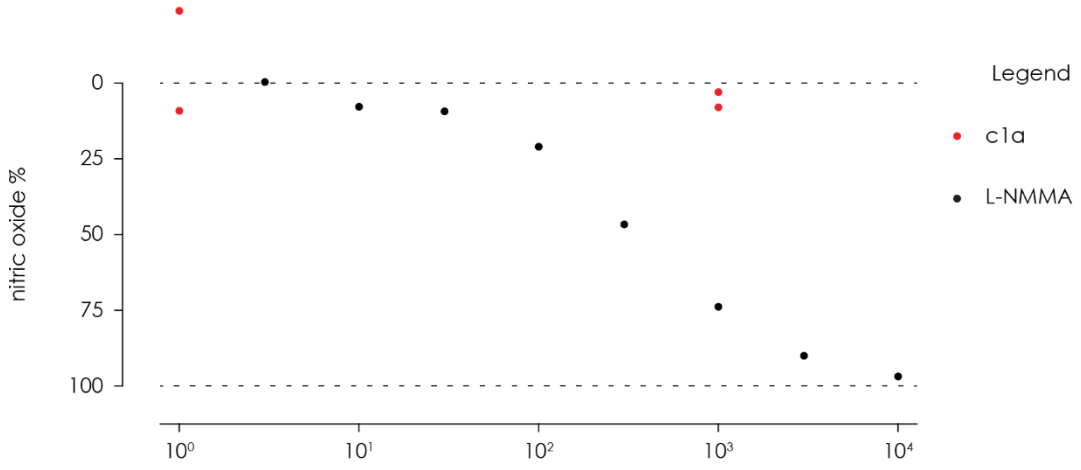

Figure 3.45: Modulation of the nNOS enzyme activity by compound C1.0a

3.15 The pharmacokinetics and ADME of C1.0 in healthy adult mice.

To assess the bioavailability in mammals we performed pharmacokinetic studies in wildtype mice. All pharmacokinetic studies were conducted by the company touchstone bioscience. They provided the experimental data and I performed the corresponding analysis.

3.15.1 Mice survive C1.0 for at least 24 hours.

In the first step, we evaluated the blood plasma level and survival in healthy wildtype mice over a period of 24 hours. 3 male adult healthy wildtype mice (strain CD-1) were fasted overnight, before 5 mg/kg of the diastereomer mixture C1.0 was injected intravenously in one shot. Blood samples were collected after 5, 15, and 30 minutes and 1, 2, 5, 6, 8, and 24 hours from the vein and the compound concentration was calculated using liquid chromatography mass spectrometry. After 24 hours all mice were killed. The

plasma concentration showed a continuously decrease over time. After 5 minutes the detected blood plasma concentration of the C1.0 was at 6.15 µg/mL (0.83 µg/mL SEM) equal to 11.9 µM (1.6 µM SEM). Within 1 hour this value dropped to 0.58 µg/mL (0.07 µg/mL SEM) equal to 1.1 µM (0.138 µM SEM) and after 4 hours to 0.012 µg/mL (0.003 µg/mL SEM) equal to 0.023 µM (0.007 µM SEM). After 24 hours the plasma concentration of C1.0 was at 0.653 ng/mL (0.184 ng/mL SEM) equal to 0.001 µM ($3.6\ 10^{-4}$ µM SEM). The blood plasma concentration of C1.0 remained above the calculated cell based IC_{50} value of 0.2 µM for the first 2 hours after the intravenous injection.

All mice survived this experimental setup, showing that the compound does not have severe side effects on the health of mice.

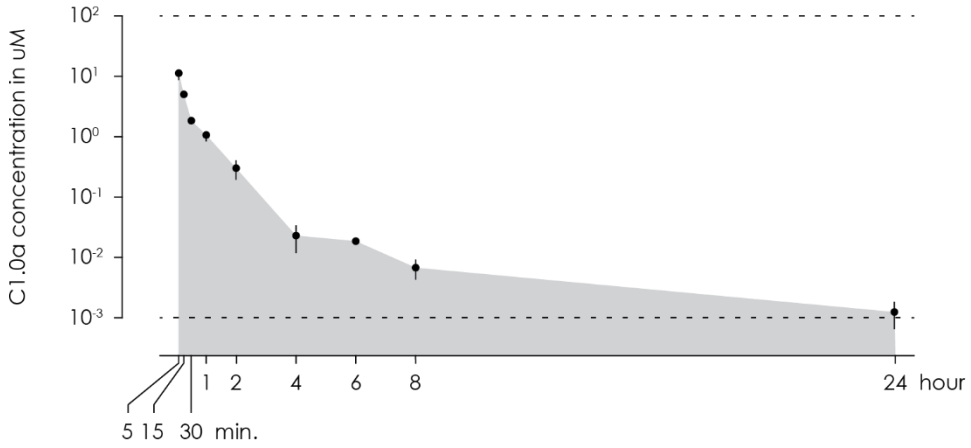

Figure 3.46: C1.0a's blood plasma concentration over a time period of 24 hours after a single shot intravenous injection.

3.15.2 C1.0 passes the blood brain barrier in healthy adult mice.

Showing that C1.0 can be detected in concentrations above the IC_{50} value in the blood plasma for more than 2 hours and that the mice survive the compound treatment, we setup a more detailed pharmacokinetic experiment in which we measured the concentrations in the blood plasma, liver, kidney, heart, and brain. The blood plasma is the main drug distribution organ, the liver the main metabolism organ, the kidney the main organ

for excretion, the heart a common organ for severe side effects, and the brain is our organ of interest. The experimental setup is similar to the one described above. 4 groups of 3 male adult healthy wildtype mice (strain CD-1) were fasted overnight, before 5 mg/kg of the diastereomer mixture C1.0 was injected intravenously in one shot. After 30 minutes, 1, 2, and 4 hours the mice were sacrificed, and the organs of interest were taken out, weighted and the concentration of C1.0 was calculated. The calculated blood plasma concentration of C1.0 was similar to those measured in the previous experiment (chapter 3.15.1 on page 106). The concentrations calculated for the liver, kidney, heart, and brain did not reach the high concentrations of the blood plasma but did show a similar drop over time. The liver and kidney reached of half the plasma concentration (plasma: 1.926 µM, 0.025 µM SEM; liver: 0.853 µM, 0.129 µM SEM; kidney: 0.961 µM, 0.112 µM SEM), the heart a quarter (0.440 µM, 0.039 µM SEM), and the brain 10 % of the plasma concentration (0.194 µM, 0.095 µM SEM). It is worth noting that the compound passed the blood brain barrier and that the concentration was in close approximation to the calculated IC_{50} value.

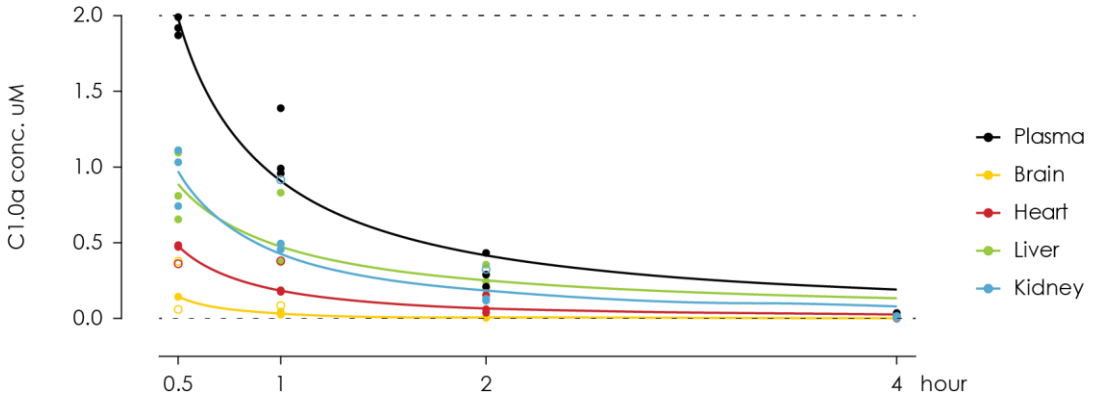

Figure 3.47: Tissue specific concentration of C1.0a over time period of 4 hours.

To investigate possible but unwanted enrichments in organs beside the brain, I normalised the concentration levels to the blood plasma level over time. In the heart, the relative concentration level remained constant between 22.3 and 27.3 % for the first 2 hours and dropped at 4 hours to 10.1 %. The kidney showed a similar result over time at a higher level. Up to 2 hours the relative concentration remained between 49.9 % and 61.3 % and dropped afterwards slightly to 46.6 %. In the liver, the relative concentration increased

over time from 44.3 % at 30 min to 84.9 % at 2 hours and dropped again to 41.4 % at 4 hours. The relative concentration in the brain started at only 10.1 % and decreased over time to 2.1 % at 2 hours, but in contrast to the other organs remained at this value 2 more hours (4h: 2.1 %). These relative concentrations indicate no enrichment in the heart and kidney and a reduction in the brain. The enrichment over time in the liver indicates a metabolic processing of the compound. This metabolic processing could lead to an inactive compound and/or to be not detected by the liquid chromatography mass spectrometry anymore.

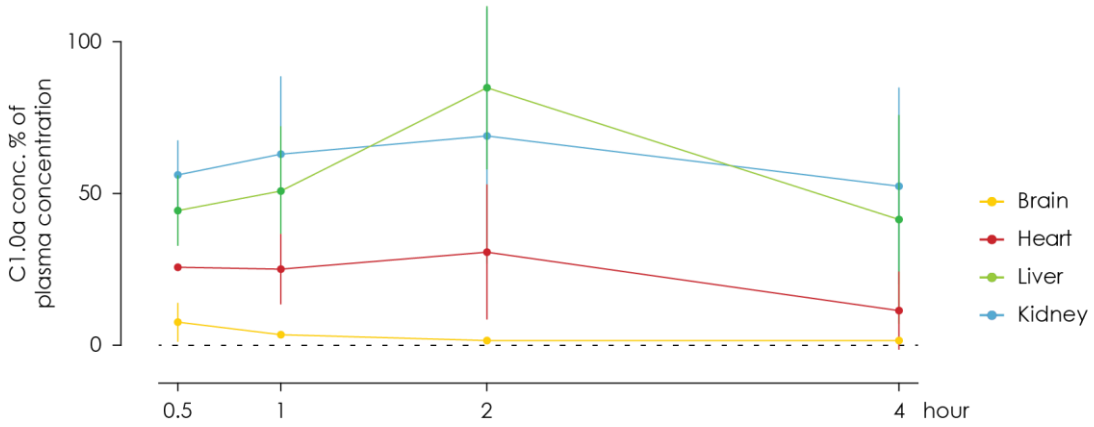

Figure 3.48: Tissue specific concentration of C1.0a in relation to the blood plasma concentration.

3.16 Compound 1.0 ameliorates neuronal deficits in a rodent model of mild cerebral arterial occlusion (MCAO)

A potential therapeutic use for compound C1.0 is an ischemic injury. It has been shown that in the acute and intermediate phase of an ischemic injury microglia and infiltrating macrophages become pro-inflammatory activated and release NO in a huge amount. As a proof of concept, we used the model of a 30 minutes middle cerebral artery occlusion

(MCAO) and treated those mice with compound C1.0. As a functional read out of neurological parameters, the motor coordination was tested with the accelerated rotarod test and their extrapyramidal motor locomotion was assessed using the pole test. Those parameters can be seen and tested in patients. The baseline of the corner test was assessed 5 days before the MCAO, the rotarod and pole test were trained for 2 days (day 3 and day 2 before the MCAO) and the baseline was assessed the day before the MCAO. On day 0 a 30 minutes MCAO was applied to adult male mice (C57Bl/6). Afterwards, the mice were treated daily for 7 consecutive days with an injection of 5 mg/kg of C1.0 diluted in $125x10^{-5}$ v/v DMSO and PBS or $125x10^{-5}$ v/v DMSO in PBS alone as a control. On day 2 and 5 after MCAO, the compounds influence on rotarod and pole test was measured, on day 6 the influence on the corner test was assessed. The lesion volume was measured on day 3 after MCAO using magnetic resonance imaging (MRI).

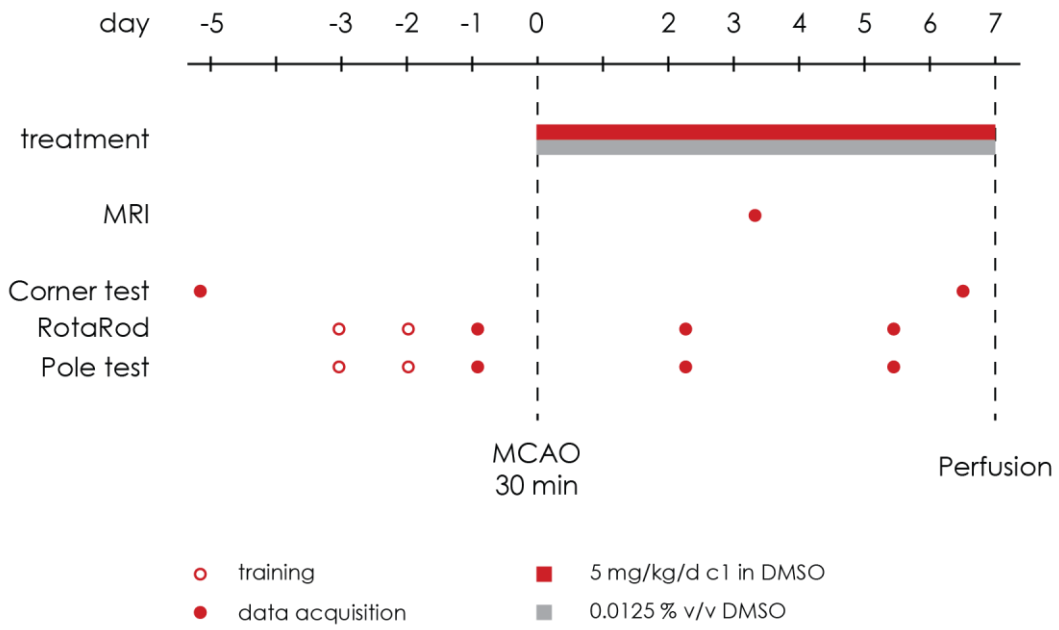

Figure 3.49: Illustration of the time line of the stroke application and the behaviour test.

3.16.1 C1.0 treatment has no significant impact on the stroke lesion volume.

The lesion volume after 6 days after MCAO was reduced from 12.74 mm³ (1,996 mm³ SEM) to 10.55 mm³ (1.420 mm³ SEM) but did not show a significant difference between the control and treatment group ($p = 0.3959$).

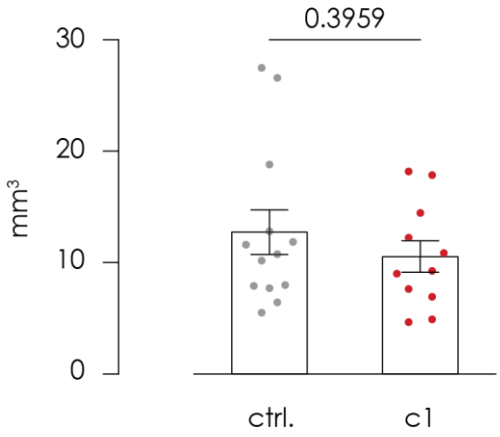

Figure 3.50: Volume of the stroke lesion 7 days after stroke.

3.16.2 C1.0 improves the laterality in mice.

Another important neurological parameter is laterality (the pathologic preference to turn to one side). Due to the right sided MCAO, mice tend to choose a left turn in situations of right-left choices. Before the MCAO was applied, mice turn to left in 5.538 (0.291 SEM) out of 10 observed cases in the control group and 4.545 (0.366 SEM) out of 10 cases in the treatment group, not significantly different from the statistical mean of 5 out of 10. 6 days after the MCAO the preference for a left turn increased significantly to 8.538 (0.312 SEM) out of 10 turns ($p < 0.0001$) in the control group and to 7.000 (0.632 SEM) out of 10 turns in the treated group ($p < 0.0001$). This decrease between the groups from 8.538 to 7.000 is significant ($p = 0.0213$).

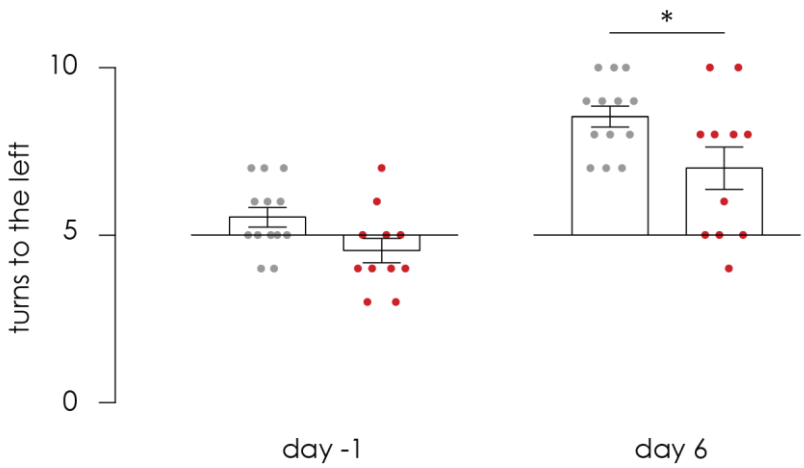

Figure 3.51: Head turning preference before and after stroke with and without compound treatment.

3.16.3 The forced movement on the rotarod is not improved by C1.0.

2 days after MCAO the time the mice spend on the accelerated rotarod decreased from baseline with 274 seconds (5.5 s SEM) to 220 seconds (12.2 s SEM) in the control group. After 5 days the time on the rotarod increased to 260 seconds (9.9 s SEM). The same pattern was observed for the treatment group with no significant difference (baseline: 276 s, 7.9 s SEM; day 2: 241 s, 16.4 s SEM; 261 s; 11.5 s SEM). However, the treated group did not show a decrease in time as strong as the control group did.

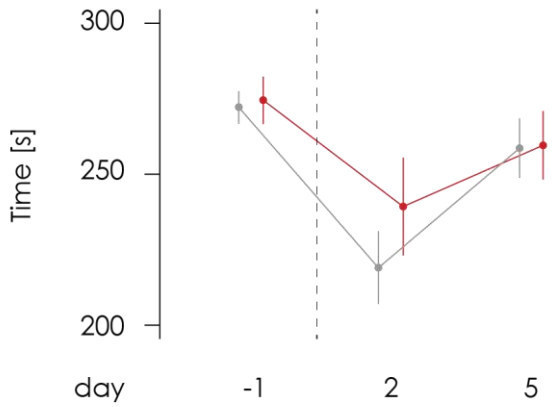

Figure 3.52: Time spend on the rotarod before and after stroke with and without compound treatment.

3.16.4 C1.0 treatment enhances the mice capability in the pole test.

The time the mice needed to turn upside down on the pole, and the time do climb down that pole was measured separately. 2 days after MCAO, mice of the control group needed longer to turn upside down (2.328 s, 0.378 s SEM) and to climb down (10.469 s, 1,966 s SEM) compared to the baseline (turn: 0.807 s, 0.071 s SEM; down: 5.292 s, 0.321 s SEM). On day 5 after MCAO, this increase normalised to the baseline for the time needed to climb down (6.076 s, 0.586 s SEM), but not the time needed to turn upside down (2.170 s, 0.491 s SEM). Treatment with C1.0 had a positive influence on both, the time needed to turn upside down and to climb down. 2 days after MCAO, the time to turn upside down and to climb down remained on a level similar to the baseline (turn: 1.175 s, 0.261 s SEM; down: 1.175 s, 0.261 s SEM) resulting in significant difference compared to the control condition (turn: $p = 0.0253$; down: $p = 0.0145$). On day 5 the treated group remained at a level similar to the baseline (turn: 1.350 s, 0.226 s SEM; down: 5.903 s, 0.410 s SEM), however due to change in the control group this effect is no longer significant.

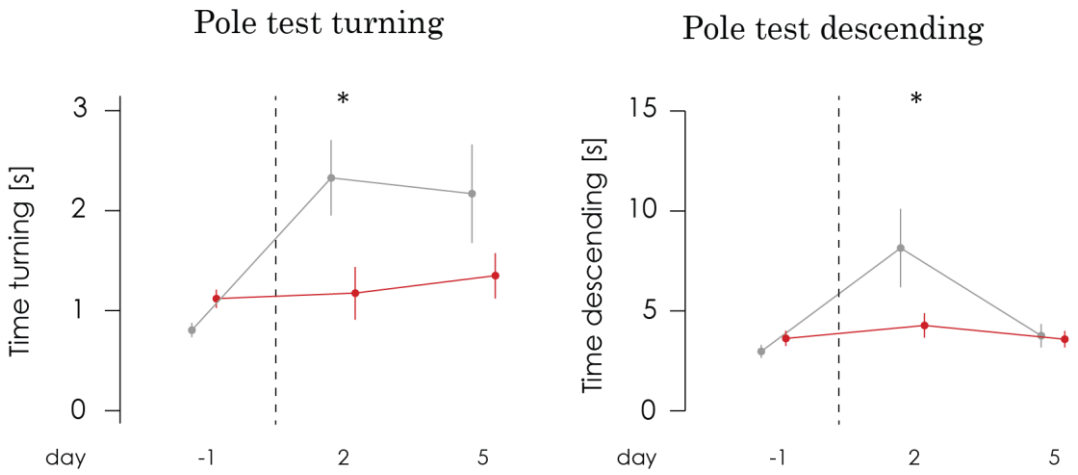

Figure 3.53: Time needed to turn and to descend in the pole test before and after stroke with and without compound treatment.

4 DISCUSSION

4.1 The distinct functions of Nitric Oxide

Nitric oxide is perhaps one of the most intensively studied transmitter molecule since its discovery by Ignarro [62] and Furchgott [173] in the early 1980s. Early investigation of nitric oxide revealed its biological function as a dilator of blood vessels. Since then, an increasing number of studies have shown the importance and the diversity of biological functions NO is involved in, resulting in over 150 000 publications on nitric oxide [174]. In addition to its role in regulating the blood pressure, NO is important in platelet aggregation, bone remodelling, inflammation and as a neurotransmitter. In mammalians NO is produced by the three isoforms, the endothelial NOS (eNOS), the inducible NOS (iNOS), and neuronal NOS (nNOS), representing the three main occupations: regulation of the blood pressure [97,98], first response mechanism of the immune system [54,58], and retrograde synaptic signalling [93,99,100]. It has been shown that NO is involved in many different physiological and pathophysiological processes [175] including diabetes [176], hypertension [177], cancer [178], drug addiction [179], memory and learning [32,90], bowel movement [180], stroke [181,182], septic shock [183], and differentiation of immune cells [184]. The impact of NO is locally restricted and originates from cells which express the distinct NOS isoforms, eNOS by endothelial cells, nNOS by neurons, and iNOS by cells of the immune system. The three NOS isoforms are regulated differently and have different catalytic proprieties and inhibitor sensitivities [59]. A misguided regulation of the NO pathway in the brain is implicated in a number of diseases, starting from an overactivated NO production by iNOS in the proinflammatory cascade in stroke up to an aberrant regulation of nNOS implicated in a number of neurological disorders, including the Alzheimer's and Parkinson's disease [32,33,185,186]. Anomalous overproduction of NO lead to neuroinflammation mainly caused by its free radical properties compromising the cellular integrity and viability and the regulation of cAMP [187,188]. The most prominent NOS isoforms of the CNS are nNOS and iNOS. A reduction in levels of NO through inhibition of NOS has the potential to be therapeutic in a multitude of indications including the treatment of stroke, neurodegenerative disorders (e.g., Parkinson's, amyotrophic lateral sclerosis (ALS), multiple sclerosis (MS) [94]),

and in the treatment of pain (e.g., migraine, chronic tension-type headache (CTTH), visceral, and neuropathic [189]). However, the therapeutic control of NO synthesis has, until recently, been unattainable due to the difficulties in achieving isoform-selective inhibition. The selective inhibition of the neuronal NOS (nNOS) enzyme and/or the inducible (iNOS) over the endothelial NOS (eNOS) enzymes for the treatment of pain or migraine would be required to avoid the cardiovascular liabilities associated with eNOS inhibition [190].

In this research, I focused NO's effect as a first response mechanism of the immune system. I identified and characterised a novel compound targeting the proinflammatory induced release of NO in microglia and macrophages.

4.2 The HTS yield two compounds of different structure and capabilities.

The initial HTS screening for compounds reducing LPS induced NO release in the microglial cell line BV2 revealed 4 compounds of different chemical structure all capable to reduce NO in a dose dependent manner. I characterised the effects of the compounds on the proinflammatory regulation in murine neonatal primary cultured microglia and murine adult bone marrow derived macrophages. Starting with the basic screen setup, I characterised the impact on the NO release induced by different stimuli, namely LPS, IFNγ, and polyIC [45]. LPS, a component of the outer membrane of gram-negative bacteria, is a ligand of the TLR-4 receptor complex inducing the iNOS derived NO production via the of the MyD88 pathway activating NF-κB [54,191]. IFNγ, a proinflammatory cytokine produced by cells of the innate and adaptive immune system, binds to its receptor (IFNγR1+IFNγR2), activating the STAT transcription factor family via the JAK-STAT pathway [192]. PolyIC, an artificial double-stranded RNA, is recognised by TLR-3 activating the transcription factors IRF3 and NF-κB via the TRIF/TRAF pathway [114,193]. The different signalling routes result in a different NO concentration released by macrophages and microglia. While LPS showed the most robust activation of microglia and macrophages, did polyIC show only a minor increase in NO release. Independent from the stimulus, do all compounds decrease the NO release in microglia and macrophages in a dose dependent manner. Treatment with C1.0 caused an outstanding reduction in NO release, reaching the level of the negative control for its

highest applied concentration. Compound C2.0 showed a similar reduction in NO release. However, it did not reach the efficiency in reduction and compound concentration. Compound C3.0 decreased NO robustly to a similar level as C2.0 upon the different stimuli, however, never fell below the 50 % level of the stimulated positive control. C4.0 shows a mediocre reduction of NO while employing the highest dosage of all compounds. The similar dose dependent reduction in NO upon all three different stimuli suggest a modulation of a protein common in all utilized pathway. These results lead to the hypothesis that the compounds regulate the NO release at a transcriptional level or later in the cascade [54,95,194,195]. Another plausible reason for the universal inhibition in NO release could be a general reduction in cell activity or cell death. The Alamar-Blue experiments executed in parallel showed no major decrease in metabolic cell activity nor did the values indicate a general cell death, declining this concern [196,197].

Beside the induction of NO does the stimulation proinflammatory cascade induce the release of cytokines. The most prominent proinflammatory cytokines are TNFα, IL1ß, and IL6. All three cytokines are acute phase cytokines and a released upon a proinflammatory stimulus. They themselves do activate proinflammatory pathways in an autocrine and paracrine loop [198].

Compound C1.0 did not interfere with LPS induced release of IL1ß, IL6, and TNFα in microglia and macrophages, supporting the previous hypothesis, that it acts on the transcriptional level or later in the NO cascade. However compound C2.0, C3.0, and C4.0 modulated the referred cytokines release in various ways. Treatment with C2.0 exceeded the LPS induced release of all evaluated proinflammatory cytokines in a dose dependent manner, counteracting the aim of this study to decrease the proinflammatory load in microglia. C3.0 showed an ambivalent effect on the concentration of cytokines. While it decreased IL1ß release slightly but significant in a dose dependent manner, it increased the IL6 dose dependently and TNFα independent of the applied dosage. It is likely that that C3.0 binds multiple targets, thus regulating different pathways on various levels causing this mixed image [198]. Out of the 4 tested compound, only C4.0 was able to reduce IL1ß, IL6, and TNFα in a dose dependent manner. The comprehensive reduction of NO and cytokines indicates a modulation of a major regulator in the proinflammatory pathway [40].

Based on these results, I suspended compound C2.0 and C3.0, leaving compound C1.0 and C4.0 as the main targets reducing the proinflammatory activation in microglia. The increase in ILß, IL6, and TNFα release provoked by C2.0 opposes this reduction. The mixed result on the cytokine release in combination with the poor reduction on the induced NO release fails compound C3.0. The data given in this initial evaluation propose C1.0 as selectively inhibitor of induced NO release which acts independent from the proinflammatory stimulus, and C4.0 as a more

global regulator, reducing the NO release as well as the proinflammatory cytokines. Compound C4.0 and C1.0 will be discussed in detail in the chapters below.

4.3 Compound C4.0 misses a structure action relationship.

The first characterisation of compound C4.0 done in primary cultured neonatal microglia indicates it as a global regulator of the proinflammatory pathway. Here, I further evaluate C4.0's regulatory impact on the NO and cytokine release in bone marrow derived macrophages, as well as the effect on microglial migration and phagocytosis, and the effect on the metabolism, cell death and cell number of other cells of the brain.

Microglia and macrophages share many features and pathways [11,50,199,200]. Among these is the proinflammatory induction of NO and upregulation of cytokine release, based on the same regulatory pathways in both cell types. Although both pathways are coherent in microglia and macrophages, they differ in the fine-tuned regulation upon different stimuli. [200] Equivalent to the similarities in-between microglia and macrophages, does C4.0 modulate the induced release of NO and the proinflammatory cytokines IL1ß, Il6, and TNFα analogously. It reduces the NO release independent of the applied stimuli in a dose dependent manner. Interestingly, did a treatment with 10 µM C4.0 lead to a stronger reduction in macrophages compared to microglia for all stimuli. The reduction of the cytokines in macrophages is almost identically to the reduction in microglia. This cell and stimuli independent regulation of NO and the proinflammatory cytokines fortifies the hypothesis of C4.0 as a global regulator in the proinflammatory cascade.

Microglial activation is often linked to increased phagocytosis [172] and directed migration [40,41] towards injury. Both migration and phagocytosis are highly complex processes requiring a multifaceted regulation. I evaluated the effect of compound C4.0 in a black-box fashioned experiment, altering the initial stimulation and treatment, and quantify the phagocytic and migration activity without further investigation into the underlying pathways. While showing no effect on microglial phagocytosis, unstimulated as well as LPS stimulated, C4.0 does modulate microglial migration in a miscellaneous way. C4.0 acts as a chemoattractant on its own but has no effect on the motility. However, in the presents of ATP this effect reverse, not elevating the induced

chemotaxis but reducing the ATP induced motility. This diverse action suggests that C4.0 attracts microglia, but once in place C4.0 reduces microglial motility to lock them in place. The missing impact on phagocytosis attenuates the hypothesis of C4.0 as a global proinflammatory regulator [172]. The changes in migration could be the result of a compound triggered regulation of migration pathways, or due to the recognition as a danger signal [187,201]. Danger signals do increase the directed migration towards the point of danger and lock them there to fight the source of the danger single.

One aim of this work is the compounds application in CNS related diseases. To exclude possible negative effects on the health of other prominent cell types within the CNS, namely neurons, astrocytes, and oligodendrocytes [202]. I studied the consequences of C4.0 treatment on the metabolic activity, proliferation, and cell death. C4.0 shows no impact on the cell death of astrocytes, oligodendrocytes, or neurons. However, it decreases the metabolic activity in astrocytes while increasing the proliferation rate at the same time, potentiating the effect on metabolic activity. In addition, C4.0 decreases the metabolic activity in oligodendrocytes slightly but significantly. These data were gained *in-vitro* for each cell type separately, omitting the intercellular communication and regulation of these cells in the CNS [203]. Though I used primary cultures for most of the cell types I had to substitute the oligodendrocytes for a cell line. The missing intercellular exchange and the use of cell lines diminish the significance of these data. However, it provides an indication of possible complications with those tested cell types.

A significant step in drug development is the identification of the compounds chemical lead structure that causes the observed reactions [204,205]. A lead structure is a defined representative of a chemical compound class, which contains the main target binding elements [206]. In most cases, the lead structure is smaller than the initial hit compound of the HTS. It is missing additional side groups like carboxylic acid, methyl, benzol, and many more. Starting from the lead structure it is possible to add side groups back on to modify the solubility, chemical and biochemical stability, target specificity and diminish off target binding, just to name a few. To identify the lead structure of compound C4.0 I performed in collaboration with Edgar Specker (FMP) a structure action relationship (SAR) analysis [207]. The compound C4.0 was altered at 3 distinct positions resulting in 19 structural different compounds. Unfortunately, did the SAR expose no lead structure for C4.0. The most potent chemical of the SAR is the initial compound C4.0 itself. The analysis of the observed biological reactions does not match with the chemical structures of the side groups. It is missing a clear structure action relationship. This could be caused by a unique solitaire chemical structure of C4.0, that has no additional related chemical range, caus-

ing all modifications to decrease its potency. A more likely explanation is the existence of multiple binding targets of C4.0. An accurate interpretation of biological experiments, target finding, and chemical optimisation of the compound with multiple targets is nearly impossible.

Due to the data of the SAR, I suspended compound C4.0, leaving compound C1.0 as the main target.

4.4 The selective NO inhibition by C1.0.

The data of the initial evaluation described above, suggests C1.0 as a selective inhibitor of NOS, acting on the transcriptional level or further down in the NO cascade. To verify this preliminary hypothesis, I conducted the same experiments done with C4.0 with compound C1.0, excluding the SAR analysis.

Treatment with C1.0 causes almost identical results in bone marrow derived macrophages as it does in primary cultured neonatal microglia. It reduces the induced NO release in a dose dependent manner independent from the applied stimulus, be it LPS, IFNγ, or polyIC. C1.0 is able to decrease the NO concentration to levels indifferent to the unstimulated negative control for all three referred stimuli. This reduction in the NO release can be seen in the LPS induced release of proinflammatory cytokines or the modulation of the metabolic activity. Both, the cytokine release and the metabolic activity remains untouched in the present of C1.0. This result underlines C1.0s ability to selectively inhibit the induced NO release, supporting the hypothesis acting on the transcriptional level or further downstream in the NO regulating cascade. Furthermore, do these experiments show that the reduction in NO is not microglial specific. It is likely that all cell types which share the same NO releasing cascade with microglia and macrophages will be affected by a treatment with C1.0 [58,95,194,208]. The evaluation of microglial phagocytosis and migration revealed a modulatory effect on the chemotaxis and motility. The basal and stimulated phagocytosis was not affected by the compound. C1.0 showed a chemoattracted property, increasing microglial migration towards itself slightly but significant, while it reduces the motility almost completely. As discussed earlier for compound C4.0, could this be the result of a direct interference with a regulatory pathway or the detection of C1.0 as a danger signal. Furthermore, could the lack of NO in the cell medium change the migration, which would contradict recent literature [187,201]. The evaluation of C1.0s impact on the health of other prominent

cell types within the CNS, namely neurons, astrocytes, and oligodendrocytes, showed no negative results allowing an application in the CNS. Even though this experiment does not reproduce the complex cellular structure of the brain, a negative result does keep the compound in the pipeline for further characterisation.

So far, the data provided in this study support the hypothesis that C1.0 modulates the induced NO release at a transcriptional level, or the responsible enzyme directly. Upon a proinflammatory stimulus microglia and macrophages release NO into the extracellular space as a first response mechanism of the immune system. Responsible for this NO production in microglia and macrophages is the inducible NOS isoform: iNOS. iNOS is mainly regulated at its transcriptional level via the proinflammatory transcription factors NF-κB and STAT1 [54]. The promoter region of the mouse iNOS gene contains several binding sites for transcription factors like NF-kB as well as Jun/Fos heterodimers, some C/EBTs, CREBs and the STAT family of transcription factors, within its proximal and distal regions [102,103,111,209]. The human promoter region shares sequences homologous to the mouse. Activation of the transcription factors inducing iNOS mRNA, resulting in the generation of the iNOS proteins, which then forms a homo-dimer including the needed cofactors to generate an active iNOS protein complex. While the activation of iNOS is incorporated into the highly regulated proinflammatory pathway cascade, the regulation and inhibition do take place in a much broader spectrum. iNOS driven NO production is directly connected to the accessibility of its substrate L-arginine and the electron donor NADPH. Both factors are available in a vast amount within the cell [210]. Another mechanism regulating iNOS driven NO production is the modification of the mRNA transcription speed and stability [211], and the protein translation speed and stability [95,96,212]. The regulation of both, transcription and translation, are not iNOS specific but shows a systematic effect. Such a broad regulation by compound C1.0 is very unlikely since the release of pro-inflammatory cytokines remains untouched. To determine a translational impact of C1.0 on iNOS, I analysed iNOSs mRNA levels in physiological and proinflammatory activated microglia in the presents of compound C1.0. As reported in the literature is the iNOS mRNA barely detectable in physiological conditions and massively upregulated upon proinflammatory activation [54]. Treatment with C1.0 does not change this behaviour. This result shows clearly that C1.0 does not interfere with the iNOS regulation prior to its translation into mRNA, supporting the data from the experiments above showing a stimulus independent downregulation of NO release. It narrows the down the possible targets of C1.0 regulating the NO production and rejects part of the hypothesis, that C1.0 modulates the induced NO release in a pathway posterior its mRNA translation or at the level of the responsible enzyme directly.

Nevertheless, a direct enzyme activity assay conducted by Eurofins show no direct inhibition of iNOS or its isoforms eNOS and nNOS by C1.0a. This data excludes a direct iNOS inhibition but also the required dimerization of the protein [59]. It suggests a regulation of iNOS posttranscriptional but prior to the enzyme ensemble. A NO specific regulation within this range of the pathway would be new to literature.

In a timeline experiment, in which microglia were stimulated with LPS prior to the treatment with C1.0, I could show that C1.0 is able to reduce the NO release of already activated microglia, resulting in a power function leading towards a defined maximum in the NO concentration. This shape can be explained by the traditional interaction between a substrate and an enzyme, in which the substrate binds the enzyme irreversible [213]. This would indicate that C1.0 binds iNOS irreversible and routes it to protein degradation [214] supporting the hypothesis that C1.0 acts directly on the NO synthase. This reduction in NO production posterior to the activation has some great advantage in the application as a drug. C1.0 could not only prevent the NO production in a cell that will be activated, but also in already activated cells opening up a vast field of acute applications.

Compound C1.0 exists in two diastereomeric forms: C1.0a and C1.0b. The chemical structure of the compound will be discussed in detail below. In the previous experiments, a mixture of both diastereomeric forms was used (approximately 43 % C1.0a and 57 % C1.0b calculated using HPLC). A microglia based dose dependency experiment showed a shift in the IC_{50} value of C1.0a towards 104 nM, while the IC_{50} value of C1.0b shifted to 43 µM. In the concentration range used in the previous experiments, 0.025 to 2.5 µM, does C1.0b shows only a minor impact on the NO reduction, while C1.0a diminishes the NO release almost completely. Combined with the knowledge about the composition of the diastereomeric mixture C1.0 explains the previously calculated IC_{50} value of 252 nM. The cell based IC_{50} value of C1.0a (104 nM) outreaches the most common used NOS inhibitors: L-NAME, a non-selective NOS inhibitor, and 1400W, an iNOS-selective inhibitor. Their IC_{50} values are 200 nM and 13.5 µM respectively, measured in an enzyme-activity assay [182,215]. The different assays used do not allow a direct correlation since IC_{50} values measured in cell-based assays tend to be higher than those in enzyme-based assays.

The first inhibitor of nitric oxide production was found and applied before the responsible enzyme was identified [216]. This inhibitor, named L-NMMA, was a modified form of the NOS substrate L-arginine. So far, the development of NOS inhibitors focused on mimicking the NOS substrate L-arginine and the co-factor BH-4 antagonising their binding [190,208,217–224]. This approach resulted in a broad list of chemical structures with only a little diversity. Most of those chemical structures are closely related to pyridine, imidazole, indazole as these are part of BH-

4 or the already named L-arginine. The binding site of L-arginine and the co-factor BH-4 are highly conserved in-between the different isoforms of NOS, causing an unselective inhibition of all isoforms for most of the chemical structures [225]. Inhibitors selective for only one isoform are seldom. Inhibitors more selective for one isoform of NOS show a larger variance in their chemical structure but are still based on the same original chemical structure.

Our compound C1.0 has a unique chemical structure compared to the broad list of known NOS inhibitors. It does neither resemble the substrate L-arginine, nor the co-factor BH-4. C1.0 has a small peptide like structure based on 1 natural - proline - and 3 artificial amino acids connected via peptide bonds.

Drugs made from small peptides do have as many advantages as disadvantages compared to small molecule-based drugs. Peptide based drugs are highly specific combined with a low cell toxicity derived from their tight binding to their targets [226]. Peptide based drugs adopt chemical interactions of the side chains of the natural amino acids and add a vast list of new interactions by utilising artificial amino acids. This results in highly divers and specific small peptides. The target recognition can occur with as low as a few amino acids [227]. The imitation of natural proteins causes less side effects with a reduced intensity compared to small molecules. Peptides outperform small molecules at Phase II to Phase III transition stage with 29% for small molecules and 42% for larger drug candidates [226,228,229]. Even larger peptides, which violate Lipinski's of five, are feasible for drug development. Modifications for passive or active transport thought biological barriers can be added utilising natural peptide structures [229], as well as cell and tissue penetration [230,231], or nuclear uptake [232]. The advantage of adopting the natural amino acid does provoke one of the major disadvantages: the enzyme degrading system. The synthesis of protein/peptides and their degradation are precisely regulated. Small artificial peptides are likely to be rapidly degraded [226,228]. An accelerated peptide deration can be prevented or slowed down by the incorporation of artificial amino acids, altering the amino acid conformation form L to D, removing the characteristic n- and c-terminus, modification of the peptide backbone, or masking the peptide backbone. All these steps can be incorporated into the peptide-based drug using an entirely chemical synthesis. A rather unpredictable disadvantage of peptide-based drugs is the possible detection by the immune system as foreign. The detection of foreign proteins/peptides by the immune system is a highly complex mechanism and can cause a severe immune reaction.

Composed of only 4 amino acids, our compound C1.0 is below all FDA approved peptide-based drugs, starting with 7 amino acids for Eptifibatide (excluding peptide-based drugs with unknown sequence) [233]. The list of approved peptide-based drugs can be divided into a group of short peptides composed of up to 100 amino acids (41 out of 148) and a group of long peptides

with ranging from 100 to 300 amino acids (97 out of 148). 10 peptide-based drugs are composed of up to 2768 amino acids[233].

The short length of C1.0 increases the probability to pass a cell's membrane, barriers like the mucosa or the blood-brain barrier and to be taken up orally. In this study, I could indirectly show that C1.0 passes a cell's membrane, and directly show that C1.0 passes the blood brain barrier. Treating microglia with LPS induced the transcription of iNOS mRNA and initiated the iNOS dependent NO production. One hour pre-treatment with C1.0 did not change the LPS induced mRNA level of iNOS but decreased the NO production in a dose dependent manner. The iNOS protein is found in the particulate and cytosolic cellular pools [234]. The combination of both experiments indicates that C1.0 do cross the cell membrane to down-regulate the function of the iNOS protein. However, I did not measure the compound concentration within the cytosol directly. In the ADME and pharmacokinetic experiments, provided in this study, C1.0 was applied in single shot intravenously into healthy mice. In the blood plasma C1.0 could be detected with HPLC for at least 24 hours after application (the experiment not perpetuated). In the brain of healthy mice, C1.0 was detectable for at least 4 hours (the experiment was not perpetuated). The amount of C1.0 in the brain reached a maximum of 10 % of the blood plasma concentration, whereas the concentration in the heart, liver, and kidney reached 27%, 85%, and 22% respectively. The detection within the brain indicates that C1.0 passes the blood-brain barrier. However, since these experiments were performed by an external company I cannot exclude a contamination of the brain sample with blood plasma. A contamination should result in an invariant change in values over time compared to blood plasma. This is not the case. A prominent way to bypass the blood-brain barrier is a break-down of those, which I also cannot exclude.

The four amino acids C1.0 is composed are the natural amino acid proline, and 3 artificial amino acids resemble phenylalanine and two times tyrosine. The sequence, starting with the n-terminus, is phenylalanine-like amino acid, natural proline, and 2 times tyrosine-like amino acids. All four amino acids are connected by a peptide bond, in which a primary amine group coupled with a carboxylic acid group. A basic peptide backbone is vulnerable to enzymatic degradation by endo- and exopeptidase [235]. Natural peptide backbones start with a primary amine group at the n-terminus and end with and the carboxylic acid group at the c-terminus. Both groups are chemically reactive. The peripheral peptides bones of C1.0 do not follow the stringent peptide bond nomenclature. The subgroup of phenylalanine-like amino acid at the n-terminus is coupled to the hydrogen atom of the carboxylic acid group instead to the carbon atom, forming an ester. In addition, this subgroup misses the primary amine group. Both modifications shield peptides n-terminus against exonucleases. The modifications of the c-terminus are mirror-inverted. The tyrosine-like amino acid is directly coupled to the nitrogen atom forming a secondary amine, and

the carboxyl acid group missing. The incorporation of proline protects C1.0 against many endopeptidases. The endopeptidases trypsin, chymotrypsin, elastase, thermolysin, and pepsin – only to name a few – do cut peptide bones specifically unless their recognised motive is followed or proceeded by proline [235]. Endonucleases do recognise specific motives of amino acids more or less stringent, depending on the specific peptidase. The artificial amino acids of C1.0 reduce the change of being cleaved by those. Taken together, does C1.0's innate chemical structure support the chemical and biological stability, by reducing the number of functional chemical reactive groups, shielding the peptide characteristic n- and c-terminus, and the incorporation of proline. In this study, I demonstrated indirectly that C1.0 has a long-term stability in *in-vitro* and *in-vivo* experiments. The experiments described above do not only indicate that C1.0 passes several biological barriers but also that it is stable for more than 24 hours in the blood plasma in healthy mice and for more than 48 hours in cell culture experiments. However, there is still a possibility that C1.0 is enzymatically cleaved or chemically modified. This study does not provide a direct verification of the chemical and biological stability of C1.0.

Proline is the only natural occurring proteinogenic amino acid in the peptide structure. It contains one of the chiral centres within C1.0, being fixed in the L- / S-conformation equal to the natural occurring proline. Prolines side chain pyrrolidine is connecting directly with the amine converting this into a secondary amine. This unique structure of proline causes unique characteristics [236]. Unlike other proteinogenic amino acids, prolines side chain is fixed in its 3-dimensional space. In addition, it changes the rotational behaviour of the peptide backbone, a reason why proline is incorporated much slower into a peptide in nature and prevents peptide cleavage. Due to its special characteristics, does proline provide certain conformational stability in C1.0.

Phenylalanine- and tyrosine-like amino acids share the benzene ring as a common chemical characteristic. Benzene rings do line up with each other caused by van der Waals force, providing spatial stability within on proteins, in-between proteins, and between protein co-factors or substrates [237]. Here, the benzene rings might help to orientate and align C1.0 to the target. Benzene rings are hydrophobic and decrease the solubility in water. This is counteracted by the ester coupling of the phenylalanine-like amino acid, and the hydroxymethyl group of the tyrosine-like amino acid.

The new described compound C1.0 attenuates the NO release in microglia and macrophages in a dose dependent manner with an IC_{50} value of 250 nM determined in a cell based assay. The most common used NOS inhibitors L-NAME, a non-selective NOS inhibitor, and 1400W, an iNOS-selective inhibitor, have IC_{50} values of 200 nM and 13.5 µM respectively, measured in an enzyme-activity assay [182,215]. Due to the different assays used, those data cannot be correlated

directly with each other since IC_{50} values measured in cell-based assays tend to be higher than those in enzyme-based assays. This highlights the potency of our compound to target NO at a lower IC_{50} than currently used compounds.

4.5 C1.0 passes the blood brain barrier in *in-vivo*.

I have tested C1.0 in pharmacokinetic study *in-vivo* to assess the compounds drug-ability and its potential to use it in a disease model as a proof-of-concept study. The data provided by touchstone bioscience showed that healthy mice tolerate the application of the substance without any obvious side effects for at least 24 hours. As a first in line *in-vivo* experiment, this data provides an approximate overview of the effects and possible side-effects on the complex biological system of a mouse. This data indicates that our compound neither has a strong negative effect on the immune and cardio vascular system, which reacts within minutes or hours [87,88,238]. Moreover, does this data indicate that C1.0 does not affect the endothelia NOS isoform (eNOS). An inhibition of eNOS, responsible for the regulation of the arterial muscle tone, would cause a drop in blood pressure, leading do shock-like symptoms [59,77,181]. A closer look on the tissue specific distribution of compound C1.0 does show that our compound passes the blood brain barrier of healthy mice and reaches concentrations in the brain that exceeds its IC_{50} for iNOS inhibition. A major risk factor in drug development is offside targets in the heart, indicated by an enrichment within the organ. Commonly, those lead to an exclusion of those compounds. Compound C1.0 does enrich in the liver, presumably caused by metabolism of the compound, but not in heart, mitigating this concern [168,169,239,240].

4.6 A proof of concept study: C1.0 improves extrapyramidal motor skills and laterality in an *in-vivo* model of ischemic injury

NO plays a key role in stroke, modulating the vasodilation of arteries, parts of the immune system, and being toxic to neurons. eNOS and nNOS activity increases in the first minutes after stroke and reduces significantly afterwards [241,242], whereas iNOS is upregulated from 12 hours after stroke and is lasting for up to seven days [147]. While eNOS derived NO is neuroprotective, nNOS-derived NO [243–245] and iNOS-derived NO [150,246–248] are detrimental to tissue survival resulting in an inferior neurological outcome. This opposing effect is illustrated in the innumerable studies trying to improve the stroke outcome utilising NO-donors, NO-acceptors (-scavengers), or unspecific and specific NOS inhibitors [181,215]. The ambivalent action of NO is based on the different location (blood vessel vs. brain tissue), time (shorty term effects vs long term effects), and concentration (high vs low). Several strategies haven been used to target the neurotoxic property of NO. Only a few have reached clinical trials. Non-selective NOS inhibitors aiming at the toxic overshoot of NO produced by iNOS led to contradictory results. Some studies using L-NMMA in models of experimental stroke reported at smaller lesion models [144,249–251], neuroprotection [252], less cerebral oedema [249] and delayed onset of neuronal death [253]. In contrary, other studies reported larger infarct volume [247,254] and increases in the blood pressure [255] after L-NMMA application. Also, low doses of L-NMMA caused smaller infarcts [256–259] whilst higher doses caused increased infarct volume [260–262]. Phase I clinical studies reported an overall increase in blood pressure, indicating a systemic impact on vasoconstriction [263]. Taken together do non-selective NOS-inhibitors act on the whole spectrum of NO-regulated symptoms, with all the positive and negative consequence, and are unlikely to be neuroprotective after stroke.

iNOS specific inhibitors seem to be a more promising target in stroke, aiming for the high cytotoxic concentrations of NO. Ivanova et al could show that aminoguanidine acts as an iNOS inhibitor and to be neuroprotective in the onset of stroke, acting in addition on other targets by inhibiting production of neurotoxins [264]. Studies on the experimental model of stroke reported a dose dependent reduction in lesion volume, even when applied 24 hours after the ischemic event [133,265–267]. However, this drug has been refrained from clinical trials due to safety reasons [268]. Other compounds have also been tested, such as 1400W, which has been shown to decrease lesion volume and neurological deficits after stroke in rats [269] but also safety questions have

risen. New nitric oxide inhibitors such as GW274150 [270], GW273629 [271] show less toxicity but failed to show effectiveness for CNS diseases.

In a prove of concept experiment we applied the active form of C1.0, in an experimental model of stroke. As a model for mild ischemic injury, we used 30 minutes of middle cerebral artery occlusion (MACO) and treated the mice 7 consecutive days with an interval of 24 hours. To influence the outcome of the stroke, C1.0 has to fulfil two requirements, it has to be available at the side of the disease in adequate concentrations, and possible side effects should not outreach the disease's symptoms. Both are achieved by C1.0. In this study, I could show, that C1.0 passes the blood brain barrier in healthy mice, reaching concentrations in the brain that exceeds the IC_{50} value for iNOS inhibition. In addition, the disruption of the blood brain barrier caused by stroke supports the compounds availingly in the ischemic area [272]. The performed pharmacokinetic experiments show, that C1.0 does exhibit no noticeable impact on healthy adult mice, not interfering with the disease symptoms.

As noted beforehand, does an inhibition of eNOS exacerbate a strokes outcome [94,147,273]. In an enzyme activity assay, I could show that eNOS driven NO production is not regulated by C1.0. Yet, the complete data set of the enzyme activity assay should be considered with caution, since it does not align with the general data in this study. Despite this concern on the enzyme assay, do the results of pharmacokinetic experiments indicate no or only a minor inhibitory effect on eNOS, exhibiting no noticeable impact on the mice health. A systematic regulation of eNOS would cause a high increase – in case of an inhibition – or decrease – in the case of an excitation in NO concentration in the blood plasma. Both lead to sever shock symptoms, which are not reported in the experimental data provided.

The subsequently chronic application of C1.0 improved some but not all measured parameters after stroke. The plain volume of the lesion did not decrease significantly. Despite the unchanged lesion volume, 3 out of 4 neurological measured parameters improved at least temporary. Starting with the negative parameter, the application of C1.0 did not change the time mice spend on the rotarod compared to the control condition. Mice suffering from stroke do tent to have significant shorter times remaining on the spinning rod [274,275], lacking motor coordination as it has been reported for human survivors of stroke [276]. However, a translation of the rotarod test from mice to human is unclear, since humans are not challenged with a similar test [277]. Contrary to the rotarod, application C1.0 improved the time mice needed to turn and descending on the pole test. While the rotarod measures a forced motor coordination, the pole test evaluates a voluntary motor coordination. Taken both results together imply that C1.0 has a positive effect on planning complex motor coordination tasks. Treated mice showed an overall performance after

stroke not different from the baseline control before the stroke, while untreated mice performance decreased at day 2 and gained again at day 5 after stroke. An evaluation of this temporal increase in performance is difficult since we measured only two time points shortly after the stroke. A long-term observation to assess the impact on the overall life quality of C1.0 treated mice needs to be carried out in the future.

4.7 C1.0a is a novel compound targeting NO release in microglia and macrophages – an outlook.

In this study, I introduced a novel compound targeting the induced NO release in microglia and macrophages. The compound exhibit peptide like structure unique to all known NOS inhibitors. In a pharmacokinetic study *in-vivo*, I could show that mice tolerated the application of the substance without any obvious side effects. I have also shown that the compound can pass the blood brain barrier and can reach concentrations in the brain that exceeds its IC_{50} for its iNOS inhibition. Even at higher doses, C1.0 does not affect the viability, metabolic activity, proliferation and cell death of microglia and other brain cells like oligodendrocytes, astrocytes, and neurons. Furthermore, I could show that C1.0 can attenuate neurological symptoms after stroke. In our experimental stroke model, C1.0 improved motor skills and reduced laterality.

This work can only be the starting point in the development of a new drug targeting NO release. Even though I could narrow down the possible targets of C1.0, the exact binding partner is missing. Without the knowledge of the binding partner, further chemical and biological evaluation of impact C1.0a has is challenging. Following up this work, a target finding experiment is planned, in which a modified C1.0a molecule - joint covalent with a chemical linker - is used to pull down and analyse all binding proteins. The information about the direct binding partner of C1.0a helps to improve the biological and chemical analysis. On the biological side, a more specific pathway analysis can be performed, identifying possible side effects and target specificity. Here I propose, a mRNA sequencing of treated and untreated microglia with and without LPS stimulation. Even though I could show that both C1.0a and C1.0b did not interfere with iNOS mRNA, it will give an overview of other pathways that might be regulated directly by C1.0 or by the missing NO. On the chemical side the binding of C1.0a to the target can be studied, was

well as modifications that enhance this binding or the overall pharmacokinetics. In a first step a SAR, as it was done for compound C4.0, will give a better overview of C1.0a's lead structure and might even identify compounds with a lower IC_{50} value. An *in-silico* binding study of C1.0a and the newly discovered chemical structures from the SAR might give an inside into the binding mode of the compound to its target. Together, the analysis of the target finding, the SAR, and the *in-silico* binding studies will increase the knowledge of the mode of action of compound C1.0a. The mRNA screening might reveal unknown offside targets.

Important in the NO regulation is isoform specific modulation. The regulation of iNOS has to outbalance the regulation of eNOS and nNOS, to decrease possible side effects or even counteractions on the positive effects of a reduction in iNOS driven NO production. The data provided by Eurofins counteract all other data provided in this thesis, therefore the assay should be repeated to clarify the data. So far C1.0a was only tested in murine cells. However, the large similarity in NOS amino acid sequences and regulation in-between species makes it likely that C1.0a does show the same impact in humans as it shows in mice. A test on human microglia is possible but laborious. As I could show does C1.0 show a similar effect on murine macrophages as it does on murine microglia. Therefore, a test on human macrophages is a good approximation. Those assays are already planned.

With this knowledge, the compound can be developed step by step into a drug targeting stroke and other NO related diseases in the CNS and the whole body.

5 SUMMARY

Microglia, the resident macrophages of the brain, monitor the central nervous system (CNS) homeostasis. Alterations in homeostasis activate microglia in a variety of ways. Upon a pathological stimulus microglia change their appearance from a ramified into an amoeboid morphology, increase their phagocytic activity, and release pro-inflammatory cytokines and nitric oxide (NO). This response is involved in the pathological process in acute and chronical neuroinflammatory disease such as stroke, multiple sclerosis, or schizophrenia. A dysregulated microglial activation can improve or exacerbate the outcome of those diseases. Therefore, it is of therapeutic interest to identify new compounds, which modulate the activation process of microglia specifically.

In this thesis, I identified a novel compound which inhibits specifically the induced NO release in microglia and macrophages independent of the applied pathological stimulus. We screened a library of 16544 compounds for their ability to interfere with lipopolysaccharide (LPS) induced NO release in the microglial cell line BV-2 and verified the results in the primary cultured neonatal microglia. The compound showed a dose dependent reduction of NO after stimulation with LSP, interferon gamma (IFNγ), and polyinosinic:polycytidylic acid (polyIC) without being cytotoxic. The LPS-induced release of proinflammatory cytokines TNFα, IL1ß, and IL6 was not altered in the presents of the compound. I could show that the basal and LPS activated phagocytosis in microglia remained untouched, while it showed some influence on microglial migration. Furthermore, I could show that the compound does not interfere with the transcriptional regulation of the inducible nitric oxide synthase (iNOS), the enzyme responsible for the induced NO release in microglia and macrophages, and that it does decrease the NO release in already activated microglia.

The compound has a unique protein-like structure, composed of 4 proteinogenic and artificial amino acids. This chemical structure is new to the field of nitric oxide synthase (NOS). Its cell based IC_{50} value of 104 nM is below those of commonly used NOS inhibitors. In a prove of concept experiment, I could show that the application of this compound improves the outcome of stroke in mice.

6 ZUSAMMENFASSUNG

Mikroglia sind die immunkompetenten Zellen des zentralen Nervensystems (ZNS). Sie überwachen die Homöostase ihrer Umgebung und aktivieren sich bei Veränderungen auf unterschiedliche Art und Weise. Eine pathologische Aktivierung verändert ihr Morphologie von einem verzweigtem zu einem rundlichen Aussehen, erhöht ihr Phagozytoseaktivität, und die Ausschüttung von Proinflammatorischen Zytokinen und Stickstoffmonoxid. Dieses Verhalten spielt eine Rolle in vielen pathologischen Prozessen in akuten und chronischen neuroinflammatorischen Erkrankungen, wie zum Beispiel dem Schlaganfall, der Multiple Sklerose, oder der Schizophrenie. Eine Aktivierung von Mikroglia kann zu einer Verbesserung oder aber auch Verschlechterung dieser Erkrankungen führen. Es ist daher von therapeutischem Interesse neue Moleküle zu identifizieren, welche spezifisch den Aktivierungsprozess von Mikroglia modulieren.

In dieser Arbeit habe ich ein neuartiges Molekül identifiziert, welches die induzierte Stickstoffmonoxidausschüttung unabhängig von ihrer Aktivierung in Mikroglia und Makrophagen hemmt. Wir haben eine Bibliothek von 16544 Molekülen im Hochdurchsatzverfahren untersucht, um jene zu finden, welche in der Lage sind die Lipopolysaccharide (LPS) induzierte Stickstoffmonoxidausschüttung in der BV-2 Zelllinie zu reduzieren. Die Resultate aller positiven Moleküle wurden in primarkultivierten neonatalen Mikrogliazellen kontrolliert. Das idenfizierte Molekül zeigte eine Reduktion der Stickstoffmonoxidausschüttung unabhängig vom pathogenen Stimulus: LPS, Interferon Gamma (IFNγ), and polyinosinic:polycytidylic Säure (polyIC). Die LPS-induzierte Ausschüttung von der proinflammatorischen Zytokinen TNFα, IL1ß, und IL6 wurde nicht verändert. Zudem konnte ich zeigen, das die basal und LPS aktivierte Phagozytose nicht beeinflusst wurde, jedoch zeigte die Migration von Mikroglia Veränderung. Des Weiteren konnte ich zeigen, dass die Regulation der Transkription von der induzierten Stickstoffmonoxidsynthase (iNOS), jenes Enzym welches für die induzierte Produktion von Stickstoffmonoxid zuständig ist, nicht von unserem Molekül beeinflusst wird.

Unser Molekül hat eine einzigartige proteinähnliche Struktur. Es setzt sich aus 4 proteinogenen und künstlichen Aminosäuren zusammen. Die chemische Struktur ist einmalig im Bereich der Stickstoffmonoxidsynthaseinhibitoren. Der zellbasierte IC_{50}-Wert ist mit 104 nM unterhalb der gebräuchlichen Inhibitoren. In einem ersten in-vivo Versuch konnte ich zeigen, dass unser Molekül einen positiven Einfluss auf den Verlauf eines Schlaganfalles hat.

EIDESSTATTLICHE ERKLÄRUNG

Ich, Philipp Jordan, erkläre hiermit an Eides statt, dass ich die vorliegende Arbeit mit dem Titel "A novel compound targeting microglial activation“ selbstständig verfasst habe und keine weiteren Hilfsmittel als die angegebenen benutzt habe.

Des Weiteren erkläre ich, dass ich die vorliegende Arbeit nie in dieser oder einer anderen Form bei einem Promotionsverfahren eingereicht habe.

Philipp Jordan

Berlin, den 31.08.2018

REFERENCES

1. del Rio-Hortega, P. El “tercer elemento” de los centros nerviosos. I. La microgl_ıa en estado normal. *Boletín la Soc. Española Biol.* VIII:67–82 (1919).

2. del Rio-Hortega, P. El “tercer elemento de los centros nerviosos”. II. Intervenci _on de la microglia en los procesos patologicos (celulas en bastoncito y cuerpos granuloadiposos). *Boletín la Soc. Española Biol.* VIII:91–103 (1919).

3. del Rio-Hortega, P. El “tercer elemento” de los centros nerviosos. III. Naturaleza probable de la microglia. *Boletín la Soc. Española Biol.* VIII:108–115 (1919).

4. del Rio-Hortega, P. El “tercer elemento de los centros nerviosos”. IV. Poder fagocitario y movilidad de la microglia. *Boletín la Soc. Española Biol.* VIII:154–166 (1919).

5. Sierra, A. *et al.* The “Big-Bang” for modern glial biology: Translation and comments on Pío del Río-Hortega 1919 series of papers on microglia. *Glia* **64,** 1801–1840 (2016).

6. Ramón y Cajal, S. Contribucion al conocimiento de la neuroglia del cerebro humano. *Trab Lab Invest Biol Univer Madrid* XI:215–315 (1913).

7. del Rio-Hortega, P. Glia con pocas prolongaciones (oligodendroglia). *Boletín la Soc. Española Biol.* XXI:1–43 (1921).

8. del Rio-Hortega, P. Son homologables la glia de escasas radiaciones y la celula de Schwann? *Boletín la Soc. Española Biol.* X:1–4. (1922).

9. del Rio-Hortega, P. Tercera aportacion al conocimiento morfologico e interpretacion funcional de la oligodendroglia. *Mem. Real Soc. Esp. Hist. Nat* **14,** 40--122 (1928).

10. Grabert, K. *et al.* Microglial brain region−dependent diversity and selective regional sensitivities to aging. *Nat. Neurosci.* **19,** 504–516 (2016).

11. Ginhoux, F. & Prinz, M. Origin of Microglia: Current Concepts and Past Controversies. *Cold Spring Harb. Perspect. Biol.* **7,** a020537 (2015).

12. Ginhoux, F. *et al.* Fate Mapping Analysis Reveals That Adult Microglia Derive from Primitive Macrophages. *Science (80-.).* **330,** 841–845 (2010).

13. Blinzinger, K. & Kreutzberg, G. Displacement of synaptic terminals from regenerating motoneurons by microglial cells. *Zeitschrift für Zellforsch. und Mikroskopische Anat.* **85,** 145–157 (1968).

14. Harry, G. J. Microglia during development and aging. *Pharmacol. Ther.* **139,** 313–326 (2013).

15. Bilimoria, P. M. & Stevens, B. Microglia function during brain development: New insights from animal models. *Brain Res.* **1617,** 7–17 (2015).

16. Michell-Robinson, M. A. *et al.* Roles of microglia in brain development, tissue maintenance and repair. *Brain* **138,** 1138–1159 (2015).

17. Kettenmann, H., Kirchhoff, F. & Verkhratsky, A. Microglia: New Roles for the Synaptic Stripper. *Neuron* **77,** 10–18 (2013).

18. Wu, Y., Dissing-Olesen, L., MacVicar, B. A. & Stevens, B. Microglia: Dynamic Mediators of Synapse Development and Plasticity. *Trends Immunol.* **36,** 605–613 (2015).

19. VanRyzin, J. W., Pickett, L. A. & McCarthy, M. M. Microglia: Driving critical periods and sexual differentiation of the brain. *Dev. Neurobiol.* **78,** 580–592 (2018).

20. Lenz, K. M. & McCarthy, M. M. A Starring Role for Microglia in Brain Sex Differences. *Neurosci.* **21,** 306–321 (2015).

21. Kim, E. & Cho, S. Microglia and Monocyte-Derived Macrophages in Stroke. *Neurotherapeutics* **13,** 702–718 (2016).

22. Anttila, J. E., Whitaker, K. W., Wires, E. S., Harvey, B. K. & Airavaara, M. Role of microglia in ischemic focal stroke and recovery: Focus on Toll-like receptors. *Prog. Neuro-Psychopharmacology Biol. Psychiatry* (2016). doi:10.1016/j.pnpbp.2016.07.003

23. Ma, Y., Wang, J., Wang, Y. & Yang, G. Y. The biphasic function of microglia in ischemic stroke. *Prog. Neurobiol.* (2015). doi:10.1016/j.pneurobio.2016.01.005

24. Hambardzumyan, D., Gutmann, D. H. & Kettenmann, H. The role of microglia and macrophages in glioma maintenance and progression. *Nat. Neurosci.* **19,** 20–27 (2016).

25. Jack, C., Ruffini, F., Bar-Or, A. & Antel, J. P. Microglia and multiple sclerosis. *Journal of Neuroscience Research* **81,** 363–373 (2005).

26. Zéphir, H. Progress in understanding the pathophysiology of multiple sclerosis. *Rev. Neurol. (Paris).* **174,** 358–363 (2018).

27. Chu, F. *et al.* The roles of macrophages and microglia in multiple sclerosis and experimental autoimmune encephalomyelitis. *J. Neuroimmunol.* **318,** 1–7 (2018).

28. Najjar, S. *et al.* Neuroinflammation and psychiatric illness. *J. Neuroinflammation* **10,** 43 (2013).

29. Mattei, D. *et al.* Minocycline rescues decrease in neurogenesis, increase in microglia cytokines and deficits in sensorimotor gating in an animal model of schizophrenia. *Brain. Behav. Immun.* **38,** 175–184 (2014).

30. Mrak, R. E. Microglia in Alzheimer brain: A neuropathological perspective. *International Journal of Alzheimer's Disease* (2012). doi:10.1155/2012/165021

31. Rojanathammanee, L., Floden, A. M., Manocha, G. D. & Combs, C. K. Attenuation of microglial activation in a mouse model of Alzheimer's disease via NFAT inhibition. *J. Neuroinflammation* **12,** 42 (2015).

32. Balez, R. & Ooi, L. Getting to NO Alzheimer's disease: Neuroprotection versus neurotoxicity mediated by nitric oxide. *Oxid. Med. Cell. Longev.* **2016,** (2016).

33. Zhihui, Q. Modulating nitric oxide signaling in the CNS for Alzheimer's disease therapy. *Future Med. Chem.* **5,** 1451–68 (2013).

34. Collin, M. & Milne, P. Langerhans cell origin and regulation. *Curr. Opin. Hematol.* **23,** 28–35 (2016).

35. Malissen, B., Tamoutounour, S. & Henri, S. The origins and functions of dendritic cells and macrophages in the skin. *Nat. Rev. Immunol.* **14,** 417–428 (2014).

36. Hussell, T. & Bell, T. J. Alveolar macrophages: plasticity in a tissue-specific context. *Nat. Rev. Immunol.* **14,** 81–93 (2014).

37. Guilliams, M. *et al.* Alveolar macrophages develop from fetal monocytes that differentiate into long-lived cells in the first week of life via GM-CSF. *J. Exp. Med.* **210,** 1977–1992 (2013).

38. Epelman, S., Lavine, K. J. & Randolph, G. J. Origin and Functions of Tissue Macrophages. *Immunity* **41,** 21–35 (2014).

39. Kettenmann, H. The brain's garbage men. *Nature* **446,** 989–991 (2007).

40. Kettenmann, H., Hanisch, U.-K., Noda, M. & Verkhratsky, A. Physiology of Microglia. *Physiol. Rev.* **91,** 461–553 (2011).

41. Wolf, S. A., Boddeke, H. W. G. M. & Kettenmann, H. Microglia in Physiology and Disease. *Annu. Rev. Physiol.* **79,** 619–643 (2017).

42. Färber, K. & Kettenmann, H. Physiology of microglial cells. in *Brain Research Reviews* **48,** 133–143 (2005).

43. Nimmerjahn, A., Kirchhoff, F. & Helmchen, F. Resting Microglial Cells Are Highly Dynamic Surveillants of Brain Parenchyma in Vivo. *Science (80-.).* **308,** 1314–1318 (2005).

44. Hughes, V. Microglia: The constant gardeners. *Nature* **485,** 570–572 (2012).

45. Gulati, P. Janeway's Immunobiology, 7th Edition by Kenneth Murphy, Paul Travers, and Mark Walport. *Biochem. Mol. Biol. Educ.* **37,** 134–134 (2009).

46. Inoue, K. Microglial activation by purines and pyrimidines. *Glia* **40,** 156–163 (2002).

47. Pocock, J. M. & Kettenmann, H. Neurotransmitter receptors on microglia. *Trends Neurosci.* **30,** 527–535 (2007).

48. Pont-Lezica, L., Béchade, C., Belarif-Cantaut, Y., Pascual, O. & Bessis, A. Physiological roles of microglia during development. *J. Neurochem.* **119,** 901–908 (2011).

49. Garay, P. A. & McAllister, A. K. Novel roles for immune molecules in neural development: Implications for neurodevelopmental disorders. *Front. Synaptic Neurosci.* **2,** 1–16 (2010).

50. Glass, C. K. & Saijo, K. Microglial cell origin and phenotypes in health and disease. *Nat. Rev. Immunol.* **11,** 775–787 (2011).

51. Könnecke, H. & Bechmann, I. The role of microglia and matrix metalloproteinases involvement in neuroinflammation and gliomas. *Clin. Dev. Immunol.* **2013,** (2013).

52. Hanisch, U.-K. & Kettenmann, H. Microglia: active sensor and versatile effector cells in the normal and pathologic brain. *Nat. Neurosci.* **10,** 1387–1394 (2007).

53. Yuste, J. E., Tarragon, E., Campuzano, C. M. & Ros-Bernal, F. Implications of glial nitric oxide in neurodegenerative diseases. *Front. Cell. Neurosci.* **9,** 322 (2015).

54. Aktan, F. iNOS-mediated nitric oxide production and its regulation. *Life Sci.* **75,** 639–653 (2004).

55. Kontogiorgis, C. & Hadjipavlou-Litina, D. Nitric oxide synthases and their natural inhibitors. *Curr. Enzym. Inhib.* **12,** 3–15 (2016).

56. EMBL-EBI ChEBI: Nitric oxide. (2017). Available at: https://www.ebi.ac.uk/chebi/searchId.do?chebiId=16480.

57. Pacher, P., Beckman, J. S. & Liaudet, L. Nitric Oxide and Peroxynitrite in Health and Disease. *Physiol. Rev.* **87,** 315–424 (2007).

58. Lowenstein, C. J. iNOS (NOS2) at a glance. *J. Cell Sci.* **117,** 2865–2867 (2004).

59. Alderton, W. K., Cooper, C. E. & Knowles, R. G. Nitric oxide synthases: structure, function and inhibition. *Biochem. J.* **357,** 593–615 (2001).

60. Daff, S. NO synthase: Structures and mechanisms. *Nitric Oxide - Biol. Chem.* **23,** 1–11 (2010).

61. Hibbs, J., Taintor, R. & Vavrin, Z. Macrophage cytotoxicity: role for L-arginine deiminase and imino nitrogen oxidation to nitrite. *Science (80-.).* **235,** 473–476 (1987).

62. Ignarro, L. J., Buga, G. M., Wood, K. S., Byrns, R. E. & Chaudhuri, G. Endothelium-derived relaxing factor produced and released from artery and vein is nitric oxide. *Proc. Natl. Acad. Sci.* **84,** 9265–9269 (1987).

63. Koshland, D. E. The Molecule of the Year. *Science (80-.).* **258,** 1861 (1992).

64. 'The Nobel Prize in Physiology or Medicine 1998'. *Nobelprize.org. Nobel Media* (2018). Available at: http://www.nobelprize.org/nobel_prizes/medicine/laureates/1998/.

65. Wise, D. L. & Houghton, G. Diffusion coefficients of neon, krypton, xenon, carbon monoxide and nitric oxide in water at 10–60°C. *Chem. Eng. Sci.* **23,** 1211–1216 (1968).

66. Pokharel, S., Pantha, N. & Adhikari, N. P. Diffusion coefficients of nitric oxide in water: A molecular dynamics study. *Int. J. Mod. Phys. B* **30,** 1650205 (2016).

67. Zacharia, I. G. & Deen, W. M. Diffusivity and Solubility of Nitric Oxide in Water and Saline. *Ann. Biomed. Eng.* **33,** 214–222 (2005).

68. Ray, P. D., Huang, B.-W. & Tsuji, Y. Reactive oxygen species (ROS) homeostasis and redox regulation in cellular signaling. *Cell. Signal.* **24,** 981–990 (2012).

69. Vollhardt, P. & Schore, N. *Organic Chemistry: Structure and Function*. (W.H. Freeman, 2018).

70. Lundberg, J. O., Weitzberg, E. & Gladwin, M. T. The nitrate-nitrite-nitric oxide pathway in physiology and therapeutics. *Nat. Rev. Drug Discov.* **7,** 156–167 (2008).

71. Bogdan, C. Nitric oxide synthase in innate and adaptive immunity: An update. *Trends Immunol.* **36,** 161–178 (2015).

72. Nathan, C. & Xie, Q. wen. Nitric oxide synthases: Roles, tolls, and controls. *Cell* **78,** 915–918 (1994).

73. Calabrese, V. *et al.* Nitric oxide in the central nervous system: neuroprotection versus neurotoxicity. *Nat. Rev. Neurosci.* **8,** 766–775 (2007).

74. Fukuto, J. M., Cisneros, C. J. & Kinkade, R. L. A comparison of the chemistry associated with the biological signaling and actions of nitroxyl (HNO) and nitric oxide (NO). *J. Inorg. Biochem.* **118,** 201–208 (2013).

75. Gould, N., Doulias, P. T., Tenopoulou, M., Raju, K. & Ischiropoulos, H. Regulation of protein function and signaling by reversible cysteine s-nitrosylation. *J. Biol. Chem.* **288,** 26473–26479 (2013).

76. Helms, C. & Kim-Shapiro, D. B. Hemoglobin-mediated nitric oxide signaling. *Free Radic. Biol. Med.* **61,** 464–72 (2013).

77. Li, H. & Poulos, T. L. Structure-function studies on nitric oxide synthases. *J. Inorg. Biochem.* **99,** 293–305 (2005).

78. Li, H. *et al.* Structures of human constitutive nitric oxide synthases. *Acta Crystallogr. Sect. D Biol. Crystallogr.* **70,** 2667–2674 (2014).

79. Hall, A. V *et al.* Structural organization of the human neuronal nitric oxide synthase gene (NOS1). *J. Biol. Chem.* **269,** 33082–90 (1994).

80. Andrew, P. Enzymatic function of nitric oxide synthases. *Cardiovasc. Res.* **43,** 521–531 (1999).

81. Cho, H. J. Calmodulin is a subunit of nitric oxide synthase from macrophages. *J. Exp. Med.* **176,** 599–604 (1992).

82. Iyengar, R., Stuehr, D. J. & Marletta, M. A. Macrophage synthesis of nitrite, nitrate, and N-nitrosamines: precursors and role of the respiratory burst. *Proc. Natl. Acad. Sci.* **84,** 6369–6373 (1987).

83. Kwon, N. S. *et al.* L-citrulline production from L-arginine by macrophage nitric oxide synthase. The ureido oxygen derives from dioxygen. *J. Biol. Chem.* **265,** 13442–5 (1990).

84. Stuehr, D. J., Cho, H. J., Kwon, N. S., Weise, M. F. & Nathan, C. F. Purification and characterization of the cytokine-induced macrophage nitric oxide synthase: an FAD- and FMN-containing flavoprotein. *Proc. Natl. Acad. Sci.* **88,** 7773–7777 (1991).

85. Bredt, D. S. & Snyder, S. H. Isolation of nitric oxide synthetase, a calmodulin-requiring enzyme. *Proc. Natl. Acad. Sci.* **87,** 682–685 (1990).

86. Pollock, J. S. *et al.* Purification and characterization of particulate endothelium-derived relaxing factor synthase from cultured and native bovine aortic endothelial cells. *Proc. Natl. Acad. Sci.* **88,** 10480–10484 (1991).

87. Dudzinski, D. M. & Michel, T. Life history of eNOS: Partners and pathways. *Cardiovasc. Res.* **75,** 247–260 (2007).

88. Zhao, Y., Vanhoutte, P. M. & Leung, S. W. S. Vascular nitric oxide: Beyond eNOS. *J. Pharmacol. Sci.* **129,** 83–94 (2015).

89. Bohlen, H. G. in *Comprehensive Physiology* **5,** 803–828 (John Wiley & Sons, Inc., 2015).

90. Pitsikas, N. The role of nitric oxide in the object recognition memory. *Behav. Brain Res.* **285,** 200–207 (2015).

91. Hu, Y. & Zhu, D.-Y. in *Vitamins and Hormones* **96,** 127–160 (Elsevier Inc., 2014).

92. Murphy, S. Production of nitric oxide by glial cells: regulation and potential roles in the CNS. *Glia* **29,** 1–13 (2000).

93. Prast, H. & Philippu, A. Nitric oxide as modulator of neuronal function. *Prog. Neurobiol.* **64,** 51–68 (2001).

94. Steinert, J. R., Chernova, T. & Forsythe, I. D. Nitric Oxide Signaling in Brain Function, Dysfunction, and Dementia. *Neurosci.* **16,** 435–452 (2010).

95. Bogdan, C. Nitric oxide synthase in innate and adaptive immunity: an update. *Trends Immunol.* **36,** 161–178 (2015).

96. Bogdan, C. Nitric oxide and the immune response. *Nat. Immunol.* **2,** 907–916 (2001).

97. Shu, X. *et al.* Endothelial nitric oxide synthase in the microcirculation. *Cell. Mol. Life Sci.* **72,** 4561–4575 (2015).

98. Simmonds, M. J., Detterich, J. A. & Connes, P. Nitric oxide, vasodilation and the red blood cell. *Biorheology* **51,** 121–134 (2014).

99. Hawkins, R. D., Son, H. & Arancio, O. in *Progress in brain research* **118,** 155–172 (1998).

100. Hardingham, N., Dachtler, J. & Fox, K. The role of nitric oxide in pre-synaptic plasticity and homeostasis. *Front. Cell. Neurosci.* **7,** 1–19 (2013).

101. Lin, A. W., Chang, C. C. & McCormick, C. C. Molecular Cloning and Expression of an Avian Macrophage Nitric-oxide Synthase cDNA and the Analysis of the Genomic 5′-Flanking Region. *J. Biol. Chem.* **271,** 11911–11919 (1996).

102. Kleinert, H. *et al.* Cytokine induction of NO synthase II in human DLD-1 cells: Roles of the JAK-STAT, AP-1 and NF-κB-signaling pathways. *Br. J. Pharmacol.* **125,** 193–201 (1998).

103. Kleinert, H., Euchenhofer, C., Ihrig-Biedert, I. & Förstermann, U. In murine 3T3 fibroblasts, different second messenger pathways resulting in the induction of NO synthase II (iNOS) converge in the activation of transcription factor NF-κB. *J. Biol. Chem.* **271,** 6039–6044 (1996).

104. Zhang, H., Chen, X., Teng, X., Snead, C. & Catravas, J. D. Molecular Cloning and Analysis of the Rat Inducible Nitric Oxide Synthase Gene Promoter in Aortic Smooth Muscle Cells 11The nucleotide sequence data reported in this paper have been submitted to the GenBank with the accession number AF042085. *Biochem. Pharmacol.* **55,** 1873–1880 (1998).

105. Chu, S. C., Marks-Konczalik, J., Wu, H.-P., Banks, T. C. & Moss, J. Analysis of the Cytokine-Stimulated Human Inducible Nitric Oxide Synthase (iNOS) Gene: Characterization of Differences between Human and Mouse iNOS Promoters. *Biochem. Biophys. Res. Commun.* **248,** 871–878 (1998).

106. Xie, Q. W., Kashiwabara, Y. & Nathan, C. Role of transcription factor NF-kappa B/Rel in induction of nitric oxide synthase. *J. Biol. Chem.* **269,** 4705–4708 (1994).

107. Xie, Q. W. Promoter of the mouse gene encoding calcium-independent nitric oxide synthase confers inducibility by interferon gamma and bacterial lipopolysaccharide. *J. Exp. Med.* **177,** 1779–1784 (1993).

108. Wang, C. *et al.* Inhibition of Cellular Proliferation through IκB Kinase-Independent and Peroxisome Proliferator-Activated Receptor γ -Dependent Repression of Cyclin D1. *Mol. Cell. Biol.* **21,** 3057–3070 (2001).

109. Lowenstein, C. J. *et al.* Macrophage nitric oxide synthase gene: Two upstream regions mediate induction by interferon γ and lipopolysaccharide (NF-cB/enhancer elements/tumor necrosis factor/transcription factors/interleukin). *Biochemistry* **90,** 9730–9734 (1993).

110. Geller, D. A. *et al.* Molecular cloning and expression of inducible nitric oxide synthase

from human hepatocytes. *Proc. Natl. Acad. Sci. U. S. A.* **90,** 3491–5 (1993).

111. Hecker, M., Cattaruzza, M. & Wagner, A. H. Regulation of Inducible Nitric Oxide Synthase Gene Expression in Vascular Smooth Muscle Cells. *Gen. Pharmacol. Vasc. Syst.* **32,** 9–16 (1999).

112. Ghosh, M. *et al.* The Interplay between Cyclic AMP, MAPK, and NF- κ B Pathways in Response to Proinflammatory Signals in Microglia. *Biomed Res. Int.* **2015,** 1–18 (2015).

113. Hoesel, B. & Schmid, J. A. The complexity of NF-κB signaling in inflammation and cancer. *Mol. Cancer* **12,** 86 (2013).

114. Ullah, M. O., Sweet, M. J., Mansell, A., Kellie, S. & Kobe, B. TRIF-dependent TLR signaling, its functions in host defense and inflammation, and its potential as a therapeutic target. *J. Leukoc. Biol.* **100,** 27–45 (2016).

115. Brown, J., Wang, H., Hajishengallis, G. N. & Martin, M. TLR-signaling Networks. *J. Dent. Res.* **90,** 417–427 (2011).

116. Aittomäki, S. & Pesu, M. Therapeutic Targeting of the JAK/STAT Pathway. *Basic Clin. Pharmacol. Toxicol.* **114,** 18–23 (2014).

117. Heinrich, P. C., Behrmann, I., Müller-Newen, G., Schaper, F. & Graeve, L. Interleukin-6-type cytokine signalling through the gp130/Jak/STAT pathway. *Biochem. J.* **334,** 297–314 (1998).

118. Scholz, C. C. & Taylor, C. T. Targeting the HIF pathway in inflammation and immunity. *Curr. Opin. Pharmacol.* **13,** 646–653 (2013).

119. Yin, J.-H., Yang, D.-I., Ku, G. & Hsu, C. Y. iNOS Expression Inhibits Hypoxia-Inducible Factor-1 Activity. *Biochem. Biophys. Res. Commun.* **279,** 30–34 (2000).

120. Taylor, B. S., Alarcon, L. H. & Billiar, T. R. Inducible nitric oxide synthase in the liver: regulation and function. *Biochemistry. (Mosc).* **63,** 766–81 (1998).

121. Katsuyama, K., Shichiri, M., Marumo, F. & Hirata, Y. Role of nuclear factor-kappaB activation in cytokine- and sphingomyelinase-stimulated inducible nitric oxide synthase gene expression in vascular smooth muscle cells. *Endocrinology* **139,** 4506–12 (1998).

122. Llovera, M., Pearson, J. D., Moreno, C. & Riveros-Moreno, V. Impaired response to interferon- γ in activated macrophages due to tyrosine nitration of STAT1 by endogenous nitric oxide. *Br. J. Pharmacol.* **132,** 419–426 (2001).

123. Lee, S. K. *et al.* Exogenous Nitric Oxide Inhibits VCAM-1 Expression in Human Peritoneal Mesothelial Cells. *Nephron* **90,** 447–454 (2002).

124. Sacco, R. L. *et al.* An updated definition of stroke for the 21st century: A statement for healthcare professionals from the American heart association/American stroke association. *Stroke* **44,** 2064–2089 (2013).

125. Adams, H. P. *et al.* Classification of subtype of acute ischemic stroke. Definitions for use in a multicenter clinical trial. TOAST. Trial of Org 10172 in Acute Stroke Treatment. *Stroke* **24,** 35–41 (1993).

126. Rodgers, H. Stroke. *Handb. Clin. Neurol.* **110,** 427–433 (2013).

127. Easton, J. D. *et al.* Definition and Evaluation of Transient Ischemic Attack: A Scientific Statement for Healthcare Professionals From the American Heart Association/American Stroke Association Stroke Council; Council on Cardiovascular Surgery and Anesthesia; Council on Cardio. *Stroke* **40,** 2276–2293 (2009).

128. Mathers, C. *et al.* Estimates of country,level deaths by cause for years 2000to2015 were primarily prepared. *Evid. Res.* 34 (2017). doi:10.1016/j.mpmed.2016.06.006

129. The top 10 causes of death. *World Health Organization* (2018). Available at: http://www.who.int/en/news-room/fact-sheets/detail/the-top-10-causes-of-death.

130. Health, B. M. C. & Res, S. Post-stroke care after medical rehabilitation in Germany : a systematic literature review of the current provision of stroke. **18,** 1–2 (2018).

131. Ritter, M., Dittrich, R., Busse, O., Nabavi, D. & Ringelstein, E. Zukünftige Versorgungskonzepte des Schlaganfalls. *Aktuelle Neurol.* **39,** 27–32 (2012).

132. del Zoppo, G. *et al.* Inflammation and stroke: putative role for cytokines, adhesion molecules and iNOS in brain response to ischemia. *Brain Pathol.* **10,** 95–112 (2000).

133. Iadecola, C., Zhang, F., Xu, S., Casey, R. & Ross, M. E. Inducible nitric oxide synthase gene expression in brain following cerebral ischemia. *J. Cereb. Blood Flow Metab.* **15,** 378–84 (1995).

134. Buisson, A., Plotkine, M. & Boulu, R. G. The neuroprotective effect of a nitric oxide inhibitor in a rat model of focal cerebral ischaemia. *Br. J. Pharmacol.* **106,** 766–767 (1992).

135. Samdani, a. F., Dawson, T. M. & Dawson, V. L. Nitric Oxide Synthase in Models of Focal

Ischemia. *Stroke* **28,** 1283–1288 (1997).

136. Zhu, D. Y., Liu, S. H., Sun, H. S. & Lu, Y. M. Expression of inducible nitric oxide synthase after focal cerebral ischemia stimulates neurogenesis in the adult rodent dentate gyrus. *J. Neurosci.* **23,** 223–9 (2003).

137. Villanueva, C. & Giulivi, C. Subcellular and cellular locations of nitric oxide synthase isoforms as determinants of health and disease. *Free Radic. Biol. Med.* **49,** 307–316 (2010).

138. Stanarius, A., Töpel, I., Schulz, S., Noack, H. & Wolf, G. Immunocytochemistry of endothelial nitric oxide synthase in the rat brain: A light and electron microscopical study using the tyramide signal amplification technique. *Acta Histochem.* **99,** 411–429 (1997).

139. Chen, Z., Mou, R., Feng, D., Wang, Z. & Chen, G. The role of nitric oxide in stroke. *Med. Gas Res.* **7,** 194 (2017).

140. Wei, G., Dawson, V. L. & Zweier, J. L. Role of neuronal and endothelial nitric oxide synthase in nitric oxide generation in the brain following cerebral ischemia. *Biochim. Acta* **1455,** 23–34 (1999).

141. Ito, Y. *et al.* Nitric Oxide Production during Cerebral Ischemia and Reperfusion in eNOS- and nNOS-Knockout Mice. *Curr. Neurovasc. Res.* **7,** 23–31 (2010).

142. Huang, Z. *et al.* Enalrged infarcts in endothelial nitric oxide synthase knockout mice are a attenuated by nitro-L-arginine. *J Cereb Blood Flow Metab* **16,** 981–987 (1996).

143. Willing, A. E. & Pennypacker, K. R. Alternate approach to understanding the molecular mechanisms of stroke-induced injury. *Histol Histopathol* **22,** 697–701 (2007).

144. Gürsoy-Özdemir, Y., Can, A. & Dalkara, T. Reperfusion-induced oxidative/nitrativie injury to neurovascular unit after focal cerebral ischemia. *Stroke* **35,** 1449–1453 (2004).

145. Hazell, A. S. Astrocytes and manganese neurotoxicity. *Neurochem. Int.* **41,** 271–277 (2002).

146. SAHA, R. & PAHAN, K. Signals for the induction of nitric oxide synthase in astrocytes. *Neurochem. Int.* **49,** 154–163 (2006).

147. Niwa, M. *et al.* Time course of expression of three nitric oxide synthase isoforms after transient middle cerebral artery occlusion in rats. *Neurol. Med. Chir. (Tokyo).* **41,** 63-72; discussion 72-73 (2001).

148. Lai, T. W., Zhang, S. & Wang, Y. T. Excitotoxicity and stroke: Identifying novel targets for neuroprotection. *Prog. Neurobiol.* **115,** 157–188 (2014).

149. Chamorro, Á., Dirnagl, U., Urra, X. & Planas, A. M. Neuroprotection in acute stroke: Targeting excitotoxicity, oxidative and nitrosative stress, and inflammation. *Lancet Neurol.* **15,** 869–881 (2016).

150. Iadecola, C., Zhang, F., Casey, R., Clark, H. B. & Ross, M. E. Inducible nitric oxide synthase gene expression in vascular cells after transient focal cerebral ischemia. *Stroke* **27,** 1373–1380 (1996).

151. Förstermann, U., Xia, N. & Li, H. Roles of vascular oxidative stress and nitric oxide in the pathogenesis of atherosclerosis. *Circ. Res.* **120,** 713–735 (2017).

152. Weber, J., Slemmer, J., Shacka, J. & Sweeney, M. Antioxidants and Free Radical Scavengers for the Treatment Of Stroke, Traumatic Brain Injury and Aging. *Curr. Med. Chem.* **15,** 404–414 (2008).

153. Allen, C. L. & Bayraktutan, U. Oxidative stress and its role in the pathogenesis of ischaemic stroke. *Int. J. Stroke* **4,** 461–470 (2009).

154. Ji, H. H., Sang, W. H. & Seung, K. L. Free radicals as triggers of brain edema formation after stroke. *Free Radic. Biol. Med.* **39,** 51–70 (2005).

155. Satoh, S. *et al.* Inhibition of neutrophil migration by a protein kinase inhibitor for the treatment of ischemic brain infarction. *Jpn. J. Pharmacol.* **80,** 41–48 (1999).

156. Tobin, M. K. *et al.* Neurogenesis and inflammation after ischemic stroke: What is known and where we go from here. *J. Cereb. Blood Flow Metab.* **34,** 1573–1584 (2014).

157. Jickling, G. C. *et al.* Targeting neutrophils in ischemic stroke: Translational insights from experimental studies. *J. Cereb. Blood Flow Metab.* **35,** 888–901 (2015).

158. Thrift, A. G. *et al.* Global stroke statistics. *Int. J. Stroke* **9,** 6–18 (2014).

159. Giulian, D. & Baker, T. J. Characterization of ameboid microglia isolated from developing mammalian brain. *J. Neurosci.* **6,** 2163 LP-2178 (1986).

160. Blasi, E., Barluzzi, R., Bocchini, V., Mazzolla, R. & Bistoni, F. Immortalization of murine microglial cells by a v-raf / v-myc carrying retrovirus. *J. Neuroimmunol.* **27,** 229–237 (1990).

161. Jung, M. *et al.* Lines of Murine Oligodendroglial Precursor Cells Immortalized by an

Activated neu Tyrosine Kinase Show Distinct Degrees of Interaction with Axons In Vitro and In Vivo. *Eur. J. Neurosci.* **7,** 1245–1265 (1995).

162. Brideau, C., Gunter, B., Pikounis, B. & Liaw, A. Improved Statistical Methods for Hit Selection in High-Throughput Screening. *J. Biomol. Screen.* **8,** 634–647 (2003).

163. Endres, M. *et al.* DNA Methyltransferase Contributes to Delayed Ischemic Brain Injury. *J. Neurosci.* **20,** 3175–3181 (2000).

164. Zhang, L. *et al.* A test for detecting long-term sensorimotor dysfunction in the mouse after focal cerebral ischemia. *J. Neurosci. Methods* **117,** 207–214 (2002).

165. Lisurek, M. *et al.* Design of chemical libraries with potentially bioactive molecules applying a maximum common substructure concept. *Mol. Divers.* **14,** 401–408 (2010).

166. Berg, T. *et al.* ChemBioNet. Available at: http://www.chembionet.info. (Accessed: 12th February 2018)

167. Lipinski, C. A., Lombardo, F., Dominy, B. W. & Feeney, P. J. Experimental and computational approaches to estimate solubility and permeability in drug discovery and development settings. *Adv. Drug Deliv. Rev.* **23,** 3–25 (1997).

168. Lipinski, C. A. Rule of five in 2015 and beyond: Target and ligand structural limitations, ligand chemistry structure and drug discovery project decisions. *Adv. Drug Deliv. Rev.* **101,** 34–41 (2016).

169. Lipinski, C. A. Drug-like properties and the causes of poor solubility and poor permeability. *J. Pharmacol. Toxicol. Methods* **44,** 235–249 (2000).

170. Das, A. *et al.* Transcriptome sequencing reveals that LPS-triggered transcriptional responses in established microglia BV2 cell lines are poorly representative of primary microglia. *J. Neuroinflammation* **13,** 182 (2016).

171. Henn, A. The suitability of BV2 cells as alternative model system for primary microglia cultures or for animal experiments examining brain inflammation. *ALTEX* **26,** 83–94 (2009).

172. Sierra, A., Abiega, O., Shahraz, A. & Neumann, H. Janus-faced microglia: beneficial and detrimental consequences of microglial phagocytosis. *Front. Cell. Neurosci.* **7,** 1–22 (2013).

173. Furchgott, R. F. & Zawadzki, J. V. The obligatory role of endothelial cells in the relaxation

of arterial smooth muscle by acetylcholine. *Nature* **288,** 373–376 (1980).

174. 'Nitric Oxide' on PubMed. *NCBI* (2018).

175. Kroncke, K., Fehsel, K. & Kolb-Bachofen, V. Inducible nitric oxide synthase in human diseases. *Clin. Exp. Immunol.* **113,** 147–156 (1998).

176. Magenta, A., Greco, S., Capogrossi, M. C., Gaetano, C. & Martelli, F. Nitric Oxide , Oxidative Stress , and p66 Shc Interplay in Diabetic Endothelial Dysfunction. *Biomed Res. Int.* **2014,** 1–17 (2014).

177. Lundberg, J. O., Gladwin, M. T. & Weitzberg, E. Strategies to increase nitric oxide signalling in cardiovascular disease. *Nat. Rev. Drug Discov.* **14,** 623–641 (2015).

178. Salimian Rizi, B., Achreja, A. & Nagrath, D. Nitric Oxide: The Forgotten Child of Tumor Metabolism. *Trends in Cancer* **3,** 659–672 (2017).

179. Liddie, S., Balda, M. A. & Itzhak, Y. Nitric oxide (NO) signaling as a potential therapeutic modality against psychostimulants. *Curr. Pharm. Des.* **19,** 7092–7102 (2013).

180. Walker, M. Y. *et al.* Role of oral and gut microbiome in nitric oxide-mediated colon motility. *Nitric Oxide - Biol. Chem.* **73,** 81–88 (2018).

181. Pmw, B., Krishnan, K. & Jp, A. Nitric oxide donors (nitrates), L-arginine , or nitric oxide synthase inhibitors for acute stroke (Review). (2017). doi:10.1002/14651858.CD000398.pub2.www.cochranelibrary.com

182. Willmot, M., Gibson, C., Gray, L., Murphy, S. & Bath, P. Nitric oxide synthase inhibitors in experimental ischemic stroke and their effects on infarct size and cerebral blood flow: A systematic review. *Free Radic. Biol. Med.* **39,** 412–425 (2005).

183. Bar-Or, D. *et al.* Sepsis, oxidative stress, and hypoxia: Are there clues to better treatment? *Redox Rep.* **20,** 193–197 (2015).

184. Beyazit, Y. *et al.* Nitric oxide is a potential mediator of hepatic inflammation and fibrogenesis in autoimmune hepatitis. *Scand. J. Gastroenterol.* **50,** 204–210 (2015).

185. Togo, T., Katsuse, O. & Iseki, E. Nitric oxide pathways in Alzheimer's disease and other neurodegenerative dementias. *Neurol. Res.* **26,** 563–566 (2004).

186. Ayton, S. *et al.* Parkinson's Disease Iron Deposition Caused by Nitric Oxide-Induced Loss of -Amyloid Precursor Protein. *J. Neurosci.* **35,** 3591–3597 (2015).

187. Scheiblich, H. *et al.* Nitric oxide/cyclic GMP signaling regulates motility of a microglial cell line and primary microglia in vitro. *Brain Res.* **1564,** 9–21 (2014).

188. Russwurm, M., Russwurm, C., Koesling, D. & Mergia, E. *NO/cGMP: The Past, the Present, and the Future. Guanylate Cyclase and Cyclic GMP Methods and Protocols IN* (2013). doi:10.1007/978-1-62703-459-3

189. LaBuda, C. J., Koblish, M., Tuthill, P., Dolle, R. E. & Little, P. J. Antinociceptive activity of the selective iNOS inhibitor AR-C102222 in rodent models of inflammatory, neuropathic and post-operative pain. *Eur. J. Pain* **10,** 505–512 (2006).

190. Yang, Y. *et al.* Nitric oxide synthase inhibitors: a review of patents from 2011 to the present. *Expert Opin. Ther. Pat.* **3776,** 1–20 (2014).

191. Lu, Y. C., Yeh, W. C. & Ohashi, P. S. LPS/TLR4 signal transduction pathway. *Cytokine* **42,** 145–151 (2008).

192. Villarino, A. V., Kanno, Y., Ferdinand, J. R. & O'Shea, J. J. Mechanisms of Jak/STAT Signaling in Immunity and Disease. *J. Immunol.* **194,** 21–27 (2015).

193. Takeda, K. & Akira, S. TLR signaling pathways. *Semin. Immunol.* **16,** 3–9 (2004).

194. Lind, M. *et al.* Inducible nitric oxide synthase: Good or bad? *Biomed. Pharmacother.* **93,** 370–375 (2017).

195. de Vera, M. E. *et al.* Transcriptional regulation of human inducible nitric oxide synthase (NOS2) gene by cytokines: initial analysis of the human NOS2 promoter. *Proc Natl Acad Sci U S A* **93,** 1054–1059 (1996).

196. Hamid, R., Rotshteyn, Y., Rabadi, L., Parikh, R. & Bullock, P. Comparison of alamar blue and MTT assays for high through-put screening. *Toxicol. Vitr.* **18,** 703–710 (2004).

197. O'Brien, J., Wilson, I., Orton, T. & Pognan, F. Investigation of the Alamar Blue (resazurin) fluorescent dye for the assessment of mammalian cell cytotoxicity. *Eur. J. Biochem.* **267,** 5421–5426 (2000).

198. Hanada, T. & Yoshimura, A. Regulation of cytokine signaling and inflammation. *Cytokine Growth Factor Rev.* **13,** 413–421 (2002).

199. Prinz, M. & Priller, J. Microglia and brain macrophages in the molecular age: from origin to neuropsychiatric disease. *Nat. Rev. Neurosci.* **15,** 300–12 (2014).

200. Guillemin, G. J. & Brew, B. J. Microglia, macrophages, perivascular macrophages, and

pericytes: a review of function and identification. *J. Leukoc. Biol.* **75,** 388–397 (2004).

201. Chen, a, Kumar, S. M., Sahley, C. L. & Muller, K. J. Nitric oxide influences injury-induced microglial migration and accumulation in the leech CNS. *J. Neurosci.* **20,** 1036–1043 (2000).

202. *Neuroglia*. (Oxford University Press, 2004). doi:10.1093/acprof:oso/9780195152227.001.0001

203. James H., S., Steven A., S. & A.J., H. *Principles of Neural Science, Fifth Edition*. (McGraw Hill Professiona, 2013).

204. Lipinski, C. A. Lead- and drug-like compounds: the rule-of-five revolution. *Drug Discov. Today Technol.* **1,** 337–341 (2004).

205. Jorgensen, W. L. Efficient Drug Lead Discovery and Optimization. *Acc. Chem. Res.* **42,** 724–733 (2009).

206. Hughes, J. P., Rees, S. S., Kalindjian, S. B. & Philpott, K. L. Principles of early drug discovery. *Br. J. Pharmacol.* **162,** 1239–1249 (2011).

207. Li, Y. & Yu, J. Research Progress in Structure-Activity Relationship of Bioactive Peptides. *J. Med. Food* **18,** 147–156 (2015).

208. Heemskerk, S., Masereeuw, R., Russel, F. G. M. & Pickkers, P. Selective iNOS inhibition for the treatment of sepsis-induced acute kidney injury. *Nat. Rev. Nephrol.* **5,** 629–640 (2009).

209. Marks-konczalik, J., Chu, S. C. & Moss, J. Cytokine-mediated Transcriptional Induction of the Human Inducible Nitric Oxide Synthase Gene Requires Both Activator Protein 1 and Nuclear Factor B-binding Sites *. *J. Biol. Chem.* **273,** 22201–22208 (1998).

210. Mori, M. & Gotoh, T. Regulation of nitric oxide production by arginine metabolic enzymes. *Biochem. Biophys. Res. Commun.* **275,** 715–719 (2000).

211. Rodriguez-Pascual, F. *et al.* Complex contribution of the 3'-untranslated region to the expressional regulation of the human inducible nitric-oxide synthase gene: Involvement of the RNA-binding protein HuR. *J. Biol. Chem.* **275,** 26040–26049 (2000).

212. Rao, K. M. K. MOLECULAR MECHANISMS REGULATING iNOS EXPRESSION IN VARIOUS CELL TYPES. *J. Toxicol. Environ. Heal. Part B* **3,** 27–58 (2000).

213. *Fundamentals of Enzyme Kinetics*. (Elsevier, 2012). doi:10.1016/C2013-0-04130-8

214. Kolodziejski, P. J., Koo, J.-S. & Eissa, N. T. Regulation of inducible nitric oxide synthase by rapid cellular turnover and cotranslational down-regulation by dimerization inhibitors. *Proc. Natl. Acad. Sci.* **101,** 18141–18146 (2004).

215. Willmot, M., Gray, L., Gibson, C., Murphy, S. & Bath, P. M. W. A systematic review of nitric oxide donors and L-arginine in experimental stroke; effects on infarct size and cerebral blood flow. *Nitric Oxide - Biol. Chem.* **12,** 141–149 (2005).

216. Palmer, R. M. J., Rees, D. D., Ashton, D. S. & Moncada, S. L-arginine is the physiological precursor for the formation of nitric oxide in endothelium-dependent relaxation. *Biochem. Biophys. Res. Commun.* **153,** 1251–1256 (1988).

217. Wang, X. *et al.* Effect of L-NAME on nitric oxide and gastrointestinal motility alterations in cirrhotic rats. *World J. Gastroenterol.* **8,** 328–332 (2002).

218. Bath, P. M., Willmot, M. M., Leonardi-Bee, J. & Bath-Hextall, F. J. in *Cochrane Database of Systematic Reviews* (ed. Bath, P. M.) (John Wiley & Sons, Ltd, 2002). doi:10.1002/14651858.CD000398

219. Alderton, W. K. *et al.* GW274150 and GW273629 are potent and highly selective inhibitors of inducible nitric oxide synthase in vitro and in vivo. *Br. J. Pharmacol.* **145,** 301–312 (2005).

220. Stover, J. F. *et al.* Nitric Oxide Synthase Inhibition with the Antipterin VAS203 Improves Outcome in Moderate and Severe Traumatic Brain Injury: A Placebo-Controlled Randomized Phase IIa Trial (NOSTRA). *J. Neurotrauma* **31,** 1599–1606 (2014).

221. Boer, R. *et al.* The Inhibitory Potency and Selectivity of Arginine Substrate Site Nitric-Oxide Synthase Inhibitors Is Solely Determined by Their Affinity toward the Different Isoenzymes. *Mol. Pharmacol.* **58,** 1026–1034 (2000).

222. Tinker, A. C. *et al.* Highly Selective Inhibitors of Inducible Nitric Oxide Synthase Which Show Antiinflammatory Activity in Vivo. *J. Med. Chem.* **46,** 913–916 (2003).

223. Jafarian-Tehrani, M. *et al.* 1400W, a potent selective inducible NOS inhibitor, improves histopathological outcome following traumatic brain injury in rats. *Nitric Oxide* **12,** 61–69 (2005).

224. Poulos, T. L. & Li, H. Nitric oxide synthase and structure-based inhibitor design. *Nitric Oxide* (2016). doi:10.1016/j.niox.2016.11.004

225. Fischmann, T. O. *et al.* Structural characterization of nitric oxide synthase isoforms

reveals striking active-site conservation. *Nat. Struct. Biol.* **6,** 233–242 (1999).

226. Otvos, L. & Wade, J. D. Current challenges in peptide-based drug discovery. *Front. Chem.* **2,** 8–11 (2014).

227. Ertl, H. C., Dietzschold, B. & Otvos Jr., L. T helper cell epitope of rabies virus nucleoprotein defined by tri- and tetrapeptides. *Eur. J. Immunol.* **21,** 1–10 (1991).

228. Fosgerau, K. & Hoffmann, T. Peptide therapeutics: Current status and future directions. *Drug Discov. Today* **20,** 122–128 (2015).

229. Fasano, a. Innovative strategies for the oral delivery of drugs and peptides. *Trends Biotechnol.* **16,** 152–157 (1998).

230. Teesalu, T., Sugahara, K. N., Kotamraju, V. R. & Ruoslahti, E. C-end rule peptides mediate neuropilin-1-dependent cell, vascular, and tissue penetration. *Proc. Natl. Acad. Sci.* **106,** 16157–16162 (2009).

231. Li, Z. & Cho, C. Peptides as targeting probes against tumor vasculature for diagnosis and drug delivery. *J. Transl. Med.* **10,** S1 (2012).

232. Wender, P. A. *et al.* The design, synthesis, and evaluation of molecules that enable or enhance cellular uptake: Peptoid molecular transporters. *Proc. Natl. Acad. Sci.* **97,** 13003–13008 (2000).

233. Usmani, S. S. *et al.* THPdb: Database of FDA-approved peptide and protein therapeutics. *PLoS One* **12,** 1–12 (2017).

234. Vodovotz, Y., Russell, D., Xie, Q. W., Bogdan, C. & Nathan, C. Vesicle membrane association of nitric oxide synthase in primary mouse macrophages. *J.Immunol.* **154,** 2914–2925 (1995).

235. Alberts, B. *et al. Molecular Biology of the Cell, 4th edition*. (Garland Science, 2002).

236. Löffler, G. *Basiswissen Biochemie*. (Springer, 2008).

237. Mcgaughey, G. B., Gagne, M. & Rappe, A. K. -Stacking Interactions. **273,** 15458–15463 (1998).

238. Balligand, J.-L., Feron, O. & Dessy, C. eNOS Activation by Physical Forces: From Short-Term Regulation of Contraction to Chronic Remodeling of Cardiovascular Tissues. *Physiol. Rev.* **89,** 481–534 (2009).

239. Biosciences, B. D. In vitro adme discovery screening research services. *B. Biosci.*

240. Information, P. Mechanism of Action. *Metab. Clin. Exp.* 1–17

241. Moskowitz, M. A. Nitric oxide production during focal cerebral ischemia in rats. Editorial comment. *Stroke* **24,** 1716 (1993).

242. Kader, A., Frazzini, V. I., Solomon, R. A. & Trifiletti, R. R. Nitric oxide production during focal cerebral ischemia in rats. *Stroke* **24,** 1716 (1993).

243. Hara, E. *et al.* Expression of heme oxygenase and inducible nitric oxide synthase mRNA in human brain tumors. *Biochem. Biophys. Res. Commun.* **224,** 153–8 (1996).

244. Huang, Z. *et al.* Effects of cerebral ischemia in mice deficient in neuronal nitric oxide synthase. *Science* **265,** 1883–5 (1994).

245. Zaharchuk, G. *et al.* Neuronal nitric oxide synthase mutant mice show smaller infarcts and attenuated apparent diffusion coefficient changes in the peri- infarct zone during focal cerebral ischemia. *Magn. Reson. Med.* **37,** 170–175 (1997).

246. Iadecola, C., Zhang, F., Casey, R., Nagayama, M. & Ross, M. E. Delayed reduction of ischemic brain injury and neurological deficits in mice lacking the inducible nitric oxide synthase gene. *J. Neurosci.* **17,** 9157–9164 (1997).

247. Zhang, Z. G. *et al.* ARL 17477, a potent and selective neuronal NOS inhibitor decreases infarct volume after transient middle cerebral artery occlusion in rats. *J. Cereb. Blood Flow Metab.* **16,** 599–604 (1996).

248. Zhao, X., Ross, E. & Iadecola, C. L-Arginine increases ischemic injury in wild-type mice but not in iNOS-de cient mice. *Imaging* **i,** 308–311 (2003).

249. Nagafuji, T., Sugiyama, M., Matsui, T., Muto, A. & Naito, S. Nitric oxide synthase in cerebral ischemia. *Mol. Chem. Neuropathol.* **26,** 107–157 (1995).

250. Carreau, a *et al.* Neuroprotective efficacy of N omega-nitro-L-arginine after focal cerebral ischemia in the mouse and inhibition of cortical nitric oxide synthase. *Eur. J. Pharmacol.* **256,** 241–9 (1994).

251. Spinnewyn, B., Cornet, S., Auguet, M. & Chabrier, P.-E. Synergistic Protective Effects of Antioxidant and Nitric Oxide Synthase Inhibitor in Transient Focal Ischemia. *J. Cereb. Blood Flow Metab.* **19,** 139–143 (1999).

252. Trifiletti, R. R. Neuroprotective effects of N-Nitro-L-Arginine in the Rice-Vannucci model

of focal stroke in the 7-day-old rat pup. *Ann. Neurol.* **32(3),** 463 (1992).

253. Skaper, S. D. & Leon, A. Monosialogangliosides, neuroprotection, and neuronal repair processes. *J. Neurotrauma* **9 Suppl 2,** S507-16 (1992).

254. Kidd, G. A., Dobrucki, L. W., Brovkovych, V., Bohr, D. F. & Malinski, T. Nitric oxide deficiency contributes to large cerebral infarct size. *Hypertension* **35,** 1111–1118 (2000).

255. Buchan, A. M. *et al.* Failure to prevent selective CA1 neuronal death and reduce cortical infarction following cerebral ischemia with inhibition of nitric oxide synthase. *Neuroscience* **61,** 1–11 (1994).

256. Ashwal, S., Cole, D. J., Osborne, S., Osborne, T. N. & Pearce, W. J. L-NAME reduces infarct volume in a filament model of transient middle cerebral artery occlusion in the rat pup. *Pediatr. Res.* **38,** 652–6 (1995).

257. Ashwal, S., Cole, D. J., Osborne, T. N. & Pearce, W. J. Dual effects of L-NAME during transient focal cerebral ischemia in spontaneously hypertensive rats. *Am. J. Physiol.* **267,** H276–H284 (1994).

258. Iuliano, B. A., Anderson, R. E. & Meyer, F. B. Effect of intermittent reperfusion and nitric oxide synthase inhibition on infarct volume during reversible focal cerebral ischemia. *J. Neurosurg.* **83,** 491–495 (1995).

259. Margaill, I., Allix, M., Boulu, R. G. & Plotkine, M. Dose- and time-dependence of L-NAME neuroprotection in transient focal cerebral ischaemia in rats. *Br. J. Pharmacol.* **120,** 160–163 (1997).

260. Kamii, H. *et al.* Effects of nitric oxide synthase inhibition on brain infarction in SOD-1-transgenic mice following transient focal cerebral ischemia. *J.Cereb.Blood Flow Metab.* **16,** 1153–1157 (1996).

261. Stagliano, N. E. *et al.* The effect of nitric oxide synthase inhibition on acute platelet accumulation and hemodynamic depression in a rat model of thromboembolic stroke. *J. Cereb. Blood Flow Metab.* **17,** 1182–1190 (1997).

262. Kuluz, J. W., Prado, R. J., Dietrich, W. D., Schleien, C. L. & Watson, B. D. The effect of nitric oxide synthase inhibition on infarct volume after reversible focal cerebral ischemia in conscious rats. *Stroke* **24,** 2023–2029 (1993).

263. Haynes, W. G., Noon, J. P., Walker, B. R. & Webb, D. J. Inhibition of nitric oxide synthesis increases blood pressure in healthy humans. *J. Hypertens.* **11,** 1375–80 (1993).

264. Ivanova, S. *et al.* Cerebral ischemia enhances polyamine oxidation: identification of enzymatically formed 3-aminopropanal as an endogenous mediator of neuronal and glial cell death. *J. Exp. Med.* **188,** 327–40 (1998).

265. Cockroft, K. M. *et al.* Cerebroprotective Effects of Aminoguanidine in a Rodent Model of Stroke. *Stroke* **27,** 1393–1398 (1996).

266. Nagayama, M., Zhang, F. & Iadecola, C. Delayed treatment with aminoguanidine decreases focal cerebral ischemic damage and enhances neurologic recovery in rats. *J. Cereb. Blood Flow Metab.* **18,** 1107–1113 (1998).

267. Cash, D. *et al.* Neuroprotective effect of aminoguanidine on transient focal ischaemia in the rat brain. *Brain Res.* **905,** 91–103 (2001).

268. Keen, H., Fukker, J. & Menzinger, G. Early closure of European Pimagedine trial. *Lancet* **350,** 214–215 (1997).

269. Parmentier, S. *et al.* Selective inhibition of inducible nitric oxide synthase prevents ischaemic brain injury. *Br. J. Pharmacol.* **127,** 546–552 (1999).

270. Cuzzocrea, S. *et al.* Role of induced nitric oxide in the initiation of the inflammatory response after postischemic injury. *Shock* **18,** 169–176 (2002).

271. Van Der Schueren, B. J. *et al.* Does the unfavorable pharmacokinetic and pharmacodynamic profile of the iNOS inhibitor GW273629 lead to inefficacy in acute migraine? *J. Clin. Pharmacol.* **49,** 281–290 (2009).

272. Kassner, A. & Merali, Z. Assessment of Blood-Brain Barrier Disruption in Stroke. *Stroke* **46,** 3310–3315 (2015).

273. Garry, P. S., Ezra, M., Rowland, M. J., Westbrook, J. & Pattinson, K. T. S. The role of the nitric oxide pathway in brain injury and its treatment — From bench to bedside. *Exp. Neurol.* **263,** 235–243 (2015).

274. Bouët, V. *et al.* Sensorimotor and cognitive deficits after transient middle cerebral artery occlusion in the mouse. *Exp. Neurol.* **203,** 555–567 (2007).

275. Rogers, D. C., Campbell, C. A., Stretton, J. L. & Mackay, K. B. Correlation Between Motor Impairment and Infarct Volume After Permanent and Transient Middle Cerebral Artery Occlusion in the Rat. *Stroke* **28,** 2060–2066 (1997).

276. Brooks, S. P. & Dunnett, S. B. Tests to assess motor phenotype in mice: a user's guide.

Nat. Rev. Neurosci. **10,** 519–29 (2009).

277. Schaar, K. L., Brenneman, M. M. & Savitz, S. I. Functional assessments in the rodent stroke model. *Exp. Transl. Stroke Med.* **2,** 1–11 (2010).